# Robust and Transparent Multi-Degree-of-Freedom Bilateral Teleoperation with Time-Delay

João Rebelo

# Robust and Transparent Multi-Degree-of-Freedom Bilateral Teleoperation with Time-Delay

**Proefschrift**

ter verkrijging van de graad van doctor
aan de Technische Universiteit Delft,
op gezag van de Rector Magnificus prof. ir. K. C. A. M. Luyben,
voorzitter van het College voor Promoties,
in het openbaar te verdedigen op maandag 18 mei 2015 om 12:30 uur

door

**João Luis PINTO REBELO**

Diplom ingenieur, Faculty of Engineering of University of Porto
geboren te Lamego, Portugal.

Dit proefschrift is goedgekeurd door de promotor:

Prof. dr. F. C. T. van der Helm

Copromotor: Dr. A. Schiele

Samenstelling promotiecommissie:

| | |
|---|---|
| Rector Magnificus, | voorzitter |
| Prof. dr. F. C. T. van der Helm, | Technische Universiteit Delft, promotor |
| Dr. A. Schiele, | Technische Universiteit Delft, copromotor |
| Prof. dr. J. Smeets | Vrije Universiteit Amsterdam |
| Dr. K. Hashtrudi-Zaad | Queen's University |
| Prof. dr. H. van der Kooij | Technische Universiteit Delft |
| Prof. dr. J. Herder | Technische Universiteit Delft |
| Dr. D. Abbink | Technische Universiteit Delft |

This research was financially supported by the Portuguese Fundação para a Ciência e Tecnologia under the doctoral grant SFRH/BD/69564/2010

*Printed by:* Ipskamp Drukkers



ISBN 978-94-6186-469-7

An electronic version of this dissertation is available at
`http://repository.tudelft.nl/`.

# Preface

It is envisioned that in future planetary exploration missions, robotic platforms equipped with multi-dof arm manipulators will be sent to the surface of planets while the astronauts stay on-board orbiting spacecraft remotely operating the robot manipulators. On the planetary surface, the tasks will range from the typical sample collection and analysis of current exploration missions to structure maintenance and assembly. While it has been proven by multiple successful Mars rover missions that motion and collection tasks can be planned offline and executed by the remote robotic system, assembling a structure composed by mating parts, connectors and soft structures, such as thermal blankets or cables, in an unknown environment, requires human-level planning and decision capabilities in real-time.

In preparation for these future robotic space exploration scenarios, the European Space Agency (ESA) has developed the Sensoric Arm Master (SAM) and the X-Arm-2 haptic master exoskeletons. To demonstrate the feasibility of these technologies, the METERON project, which has as final goal to bilaterally control a robot on the ground using a 7-DOF exoskeleton on the International Space Station (ISS), is currently ongoing.

The work presented in this thesis was developed in the Telerobotics and Haptics Lab of the European Space Research and Technology Center (ESTEC) as an integral part of the METERON project. Its main aim is to provide the necessary knowledge and algorithms for bilateral teleoperation control in systems with communication delay values corresponding to those present in the communications between the ISS and ground. For this purpose this thesis investigates how to achieve high transparency and time-delay robustness in bilateral teleoperation using dissimilar multi-dof master-slave devices.

# Contents in Brief

# Summary

Robots are particularly well suited for executing tasks that take place in locations which are too dangerous or inaccessible to human operators. For robot manipulators to execute complex activities in unknown, unstructured environments, despite the recent increases in computation power, human input is still required for task planning and execution. Most of the existing bilateral teleoperation systems, which make use of commercially available master devices to control industrial slave manipulators, show three main limitations: instability on contact with stiff environments, reduced force-feedback performance to the operator and limited master workspaces. It is the main goal of the research presented in this thesis to achieve high transparency and time-delay robustness in bilateral teleoperation using dissimilar multi-dof master-slave devices, in particular making use of impedance-type masters to command impedance-controlled slave manipulators.

This research focuses on tasks which a human operator could manually execute if physically present in the remote environment. This implies that there should be no force scaling and the motion remains within the limits of the human operator arm. It is also assumed that a high level of transparency should be provided to the operator to enable the execution of the required tasks in teleoperation. Currently, modern communication devices and the Internet allow connections throughout the world with round-trip communication delays in the range of hundreds of milliseconds. Throughout this work, communication delay values smaller or equal to 250 ms, for which direct bilateral teleoperation is the most usable, are considered.

Under these premises, the research approach followed on this thesis is divided in three main parts. These parts are:

(1) *Effect of different parameters on system stability and performance for a system with impedance-type master commanding an impedance-controlled slave*

To enable the usage of systems composed by impedance-type masters commanding impedance-controlled slaves, it is important to quantify how control system parameters, master and slave physical characteristics and human operator and environment, together with time-delay, affect the stability and performance of the teleoperation system. A 4-channel control architecture is used for both analyses, since this architecture ensures a high level of transparency and can, by adequate control system parameter selection, allow other control architectures to be studied. Since the goal is to determine guidelines for control parameters design, all the analysis is done considering a 1-dof system to avoid the additional complications introduced by multi-dof systems. To overcome the limitations introduced by passivity analysis methods, a numerical method based on the Lambert W function is used to analyse a state-space model of the time-delay system.

The performance of the system, quantified using transparency is studied both in free-air and contact situations in the presence of time-delay.

Using the numerical method based on the Lambert W function, exact solutions of the time-delay state-space description of a 1-DOF system are obtained. The theoretical results, experimentally validated using a one degree-of-freedom setup, shows that increasing the damping or reducing the stiffness of the master and slave controllers increases the system robustness to time-delay. In particular, having a master device with higher controller stiffness commanding a slave with low stiffness, provides the highest stability margin in rigid contact whereas configuring lower stiffness in the master and a higher stiffness in the slave provides higher stability in free-air motion. The results also show that using the Lambert W function analysis it is possible to determine an accurate stability border for the linear time-delay state-space system.

To evaluate the system performance, both "transparency" and the newly introduced "reflected damping in free-air" criterion are used. Using this criterion it is shown that the damping felt by the human operator interacting with the system while the slave is in free-air is dependent on the master and slave local controller parameters and increases linearly with the time-delay with a factor dependent on the master and slave proportional controller gains. The steady-state transparency analysis of the system shows that, independently of the time-delay or controller parameters, a stiffness equal to that of the environment is transmitted to the operator as long as the transparency optimized tuning rules are used. The experimental validation, using a 1-dof master-slave teleoperation system, shows that the proposed criterion can approximate the identified damping with an accuracy of 5% for time-delay values up to 30 ms.

(2) *Robust stability methods for 4-channel architecture under time-delay*

Time-domain passivity control has been used successfully to stabilize teleoperation system with position-force and position-position controllers, however the performance with these control architectures is sub-optimal both with and without time-delay. This thesis extends the network representation of the time-domain passivity controller to the 4-channel architecture. The proposed architecture is based on the previously presented time-delay power network concept and modelling all the controllers as dependent voltage sources and using only series passivity controllers. The obtained results on a one degree-of-freedom setup show that, using this method, the system can be made stable for time-delays up to 1s as well as in the presence of data losses and complete data blackouts in the communication channel. Using the 4-channel time-domain passivity framework, a better performance in terms of transparency, when compared to other time-domain passivity architectures, is obtained both with and without time delay.

Since multiple degrees-of-freedom are typically needed to execute meaningful tasks in teleoperation, the 4-channel time-domain passivity control architecture is then extended to multi-dof. The proposed multi-dof 4-channel time-domain passivity control framework is validated using the Sensoric Arm Master arm exoskeleton controlling a Kuka Lightweight Robot in Cartesian space with a round-trip communication delay of 300 ms. The proposed time-domain passivity method is able to stabilize a time-delay multi-dof bilateral system being controlled using the 4-channel architecture while still providing a level of transparency of 0.8, similar to that of the case without time-delay.

Two different energy dissipation strategies are used and it is shown that, while both can ensure stability of the system, they result in different forces being transmitted to the operator during teleoperation.

(3) *Propose hardware/software architectures for multi-dof teleoperation*

Currently existing state-of-the-art haptic master devices with human-like workspaces are based on heavy robotic manipulators which are not wearable and not easily portable. In many applications, in particular in space teleoperation, portable lightweight master devices are needed. In this work, a complete end-to-end teleoperation system using a portable arm exoskeleton to control a 7-DOF slave manipulator with transparent force-reflection to the operator is presented. The proposed master device architecture makes use of local joint controller communicating over an EtherCAT bus for high performance and using a tablet computer for a high-level Graphical User Interface. The results show that using the developed exoskeleton haptic device as the controller for the 7-DOF Kuka Lightweight robot in impedance-mode, with a system control frequency of 1 kHz, contact with surfaces of different stiffness are able to be rendered with a ratio of 0.8 between the real stiffness and that rendered to the operator.

The teleoperation system using the SAM exoskeleton to command the Kuka Lightweight Robot, combined with the 4-channel time-domain passivity control is shown to allow execution of tasks over a bandwidth limited mobile Internet connection with an average 100 ms delay and 17% data loss. To handle the network limitations, video is compressed to keep the bandwidth usage to 96kbits/s. The ability of an operator to execute 6-DOF activities is demonstrated by performing a complex peg removal task.

However, since the existence of singularities, joint limits and manipulator redundancies can lead to instability, causing loss of control and potentially leading to dangerous situations, a mapping strategy for using only a part of the slave workspace which is reachable by the human operator during teleoperation is proposed. With convenient scaling and slave base placement using a genetic algorithm, the reachable area is placed such that singularities and joint limits are always avoided during real-time teleoperation. Combining the slave mounting optimization with an elbow angle redundancy mapping for configuration control is shown to ensure geometrical correspondence between the operator and the slave manipulator. The proposed mapping is demonstrated using a full arm master exoskeleton to command a 7-DOF slave manipulator.

# Contents

CHAPTER 1

# Introduction

Robots are particularly well suited for executing tasks that take place in locations which are too dangerous or inaccessible to human operators. For robot manipulators to execute complex activities in unknown, unstructured environments, despite the recent increases in computation power, human input is still required for task planning and execution. In these cases, the human operator interacts with a *master* device which sends commands to the remote *slave* manipulator. The human is responsible for the entire task planning and execution with different level of autonomy needed on the local and remote sites. These systems are called *teleoperation* systems. Some of the first examples appeared in the nuclear industry for handling radioactive material [1]. Other applications for teleoperation are in fields as diverse as robotic surgery [2] and space exploration [3].

In this context, the teleoperation system is used to allow the operator to efficiently execute tasks remotely. For unknown and unstructured environments, since autonomy is limited due to the lack of information on the remote environment, the operator should be linked as directly as possible to the slave manipulator such that tasks can be seamlessly executed. For this purpose, not only visual but also *haptic* feedback, in which forces from the remote side are transmitted through the master device to the operator, is needed. This is achieved by transmitting force, position and velocity data bilaterally, both from the master to the slave and from the slave back to the master. When a teleoperation system provides haptic feedback to the human operator it is called a *bilateral teleoperation system*. When the master and the slave devices are placed in distant locations, the communication channel used for data exchange introduces *time-delay* and other communication constraints in the system. Figure 1.1 shows a high-level bilateral teleoperation system diagram.

To execute meaningful tasks remotely, the operator has to be able to simultaneously control multiple degrees-of-freedom (multi-dof) of the slave manipulator and efficiently receive information from the remote site through the master. In some applications, such as, for example, robotic surgery, the tasks to be executed take place in a range of centimetres, and therefore, the human operator only has to command small motions. In many other cases, tasks may involve grasping and moving objects or press buttons on a task panel. In these cases, the operator should be able to use the master device to command motions and sense forces in a range comparable to that of the human arm. Currently available state-of-the-art commercial teleoperation systems, such as the Da Vinci surgical system [2], allow controlling robots in multi-dof, however no force-feedback is provided to the operator. While the system enables various surgical tasks to be executed, operations require a large amount of training and complex activities are limited to a few, very skilled operators [4]. It is generally agreed that force-feedback could allow simpler and more efficient task execution using the system [5]. Most of the existing bilateral teleoperation systems make

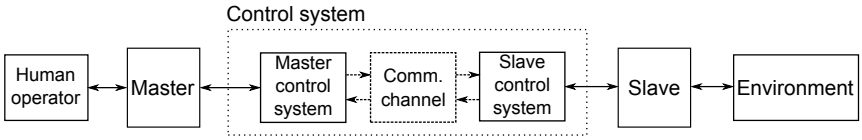


Figure 1.1: Bilateral teleoperation high-level system diagram

use of commercially available master devices, such as the Geomagic Touch[1] [6] or the sigma.7 [7], to control industrial slave manipulators [8, 9, 10]. These bilateral teleoperation systems show three main limitations: instability on contact with stiff environments [9], reduced force-feedback performance to the operator [8] and limited master workspaces.

These limitations can be related to characteristics of the devices used on both the master and slave sides. An analysis of the performance limits of a teleoperation system done by Daniel and McAree [9] showed that the maximum force-feedback gain for stable contact interaction in bilateral teleoperation is limited by the ratio between the master and the slave inertia. Classical industrial manipulators are designed to execute position tasks with high accuracy and velocity. Using this type of manipulators as slave devices results in large forces occurring at contact that can easily destabilize the system [8, 11].

Impedance-control has been proposed as a solution for contact task execution in robotics [12]. In this case, impedance, a relationship between force/position, is controlled in the robot manipulator, which allows executing contacts at the expense of position accuracy and speed of motion. The usage of "soft" (low impedance) slave manipulators has been explored for teleoperation and a higher stability in contact situations has been reported both with and without the presence of time-delay in the communication channel [8, 13]. However, even when using external force sensors to implement impedance-control using classical industrial manipulators, performance is still limited by the control bandwidth limitations and the large inertia of these devices [8]. Novel impedance-controlled lightweight manipulators, such as the Kuka Lightweight Robots (LWR) [14] or the NASA Robonaut arms [15] are designed to be able to reliably execute a large range of contact tasks using variable impedance.

The master devices typically used, introduce additional limitations in the absolute levels of force-feedback rendered to the operator and available workspace. Most of the existing commercial devices (e.g. [6, 7]) have small workspaces, with motion ranges in the order of centimetres and typically allow applying forces in magnitudes up to 10 N. When larger forces and workspaces are needed, the master devices tend to increase in size and complexity, becoming more similar to classical industrial manipulators [16, 17]. In both cases the devices show limited capability to render stiff environments to the operator and are often hard or uncomfortable to use by the operator [18]. To address these limitations, exoskeleton master devices, which are portable, lightweight and developed for ideal ergonomic use were developed to allow executing tasks requiring motion and force ranges comparable to that of the human arm [18].

It is expected that replacing classical teleoperation systems (Figure 1.2(a)), in which a

[1] formerly known as Sensable Phantom Omni

small haptic master with a complex user-interface is used to command an industrial slave manipulator, by wearable exoskeleton masters commanding slave impedance-controlled manipulators (Figure 1.2(b)) results in a teleoperation system which allows the human operator to remotely execute a broad range of tasks. Previous research was done using impedance-controlled slave manipulators using external force-torque sensors [19] and impedance-controlled master and slaves [20]. Before the start of this work, to the author's knowledge, no setup has been reported which makes use of state-of-the-art master devices to command modern impedance-controlled manipulators over modern packet-switched communication links with time-delay. The work presented in this thesis focuses on bilateral teleoperation control systems between impedance-type masters commanding impedance-controlled slaves.


(a) Classical teleoperation system with Sensable Phantom device (pictured on the left) used to control an industrial Puma 200 robot (right)

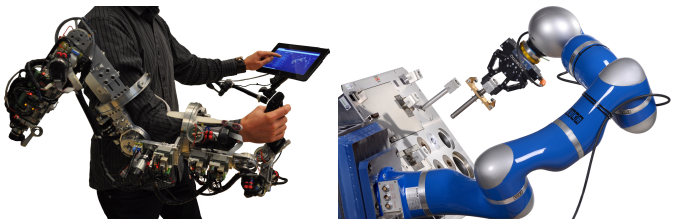

(b) Proposed teleoperation system with exoskeleton device (left) used to command a Kuka Lightweight Robot (LWR) (right)

Figure 1.2: Currently existing and proposed bilateral teleoperation systems

## 1.1 Bilateral teleoperation control

In the scope of control system design for bilateral teleoperation, two aspects play a key role: performance and stability. A system is said to be *stable* if every bounded input results in a bounded output. When considering time-delay bilateral teleoperation, this means that the human operator can interact with the system using the master device without introducing

persistent and increasing involuntary oscillations. In haptic systems, instability not only prevents tasks from being executed but can result in harm to the human operator through the application of large, uncontrolled forces through the master device. A bilateral teleoperation system is said to be *robust* to delay if stability can be ensured for certain bounded values of time-delay in the communication channel.

The *system performance* in bilateral teleoperation is defined by the relation between the impedance rendered to the human operator by the master device and that of the remote environment with which the slave is interacting. Given that the teleoperation system should allow the operator to execute tasks remotely in a way comparable to when these tasks are being executed locally, it is expected that the best task performance will result from giving the operator the same "feeling" as if physically present in the remote environment. Based on this principle, an ideal system is the one which renders precisely the remote environment impedance to the human operator. The relation between system performance and task performance is still an open question in the field and is largely beyond the scope of this thesis. Other performance measurements might take into account the performance and behaviour of the human operator or the type of interactions taking place. As this work concentrates on the design, implementation and evaluation of control systems, the focus is on system performance. Human performance is evaluated in a qualitative, subjective manner.

A large body of literature addressing the design of bilateral teleoperation systems, published over the last 40 years, exists [21]. The review presented in the remaining of this section shows that the performance and stability of teleoperation system composed by impedance-controlled slaves being commanded by impedance-type master has so far not been explicitly considered in literature.

### 1.1.1 Bilateral teleoperation system performance

To evaluate the performance of a bilateral teleoperation system, i.e. the relation between the remote environment impedance and that rendered to the operator, criteria, such as *transparency* [22], "Ideal Response"[23] or *Z-Width* [24] have been defined in literature.

A common way to evaluate the system performance is to establish a ratio between the impedance rendered by the master device to the human operator and that of the remote environment. This relation, defined as *transparency*, was introduced by Lawrence [22]. In the same work, the transparency of the common position-position and position-force architectures was studied and it was shown that, for perfect transparency to be achieved, both the position and forces of the master and the slave have to be transmitted to the opposite side, which corresponds to a 4-channel architecture. The work of Lawrence [22] was later extended by Hashtrudi-Zaad and Salcudean [25] who demonstrated that, having a local force-feedback compensation loop, allows a 3-channel architecture to achieve perfect transparency.

Following a similar approach, Yokokohji and Yoshikawa [23] defined the system "Ideal Responses" for kinaesthetic coupling, which involved both perfect force and position tracking between the master and the slave in contact and free-air.

The Z-Width [24], which represents the range of impedances that an haptic device can render in a stable fashion, has also been used to evaluate the performance of a haptic system. This criteria takes into account the limit situations of free-air and rigid contact over the

entire frequency domain to establish the frequencies that are transmitted to the operator through the master.

The performance of systems composed by impedance- or admittance-type master and slave devices in different combinations has been studied by Hashtrudi-Zaad and Salcudean [26]. So far, no analyses were done using devices which use impedance-controlled slaves with either admitance- or impedance-type master devices.

### 1.1.2 Time-delay teleoperation system stability

Stability is a key issue in all areas of control theory. In bilateral teleoperation, the communication channel between the master and the slave substantially increases the complexity of the system due to the introduction of time-delay, data loss and other signal distortions.

The negative effects of time-delay on the stability and performance of teleoperation systems were reported as early as 1965 by Ferrell [27]. The first strategy that guaranteed stability of teleoperation systems under constant time-delay, proposed by Anderson and Spong [28], was based on passivity and the scattering operator. Modelling the system using the hybrid matrix [29] and applying scattering theory, allowed making the communication system behave as a lossless transmission line. This framework was later extended by Niemeyer and Slotine [30] with the introduction of wave variables, which guaranteed the same communication channel behaviour, but enabled the inclusion of filters and predictors while keeping the system stable due to its passivity guarantees.

Initially, the proposed passivity theory was adequate for stabilizing systems with constant time-delay, however, with the expansion of the Internet in the mid 1990's, communicating information over a packet-switched network became a standard. In this case, communication has a variable time-delay and packet loss or reordering can occur. Using passivity design methods under these conditions, resulted in loss of position tracking between the master and slave and distortion of the force-feedback signal [31]. One simple way of solving these problems while using previously existing control methods, consisted on buffering the data to ensure a constant, worst-case delay [32]. However, this results in additional delay and overhead which is not always desired. To solve these issues, Niemeyer and Slotine [31] proposed sending an additional wave variable integral as a way of keeping the positions of the master and the slave synchronized. Benedetti et al. [33] argued that the existence of wave variable impedance matching elements on both the master and slave side caused the position offsets and proposed an implementation without the master matching element.

While passivity design frameworks can ensure system stability at all time, the implementations are generally limited to position-force architectures which have low transparency both with and without time-delay. The transparency of these systems is further reduced by designing the control to remain passive for any value of communication delay. To address this problem, the time-domain passivity controller, which measures and maintains system passivity in real-time, was proposed by Hannaford and Ryu [34] for haptic interfaces and later extended by Ryu et al. [35] and Artigas et al. [36] for teleoperation in both position-force and position-position architectures. This method, using the position-force architecture, has also been extended for 6-dof teleoperation [37] and the possibilities of using different energy dissipation strategies in multi-dof scenarios were explored by Hertkorn

et al. [38]. Similar approaches, which consist on limiting the energy transmitted by the system to an amount which can be dissipated by the device mechanical damping [39, 40] or limiting the energy transmitted by the communication channel to that injected in the system by the master [41] were also presented for 1-dof teleoperation.

Passivity has been used not only to ensure stability of the system but also as an analysis tool to determine control parameters and delay boundaries for the system. The Llewelyn's criterion for two-port stability was used by Adams and Hannaford [42] to determine conditions for the absolute stability of the system. The analysis was extended by Jazayeri and Tavakoli [43] to enable considering non-passive environments and operators. It was shown by Colgate and Schenkel [44], in the scope of haptic interfaces interacting with virtual environments, that the maximum achievable stiffness depends on the amount of damping present in the system. Methods which do not involve passivity, such as frequency-domain approaches, have also been used in [45] and [46] for system analysis, to derive criteria which ensure closed-loop stable behaviour.

Even though passivity methods have been the most widely presented in literature, other control strategies have been used either to analyse or ensure system stability. $H_\infty$ and $\mu$-synthesis design procedures were used to compute controllers taking into account worst case communication delay [47, 48] and later extended using the small gain theorem to position-position architectures with possible unbounded communication delays [49]. To account for the varying delays, Sano et al. [50] proposed using a gain-scheduling method which adapted the controller values according to the current estimated delay value. Linear-quadratic design methods to determine the parameters of the system have been used by Polat and Scherer [51]. Considering variations that occur in the system, for example in terms of environment, time-delay or master and slave characteristics, some authors have proposed using adaptive control methods [52, 53, 54] and sliding-mode control [55, 56]. Lee and Huang [57] proposed using directly a PD controller and showed its stability up to certain amounts of time-delay. Using these design methods, system stability can be ensured under well defined conditions, however, higher performance when compared with using manually tuned classical controllers has not been demonstrated.

In summary, stability analysis in time-delay bilateral teleoperation has mostly focused on using impedance-type devices used both as master and slave. So far, no analysis has been done to the specific case of impedance-type master devices commanding impedance-controlled slave manipulators. Nonetheless, previous research has shown the advantages of using low impedance slaves, in particular in contact with rigid surfaces. However, the implementation of these systems had been limited to one-dof and the experiments have been done in scenarios without time-delay. In multi-dof, the controlled slave devices had been limited to admittance-type devices for which contact task performance is restricted.

## 1.2 Problem statement

Despite the large body of literature existing on the stability and performance analysis of bilateral teleoperation, currently available teleoperation systems are typically either limited to one degree-of-freedom, which does not allow complex tasks to be executed, or show limitations in terms of stability and performance. So far, no bilateral teleoperation system

has been reported which can provide a level of transparency to the user in multi-dof close to that achieved by one-dof setups using the 4-channel architecture, while being stable when functioning over time-delay and other constraints present in modern packet switched communication channels.

The limitations on existing teleoperation systems can be related to issues in their different components. On the master side, most of the commercially available devices have either small workspaces, which do not allow human-like manipulation tasks to be executed in an intuitive manner, and/or limited force-feedback capabilities due to limitations on the actuators. When larger workspaces or higher forces are needed, these device tend to get heavy and bulky, making them hard for a human operator to interact intuitively with. On the slave side, classical industrial manipulators, which are heavy and do not have the adequate capabilities to execute contact tasks, are used as slave devices [8, 11]. A teleoperator using this type of slave device shows limited transparency since the large forces occurring at contact can easily destabilize the system [9]. Even when using external force sensors to implement impedance-control, performance is limited by the control bandwidth limitations and the large inertia [8].

Recently developed impedance-controlled lightweight manipulators, such as the Kuka Lightweight Robots [14] or the NASA Robonaut arms [15], are able to reliably execute control tasks in a similar fashion to the human arm. Modern master devices, such as exoskeletons [58], have been designed as optimal human-machine interfaces and allow rendering large forces to the operator while still being lightweight and backdrivable. Using this type of master devices to command impedance-controlled slave manipulators should enable the remote execution of human-like tasks using teleoperation. However, as the review in Section 1.1 shows, no theoretical analysis or implementation of such bilateral teleoperation systems exists. In terms of control, the effects of controller parameters, master/slave device characteristics and human operator/environment on both the stability and performance of the system are currently unknown. Furthermore, from the stabilization methods presented in literature, the capability to ensure stability for teleoperation systems with impedance-type masters commanding impedance-controlled slaves in the presence of variable time-delay, data loss and other communication channel constraints, while ensuring as high as possible level of transparency has so far not been shown.

For teleoperation in multi-dof, currently, no hardware and software architectures have been presented that can ensure the level of performance needed for bilateral teleoperation with high transparency. In addition, since the master and slave devices will likely have different kinematic structures, the best position mapping between them needs to be determined. This problem has also not been considered in literature.

The key questions can be summarized as follows:

(1) How do controller parameters, master/slave device and human operator/environment characteristics affect the stability and performance of the bilateral teleoperation system?

(2) How can stability of a teleoperation system be ensured with impedance-masters commanding impedance-controlled slaves with variable time-delay, data loss and other communication channel constraints?

(3) Which hardware/software architectures allow achieving maximum transparency in multi-dof bilateral teleoperation both with and without time-delay?

## 1.3 Goal

It is the main goal of this research to achieve maximum transparency and time-delay robustness in bilateral teleoperation using dissimilar multi-dof master-slave devices, in particular when using impedance-type masters to command impedance-controlled slave manipulators.

This overall goal can be divided into the following sub-goals:

- Understand the influence of human operator, environment, control system parameters and time-delay on the stability and performance of a teleoperation system composed by an impedance-type master device and an impedance-controlled slave.
- Develop a control strategy that ensures system stability, independent of time-delay and other communication constraints, while still providing a maximum level of transparency to the operator.
- Propose a hardware and control architecture, as well as a master/slave position mapping, which allows transparent bilateral teleoperation using kinematically dissimilar multi-dof master-slave devices while being robust to time-delay and other communication channel constraints.

## 1.4 Research scope

To achieve the proposed goals, it important to establish the scope of the work which is under study. The term "teleoperation" is very broad and can refer to any type of remote control of a robot manipulator in terms of force and motion scaling, control methods, existence of time-delay and the type of master and slave devices.

The focus of this work is on tasks which a human operator could manually execute if physically present in the remote environment. This implies that there should be no force scaling and the motion remains within the limits of the human operator arm. Since exoskeleton master devices with human-like workspace are used, this work concentrates on position control of the slave manipulator instead of rate-control methods typical of devices with smaller workspaces. It is also assumed that a high level of transparency should be provided to the operator to enable the execution of the required tasks in teleoperation. Based on these premises, all the research is done considering control architectures which command positions and maximize transparency or have this goal in mind.

Currently, modern communication devices and the Internet allow connections throughout the world with round-trip communication delays in the range of hundreds of milliseconds. This corresponds also to the operational range of the communication channel for real-time data transfer between the International Space Station (ISS) and ground [59], which is about 100 ms. Therefore, in this research, the focus is on short-delay teleoperation scenarios (delay smaller or equal to 250 ms), which are also the ones for which direct bilateral teleoperation is the most usable. Even when stability is ensured, larger time-delays will result in an inevitable degradation of the system and operator performance, which calls for the use of different methods such as shared control [60] or high-level commanding [61] that are beyond the scope of this work.

An unstable bilateral teleoperation system can be dangerous not only to the master and slave systems but also to the remote environment and especially the human operator. Since the communication channels that are used present not only unbounded variable time-delay but also data loss it has to be ensured that the system will remain stable at all time independently of the quality of the communication channel.

## 1.5 Thesis outline

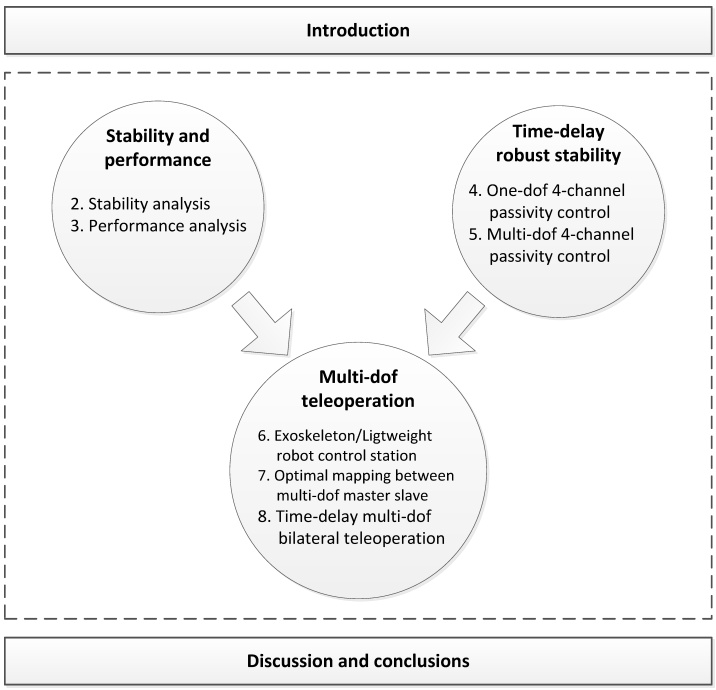


Figure 1.3: Thesis structure schematic representation

Besides this introduction and the final conclusions, this thesis is composed by three parts, each part related to the goals established in Section 1.3 and a total of 8 chapters. All these chapters are a reproduction or adaptation of submitted or published material in peer-reviewed conferences or journals, therefore some redundancy between them might occur. Figure 1.3 shows a schematic representation of the thesis structure.

**Part I** is constituted by two chapters in which the stability and performance of a time-delay bilateral teleoperation system is analysed. In **Chapter 2**, a stability analysis of a teleoperation system composed by an impedance-type master commanding and impedance-controlled slave is presented. The analysis shows how the different controller parameters influence the stability of the system under time-delay. **Chapter 3** presents the performance

analysis of this system, where the transparency in both free-air and contact situations is determined. The analysis highlights the trade-off between stability and transparency of the system.

**Part II** establishes the control methods for stable time-delay bilateral teleoperation. A method for time-delay robustness of a teleoperation system under time-delay is presented in **Chapter 4**. This method is based on an extension to the 4-channel architecture of the time-domain passivity control. In **Chapter 5**, the 4-channel time-domain passivity-control method is extended to a multi-dof 4-channel architecture.

**Part III** presents the multi-dof bilateral teleoperation system using an arm exoskeleton to control a Kuka Lightweight Robot. **Chapter 6** proposes a hardware/software architecture for an end-to-end bilateral teleoperation system with exoskeleton and multi-dof slave manipulator. The results, using the SAM exoskeleton controlling the 7-DOF Kuka Lightweight robot show that a very high level of transparency can be achieved with the proposed system. **Chapter 7** presents a complete bilateral teleoperation system using an exoskeleton commanding a Kuka Lightweight Robot over a mobile WAN network which emulates the space operation scenario. A methodology for optimal mapping between multi-dof master and slave devices is studied in **Chapter 8**. The method is shown to ensure geometrical correspondence between the operator and the slave manipulator while avoiding kinematic problems.

The overall work presented in this thesis, its achievements and limitations, possibilities of future work and the main conclusions are presented in **Chapter 9**.

**Appendix A** presents the SPANviewer, a visualisation tool for robotics, which was developed as part of the work done in this thesis for testing and debugging of different control algorithms, as well as results visualisation.

# Part I

# Stability and performance analysis

CHAPTER 2

# State-space stability analysis of 4-channel bilateral teleoperation under constant time-delay

J. Rebelo and A. Schiele

*IEEE Transactions on Control Systems Technology*, (submitted)

**Abstract**

*Recently developed impedance-controlled robots are better suited than conventional industrial robots for executing human-like contact tasks with various environments. However, performance and stability of a system when using such devices as slaves in time-delay bilateral teleoperation systems is still unknown. It is the goal of this work to research how the different system characteristics affect the stability robustness of a 4-channel time-delay bilateral teleoperation system with an impedance-type master device commanding an impedance-controlled slave. Using a numerical method based on the Lambert W function, exact solutions of the time-delay state-space description of a 1-DOF system are obtained. The theoretical results show that increasing the damping or reducing the stiffness of the master and slave controllers increases the system robustness to time-delay. The results also show that, when a master device with high controller stiffness commands a slave with low stiffness, provides the highest stability margin in rigid contact is provided. Lower stiffness in the master and a higher stiffness in the slave provides higher stability in free-air motion. Experimental validation is done using a one degree-of-freedom setup. The experimental results also show that the Lambert W function analysis allows to determine an accurate stability border for the linear time-delay state-space system.*

## 2.1 Introduction

In a teleoperation system, a human operator interacts with a master device to control a remote slave manipulator. These systems are used when human decision making capabilities are needed for executing tasks in unknown and unstructured remote environments. To improve the human operator task performance, not only visual but also haptic feedback has to be provided [22]. It is assumed that an ideal teleoperation system has perfect transparency, i.e. renders to the operator exactly the same impedance as that of the remote environment [22]. For this purpose, position, velocity and/or force information is exchanged between the master and the slave sites through the communication channel. If the two devices are placed in distant locations, the communication channel introduces delay in the signals transmitted between the master and the slave. Figure 2.1 shows the schematic diagram of a bilateral teleoperation system. This paper focuses on the stability of time-delay bilateral teleoperation control systems.

Many typical teleoperation systems make use of commercially available master devices to control classical industrial manipulators which are designed to execute position tasks with high accuracy and velocity [9]. Using admittance-type of manipulators to execute contact tasks in teleoperation results in large forces, both on the master and slave sides that easily make the system unstable [9]. Using impedance-controlled slave manipulators, which are designed to keep a relationship between force and position at the expense of position tracking accuracy, results in higher stability in contact situations both with and without the presence of time-delay in the communication channel [8, 13].

Despite the experimentally demonstrated advantages of using impedance-controlled slave manipulators in bilateral teleoperation, the effects of different stiffness and damping configurations, as well as environment and operators characteristics, on the stability of these systems in the presence of time-delay has so far not been studied. The stability of time-delay bilateral teleoperation systems is typically analysed using techniques such as passivity [28, 30, 26], frequency response [22] or Lyapunov stability theory [45]. Passivity-based methods, have provided the means to design teleoperation systems which are stable independently of time-delay [30] but the analysis are typically limited to systems represented by two-port networks elements exchanging energies and are based on assumptions of passivity for the operator and environment [62]. When both forces and velocities are transmitted in either direction, such as in the transparency optimized 4-channel architecture, stability analysis is done using a frequency response based method [22]. This allows determining the stability margins of the system, however a complex loop reshaping is required and no information on the exact pole behaviour of the system is obtained.

In other domains of automatic control, Asl *et al.* [63] used the Lambert W function to provide an analytical solution for a scalar delay differential equation and have shown that this allows computing all infinite poles of such systems from a state-space description. In [64], the same authors extended their work to a general matrix case to allow estimating unknown time-delay in processes [65] and to design optimal controllers by pole placement [66, 67]. State-space has been used earlier for non-delayed teleoperation system modelling and design in [68] and [69]. Up to now, no approach has shown the modelling and analysis of a bilateral teleoperation system by state-space analysis considering time-delay.

It is the goal of this work to understand how different system characteristics affect

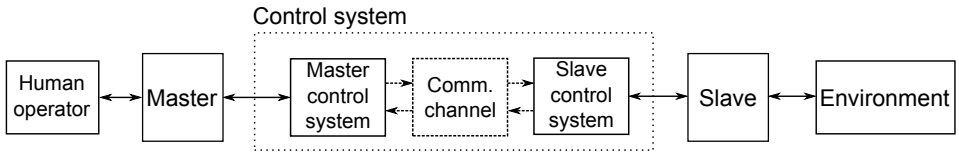


Figure 2.1: Bilateral teleoperation schematic diagram

the stability robustness of a 4-channel time-delay bilateral teleoperation system with an impedance-type master commanding an impedance-controlled slave. The analysis presented in this work is done by applying the Lambert W function to solve the time-delay differential equations of the teleoperation system. The presented results are expected to (1) determine the exact influence of human operator and environment impedances, as well as controller parameters on the system stability, both in free air and in rigid contact; (2) predict and experimentally verify the exact stability boundaries of the system against different amounts of constant time-delay and controller parameter values. Overall, such knowledge should provide guidelines for designing and tuning controllers when such systems are used in bilateral teleoperation.

## 2.2 State-space bilateral control model

For a generic one degree-of-freedom bilateral teleoperation system with impedance type master and slave devices (force input, velocity output), as illustrated in Figure 2.2, the closed-loop differential equations are represented as

$$f_m(t) + f_h = m_m \ddot{x}_m(t) + b_m \dot{x}_m(t) \tag{2.1}$$

$$f_s(t) - f_e(t) = m_s \ddot{x}_s(t) + b_s \dot{x}_s(t) \tag{2.2}$$

where $x$, $m$, $b$ are the position, mass and damping of the devices, respectively. The dot and double dot notation are used to represent the first and second derivatives and the subscripts $m$ and $s$ represent the slave and the master. The forces $f_m$ and $f_s$ are the ones applied by the master and slave and the forces $f_h$ and $f_e$ are the ones applied externally by the human operator and the environment.

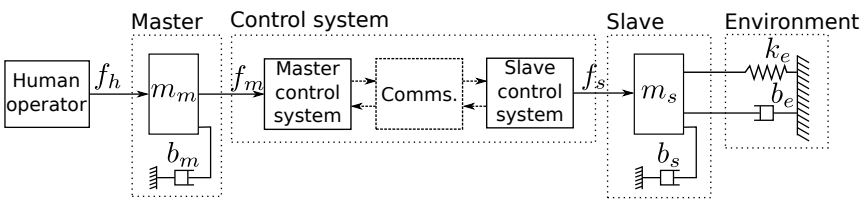


Figure 2.2: Bilateral teleoperation diagram

For an impedance-controlled slave device, the slave force can be computed as

$$f_s(t) = b_s\dot{x}_s(t) - B_s\dot{x}_s(t) + K_s\left(x_{rs}(t) - x_s(t)\right) + f_{\tilde{s}}(t) \tag{2.3}$$

where $B_s$ and $K_s$ are the user-defined damping and stiffness of the system, $x_{rs}$ the slave manipulator reference position and $f_{\tilde{s}}$ the additional commanded force [12].

Assuming that the system interacts only with passive environments which have a spring-damper behaviour, the environment force $f_e$ can be modelled as

$$f_e(t) = -b_e\dot{x}_s(t) - k_e x_s(t) \tag{2.4}$$

where $k_e$ represents the environment stiffness and $b_e$ represents the environment damping. Replacing (2.3) and (2.4) into (2.2) results in an impedance-controlled slave with an equation of motion defined as

$$\begin{aligned} f_s(t) = m_s\ddot{x}_s(t) + B_s\dot{x}_s(t) - K_s\left(x_{rs}(t) - x_s(t)\right) \\ + b_e\dot{x}_s(t) + k_e x_s(t). \end{aligned} \tag{2.5}$$

Independently of the mechanical type of the slave device used, i.e. impedance or admittance, Equation (2.5) is valid whenever active impedance-control is implemented [12].

When interacting with the system, the human operator applies a force to perform the motion while adding its own hand-arm impedance to the dynamics of the master. The force $f_h$ can be represented as

$$f_h(t) = f_{\tilde{h}}(t) + m_h\ddot{x}_m(t) - b_h\dot{x}_m(t) + k_h\left(x_{rh} - x_m\right), \tag{2.6}$$

where $f_{\tilde{h}}$ is the operator extrinsic force, $b_h$ is the damping added to the system by the operator, $k_h$ is the operator stiffness and $x_{rh}$ the operator desired target position. For the remaining of this chapter, the operator mass $m_h$ is considered as part of the master mass $m_m$ and only the latter value is shown.

In this work, the 4-channel control architecture, derived from [22], as shown in Figure 2.3, is used. This architecture is known for providing perfect transparency without time-delay and can be used to represent other common architectures such as position-position or position-force with adequate controller parameter tuning. The velocity channel controllers $C_m$ and $C_s$ are implemented as PD controllers (with the position as input), and the force channel controllers $C_2$ and $C_3$ are implemented as P controllers. The forces applied by the master and slave devices can be computed as

$$f_m(t) = -B_m\dot{x}_m(t) + K_m\left(x_s(t) - x_m(t)\right) + K_2 f_e(t) \tag{2.7}$$

$$f_{\tilde{s}}(t) = K_3 f_h(t) \tag{2.8}$$

$$x_{sr}(t) = x_m(t) \tag{2.9}$$

where $K_i$ and $B_i$ represent the proportional and derivative gains of the controller $i$ with $i = \{m, s, 2, 3\}$. Using this control scheme with time-delay present in the communication channel, the equations of motion for the complete system are

$$\begin{aligned} m_m \ddot{x}_m(t) =& k_h\left(x_{rh}(t) - x_m(t)\right) - b_h \dot{x}_m(t) + \\ &+ K_m\left(x_s(t-T) - x_m(t)\right) - B_m \dot{x}_m(t) \\ &- K_2 f_e(t-T) \end{aligned} \tag{2.10}$$

$$\begin{aligned} m_s \ddot{x}_s(t) =& K_s\left(x_m(t-T) - x_s(t)\right) - B_s \dot{x}_s(t) + \\ &+ K_3 f_h(t-T) \end{aligned} \tag{2.11}$$

where $T$ is the constant time-delay.

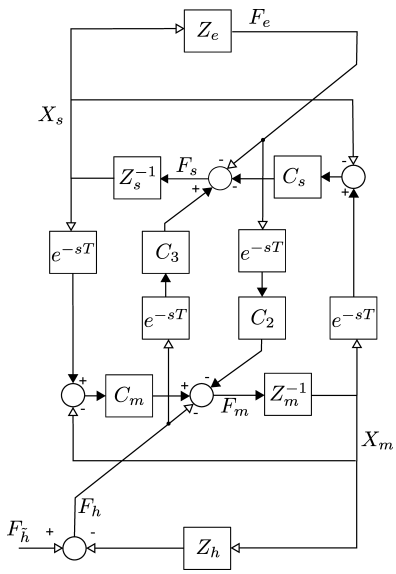


Figure 2.3: 4-channel architecture with impedance-controlled slave device. The hollow arrows represent physical signals and the filled arrows represent controller signals (adapted from [22]).

Replacing $f_h$ and $f_e$ on equations 2.10 and 2.11, the state equation of this delayed system is defined as

$$\begin{aligned} \begin{bmatrix} \dot{x}_m(t) \\ \ddot{x}_m(t) \\ \dot{x}_s(t) \\ \ddot{x}_s(t) \end{bmatrix} =& \mathbf{A} \begin{bmatrix} x_m(t) \\ \dot{x}_m(t) \\ x_s(t) \\ \dot{x}_s(t) \end{bmatrix} + \mathbf{A_d} \begin{bmatrix} x_m(t-T) \\ \dot{x}_m(t-T) \\ x_s(t-T) \\ \dot{x}_s(t-T) \end{bmatrix} \\ &+ \mathbf{B} \begin{bmatrix} f_{\tilde{h}}(t) \\ f_{\tilde{e}}(t) \end{bmatrix} + \mathbf{B}_d \begin{bmatrix} f_{\tilde{h}}(t-T) \\ f_{\tilde{e}}(t-T) \end{bmatrix} \end{aligned} \tag{2.12}$$

where $\mathbf{A}$ is the undelayed state matrix, $\mathbf{A}_d$ is the delayed state matrix, $\mathbf{B}$ is the input matrix and $\mathbf{B}_d$ is the delayed input matrix, with

$$\mathbf{A} = \begin{bmatrix} 0 & 1 & 0 & 0 \\ -\frac{K_m}{m_m} & -\frac{B_m+b_m+b_h}{m_m} & 0 & 0 \\ 0 & 0 & 0 & 1 \\ 0 & 0 & -\frac{K_s+k_e}{m_s} & -\frac{B_s+b_e}{m_s} \end{bmatrix} \tag{2.13}$$

$$\mathbf{A}_d = \begin{bmatrix} 0 & 0 & 0 & 0 \\ 0 & 0 & \frac{K_m-K_2k_e}{m_m} & -\frac{K_2b_e}{m_m} \\ 0 & 0 & 0 & 0 \\ \frac{K_s}{m_s} & 0 & 0 & 0 \end{bmatrix} \tag{2.14}$$

$$\mathbf{B} = \begin{bmatrix} 0 \\ \frac{1}{m_m} \\ 0 \\ 0 \end{bmatrix} \tag{2.15}$$

$$\mathbf{B}_d = \begin{bmatrix} 0 \\ 0 \\ 0 \\ \frac{K_3}{m_s} \end{bmatrix}. \tag{2.16}$$

## 2.3 Delay-differential system solution

Considering the bilateral control system formulated in (2.12), an analytical solution using the Lambert W function can be computed as follows.

The Lambert W function $W_k$ is a complex multivalued function defined as

$$W_k\,(a)\,e^{W_k(a)} = a, \tag{2.17}$$

where $a \in \mathbb{C}$ and $k \in \mathbb{Z}$ is an integer representing the branch of the function [70]. Since (2.17) has infinite solutions, each branch $k$ represents a solution for the equation. Figure 2.4 shows an example of the behaviour of the Lambert W function with real argument for 3 different branches. For details about the calculation of the Lambert W function when $a$ is a square matrix we refer the reader to [64].

As with typical ordinary differential equation systems, the system input does not play a role in the stability [64]. Assuming a candidate solution of the form $\mathbf{x}(t) = e^{\mathbf{S}t}\mathbf{x_0}$, the system is bounded-input bounded-output (BIBO) stable as long as the $\lim_{t\to\infty} e^{\mathbf{S}t} = \mathbf{0}$, which means that all the eigenvalues of the solution matrix $\mathbf{S}$ must have non-positive real parts [71]. The candidate solution can be replaced into (2.12) to yield the characteristic equation

$$\mathbf{S} - \mathbf{A} - \mathbf{A_d}e^{-\mathbf{S}T} = \mathbf{0}. \tag{2.18}$$

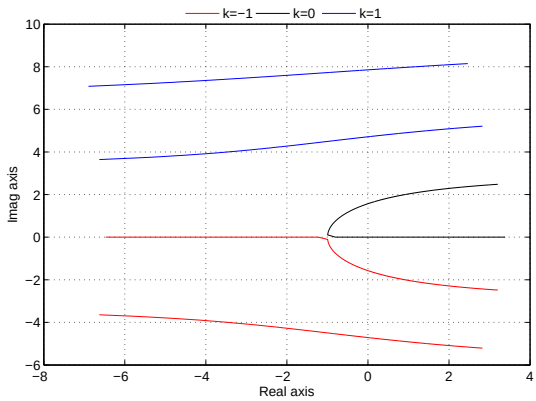


Figure 2.4: Lambert W function $W_k(x)$ range for branches $k = -1, 0, 1$ with $-100 \leq x \leq 100$

If the system is not affected by time-delay, i.e. $T = 0$, then this solution reduces to $\mathbf{S} = \mathbf{A} + \mathbf{A}_d$ which is the solution for standard ordinary differential equations in terms of the matrix exponential. In cases with time-delay, (2.18) can be reformulated as

$$T\,(\mathbf{S} - \mathbf{A})\, e^{\mathbf{S}T} e^{-\mathbf{A}T} = \mathbf{A_d} e^{-\mathbf{A}T} T. \tag{2.19}$$

In general matrix multiplication is not commutative, i.e. $\mathbf{S} \cdot \mathbf{A} \neq \mathbf{A} \cdot \mathbf{S}$ which means that it is not possible to consider $e^{\mathbf{S}T} e^{-\mathbf{A}T} = e^{(\mathbf{S}-\mathbf{A})T}$. To compensate for this inequality an unknown matrix

$$\mathbf{Q} = \begin{bmatrix} q_{11} & q_{12} & q_{13} & q_{14} \\ q_{21} & q_{22} & q_{23} & q_{24} \\ q_{31} & q_{32} & q_{33} & q_{34} \\ q_{41} & q_{42} & q_{43} & q_{44} \end{bmatrix} \tag{2.20}$$

is introduced to allow the matrix exponential product $e^{\mathbf{S}T} e^{-\mathbf{A}T}$ in (2.19) to be combined such that

$$T\,(\mathbf{S} - \mathbf{A})\, e^{T(\mathbf{S}-\mathbf{A})} = \mathbf{A_d} \mathbf{Q} T. \tag{2.21}$$

Applying the Lambert W function and solving for $\mathbf{S}$ gives

$$\mathbf{S_k} = \frac{1}{T} \mathbf{W}_k (\mathbf{A_d} \mathbf{Q} T) + \mathbf{A}. \tag{2.22}$$

Since the matrix $\mathbf{Q}$ is unknown it is not possible to determine the solution matrix from (2.22), however substituting $\mathbf{S_k}$ in (2.19) results in

$$\mathbf{W}_k(\mathbf{A_d}\mathbf{Q}T)e^{\mathbf{W}_k(\mathbf{A_d}\mathbf{Q}T)+AT} = \mathbf{A_d}T. \tag{2.23}$$

Equation (2.23) can be used to numerically evaluate the value of matrix $\mathbf{Q}$ (e.g. using Matlab *fsolve*). Conditions for the existence of this matrix have not been mathematically proven. Nonetheless, during our analysis, it was always possible to find a value for $\mathbf{Q}_k$. The same behaviour was reported by Yi *et al.* (see e.g. [64, 72, 65]).

Using this method it is possible to compute all the infinite solutions of the system, corresponding to each branch $k$. To determine the stability of the system, the rightmost poles have to be known. For the scalar case it was proven in [73] that these poles are always given by the branches $k = 0$ or $k = -1$. Such a proof does not exist for the matrix case, however the same behaviour was reported by other researchers, therefore Conjecture 1, formulated in [64], is reintroduced here:

**Conjecture 1** *The system rightmost poles are given by the solution* (2.22)–(2.23) *with* $k = 0$ *or* $k = -1$*, i.e.* $\mathbf{S}_0$ *or* $\mathbf{S}_{-1}$.

From the proposed solutions and conjecture it is possible to determine the stability of the 4-channel time-delay bilateral teleoperation system.

## 2.4 Bilateral teleoperation system stability analysis

In this section, a hardware setup is identified and its physical parameters are used to model the delayed system for which the stability boundaries are theoretically analysed and then experimentally verified.

### 2.4.1 Experimental setup hardware and model

The experimental setup used for this analysis is composed by two identical one degree-of-freedom haptic devices. Each device consists of a Maxon brushless DC motor, gearing stage (planetary gear + capstan) and output handle. The motor is equipped with a 1024 pulses per turn encoder for position measurement and a strain-gage based force-torque sensor is mounted on the output handle. Both units are controlled by the same PC104 computer running Xenomai real-time operating system at a rate of 1kHz. The constant time delay is simulated using delay buffers for the transmission between each side. The complete setup is shown in Figure 2.5.

The system state-space model is constructed based on an experimental identification of the mass and damping characteristics of the master and slave devices independently. These characteristics can be used directly on the model presented in Section 2.2. The identification is done by applying a random sinusoidal excitation by hand, and measuring the force input signal using the torque sensor and the resulting speed response of the system using the encoder.

The system parameters obtained using the frequency-domain identification [74] are $m_m = 8.4 \cdot 10^{-3}\,\mathrm{kg} \cdot \mathrm{m}^2$, $b_m = 7.38 \cdot 10^{-2}\,\mathrm{Nm} \cdot \mathrm{rad} \cdot \mathrm{s}^{-1}$, $m_s = 8.7 \cdot 10^{-3}\,\mathrm{kg} \cdot \mathrm{m}^2$ and $b_s = 1.0 \cdot 10^{-1}\,\mathrm{Nm} \cdot \mathrm{rad} \cdot \mathrm{s}^{-1}$.

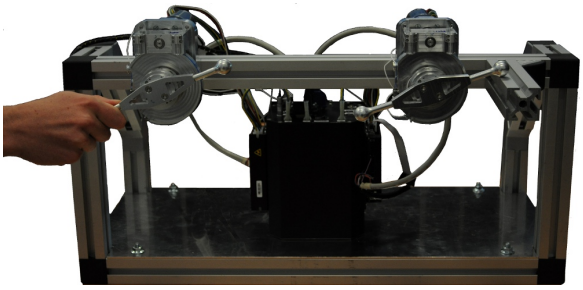

Figure 2.5: Experimental setup (master unit on the left and slave unit on the right)

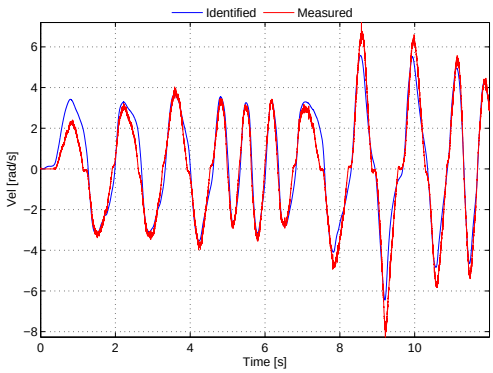


Figure 2.6: Comparison between the measured and the identified system response for the master device. The input signal used in this test is different from the one used to identify the system.

Figure 2.6 shows a comparison between the measured and the identified response. The illustrated system has a Variance Accounted For (VAF) [74] of approximately 0.94 using an independent data-set than the one used for the system identification.

### 2.4.2 Theoretical stability analysis

Using the system model (2.12) and the mechanical system parameters identified in the previous subsection, the effects of controller parameters, human impedance and time-delay on the system root locus can be studied. For all the experiments the controllers are dimensioned such that the motion and forces are not scaled, which implies $K_2 = K_3 = 1$. The analysis is done for time-delay values ranging from 0 to 100 ms or until the poles are placed on the right half-plane, meaning that the system has become unstable. The analysis was repeated with different initial conditions for $\mathbf{Q}$ and always resulted in the same pole configurations.

### *Solution branches analysis*

Since the stability of the system is studied based on Conjecture 1 for which, to the authors' knowledge, the only empirical data is given by [64], the behaviour of branches -3 to 3 of the system is analysed. The analysis is done for free-air motion, i.e. $k_e = b_e = 0$ and considering a human operator with $k_h = 1$ and $b_h = 0.02$. The controller parameters are set to $K_m = K_s = 10$ and $B_m = B_s = 0.1$ with the time-delay varying from 1 to 16 ms. Using Matlab's *fsolve*, equation (2.23) can be numerically computed to a precision of $10^{-28}$ with the characteristic equation (2.18) having a residual in the order of $10^{-12}$ for all the branches. Figure 2.7 shows the root-locus depending on time-delay for all the poles computed in these branches.

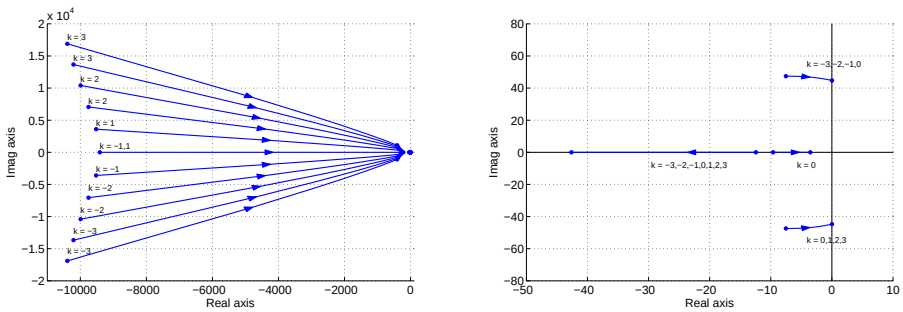


(a) Poles on the entire real-imaginary plane

(b) Detail of the poles around the origin

Figure 2.7: Root-locus in free-air motion ($k_e = b_e = 0$) for branches $k = \{-3, -2, -1, 0, 1, 2, 3\}$ with $K_m = K_s = 10$, $B_m = B_s = 0.1$, $k_h = 1$, $b_h = 0.02$ and time-delay $1 \leq T \leq 16$ ms. In all plots the arrows indicate direction of increasing time-delay. In this case T increases from 1 to 16 ms.

Figure 2.7(a) shows that, for the 7 branches analysed, there are 11 poles which have real values around $-11000$ for $T = 1$ ms which increase to around $-300$ for $T = 16$ ms. The results suggests that the negative branches give the poles on or below the real axis and the respective complex conjugate appears on the positive branch.

From Figure 2.7(b), which gives the detail of the poles around the origin, it is visible that none other than branch 0 covers all the poles close to the origin, which also cross the imaginary axis. Thus, analysing this branch is enough to get an accurate approximation of the system behaviour, since the remaining poles are considerably less significant. The pole pair which has a real value of -7 at $T = 1$ ms and a real value just above 0 at $T = 16$ ms is the one causing the system instability. A similar pole placement behaviour was observed in all the analyses, therefore, for the remaining of the paper, only the rightmost pole pair from branch 0 which crosses the imaginary axis is presented, for clarity of the results.

### *Human operator dynamics influence*

To study the effects of the human operator impedance on the system an analysis is performed considering an operator with three different grips of increasing stiffness, modelled

as $k_h = 0$, $k_h = 1$ and $k_h = 5$ and a constant damping $b_h = 0.02$. In both cases the controller values are kept constant with $K_m = K_s = 10$ and $B_m = B_s = 0.1$. In Figure 2.8 it can be observed that for the stiffer operator grip the system is stable for time-delays up to 27 ms whereas with the softer grip and without operator influence this boundary decreases to 16 ms and 15 ms, respectively.

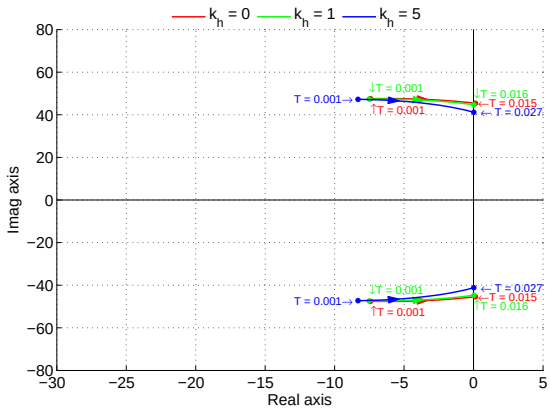


Figure 2.8: Rightmost root-locus depending on time-delay for different human stiffness values in free-air motion ($k_e = b_e = 0$) with $K_m = K_s = 10$, $B_m = B_s = 0.1$ and constant human operator damping $b_h = 0.02$.

### *Control parameters influence in free-air*

The effects of controller parameters when the system moves in free-air ($k_e = b_e = 0$) can be studied by varying $K_m$, $K_s$, $B_m$ and $B_s$ while keeping all the other parameters constant. Figure 2.9(a) shows the root-locus of the rightmost pole pair for four stiffness gain combinations $K_m = K_s = 10$, $K_m = 2\ K_s = 10$, $K_m = 10\ K_s = 2$ and $K_m = K_s = 5$ with fixed $B_m = B_s = 0.1$ in all cases. Figure 2.9(b) shows the root-locus of the rightmost pole pair for $B_m = B_s = 0.1$, $B_m = B_s = 0.3$ and $B_m = -b_m$, $B_s = 0$ with fixed $K_m = K_s = 10$ in all cases. The setting with $B_m = -b_m$, $B_s = 0$ corresponds to the transparency optimized configuration proposed in [22]. For this analysis, the human operator influence is disregarded by choosing $k_h = b_h = 0$.

Figure 2.9(a) shows that for $K_m = K_s = 10$ the system is stable with time-delay up to 15 m whereas for $K_m = K_s = 5$ the poles are placed in the unstable region at $T = 32$ ms. When a high stiffness is kept in the master and a soft slave is controlled, i.e. $K_m = 10$ and $K_s = 2$, the system remains stable up to $T = 85$ ms. For a stiff slave and a soft master, corresponding to $K_m = 2$ and $K_s = 10$, the system is stable up to the delay limit of 100 ms. Figure 2.9(b) shows that, for the system with $B_m = B_s = 0.1$, stability is kept up to 15 ms and increasing the damping to $B_m = B_s = 0.2$ allows the system to be operated in a stable manner for time-delay up to 31 ms. Using the transparency optimized tuning the system poles are placed on the imaginary axis when no time-delay is present in the system and any amount of time-delay is shown to cause instability.

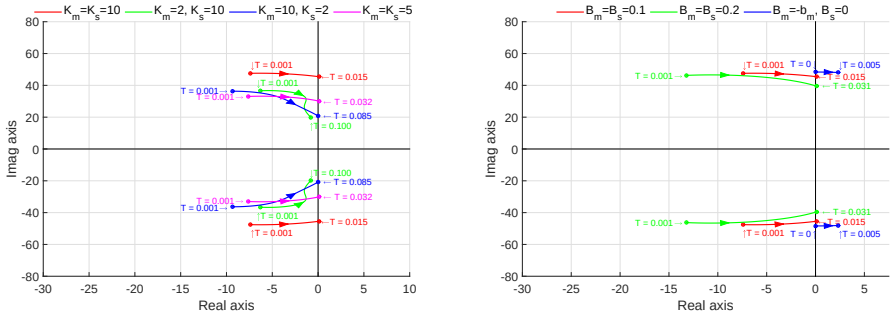


(a) $K_m$ and $K_s$ variable, $B_m = B_s = 0.1$

(b) $B_m$ and $B_s$ variable, $K_m = K_s = 10$

Figure 2.9: Rightmost root-locus depending on time-delay for different proportional and integral controller gain values in free-air motion and no operator influence ($k_h = b_h = 0$)

### *Control parameters influence in rigid contact*

To analyse the system behaviour when the slave is in permanent contact with the environment, an analysis is done considering a rigid environment with a stiffness $k_e = 250\,\mathrm{Nm} \cdot \mathrm{rad}^{-1}$ and a damping of $b_e = 0.5\,\mathrm{Nm} \cdot \mathrm{s} \cdot \mathrm{rad}^{-1}$. The effects of the control parameters on the system stability are once more studied by varying $K_m$, $K_s$, $B_m$ and $B_s$ controller parameters. The effects of the human operator are again disregarded by defining $k_h = b_h = 0$ which, also in this situation, corresponds to the worst case scenario. The rightmost root-locus of the system in these conditions is shown in Figure 2.10.

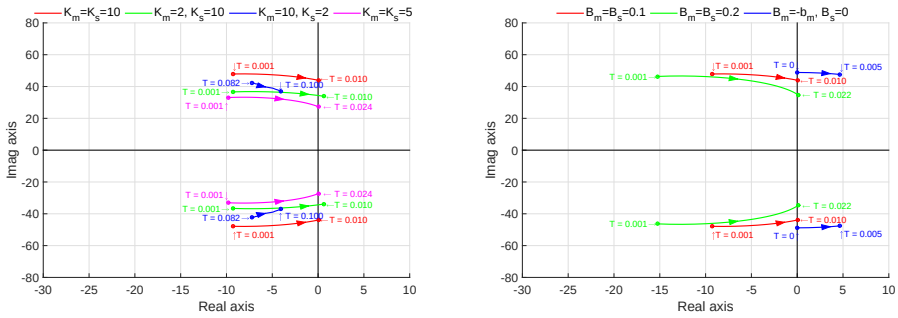


(a) $K_m$ and $K_s$ variable, $B_m = B_s = 0.1$

(b) $B_m$ and $B_s$ variable, $K_m = K_s = 10$

Figure 2.10: Rightmost root-locus depending on time-delay for different proportional and integral controller gain values in rigid contact ($k_e = 250\,\mathrm{Nm} \cdot \mathrm{rad}^{-1}$ and $b_e = 0.5\,\mathrm{Nm} \cdot \mathrm{s} \cdot \mathrm{rad}^{-1}$) without operator influence ($k_h = b_h = 0$)

From Figure 2.10(a) it can be seen that for both $K_m = K_s = 10$ and $K_m = 2$, $K_s = 10$ the system is stable for time-delay values below 10 ms. For $K_m = K_s = 2$ the system remains stable up to $T = 24$ ms and for $K_m = 10$, $K_s = 2$ the system is still stable with

communication delay values of 100 ms. For the last scenario, different discontinuous pole pairs appear for branch 0 depending on time-delay, therefore only the rightmost pole is plotted from the first time-delay value in which it is observed up to the analysis limit, corresponding to $82 \leq T \leq 100$ ms. Figure 2.10(b) shows a similar behaviour to that observed in free-air motion with the system being stable up to $T = 10$ ms and $T = 22$ ms for $B_m = B_s = 0.1$ and $B_m = B_s = 0.2$, respectively. Once more, the transparency optimized configuration is only stable for no delay with instabilities appearing for any value of time-delay in the communication channel.

### 2.4.3 Experimental stability analysis

In this section an experimental validation of the theoretical analysis using the real hardware is presented. The validation is done both for free-air and rigid contact scenarios.

#### *Free-air motion validation*

To validate the theoretical free-air stability boundaries using the real hardware, multiple boundaries are computed for $K_m = K_s$ ranging from 5 to 20 with increments of 2.5 keeping constant $B_m = B_s = 0.1$ and for $B_m = B_s$ with increments of 0.05 ranging from 0.1 to 0.3 with constant $K_m = K_s = 10$. An operator attempts to make the system unstable for different values of controller gains under a series of increasing time-delay and the experimental stability margin is compared with the theoretical value for identical controller settings. In this test, instability is defined as the appearance of increasing unbounded oscillations that continue even without further operator input. An example of this behaviour is shown in Figure 2.11 where oscillations appear after some operator action, as visible in both the master and slave position after 1 s. The time-delay was increased in steps of 1 ms starting from zero. The operator influence in the theoretical analysis was set to $b_h = k_h = 0$, therefore the operator is instructed to keep a soft grip on the handle to introduce minimum non-modelled damping in the system. The real and theoretical stability boundaries are shown in Figure 2.12.

These results show that the difference between the theoretical and experimental time-delay to instability is $9 \pm 1.5$ ms. The results variation of 1.5 ms corresponds to the sample rate of the system, which is the minimum time-delay step difference. As predicted by the theoretical analysis it is shown that higher values of damping correspond to stability for longer time-delays and higher controller stiffness values correspond to a decrease in tolerance to time-delay.

#### *Rigid contact validation*

The theoretical analysis shows that, in rigid contact, the system becomes unstable if a high controller stiffness is configured on both the master and slave, whereas, for the same time-delay, using a master with higher stiffness to control a softer slave allows contacts to be stably rendered. To validate this fact, two tests in which the operator is instructed to use the master to command the slave to contact a rigid environment are performed with a communication delay of 8 ms. In the first test both the master and slave are kept with stiffness settings $K_m = K_s = 10$ and $B_m = B_s = 0.1$. For the second test the slave

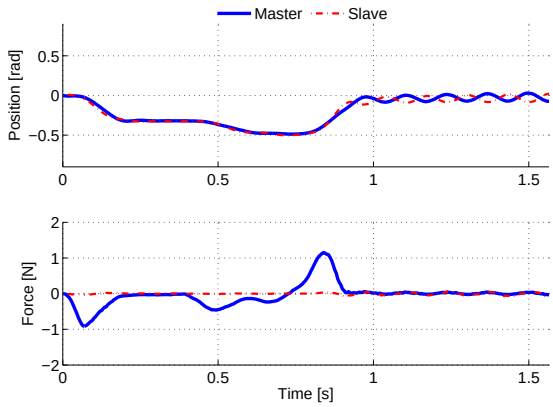


Figure 2.11: Example of unstable system position and force behaviour in free-air motion with $K_m = K_s = 10$, $B_m = B_s = 0.1$ and $T = 10\,\text{ms}$. The instability situation is visible after $t = 1\,\text{s}$.

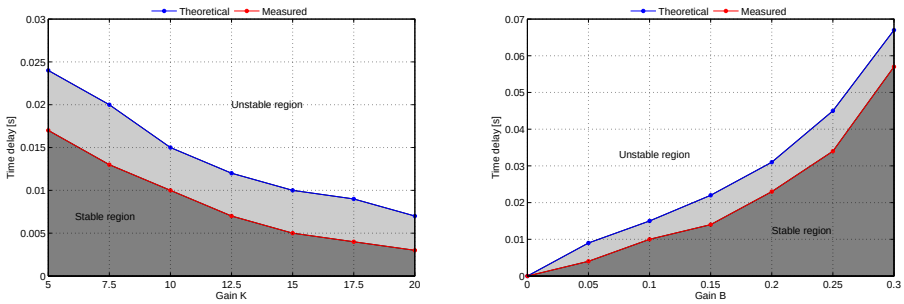


(a) $K_m = K_s$ variable, $B_m = B_s = 0.1$

(b) $B_m = B_s$ variable, $K_m = K_s = 10$

Figure 2.12: Real and theoretical stability boundaries for different controller stiffness and damping gains and time-delay in free-air motion. The points marked with a circle are the ones for which the experiment was performed.

stiffness is set to $K_s = 2$ while the master stiffness and the damping of both controllers is left unchanged.

From the system response, shown in Figure 2.13, it can be verified that the system remains stable when a the slave stiffness is configured to $K_s = 2$ with the forces on the slave side being accurately rendered to the operator. With $K_m = K_s = 10$ the operator is not able to exert forces on the environement, with unvoluntary oscillations being visible after $t = 4\,\text{s}$.

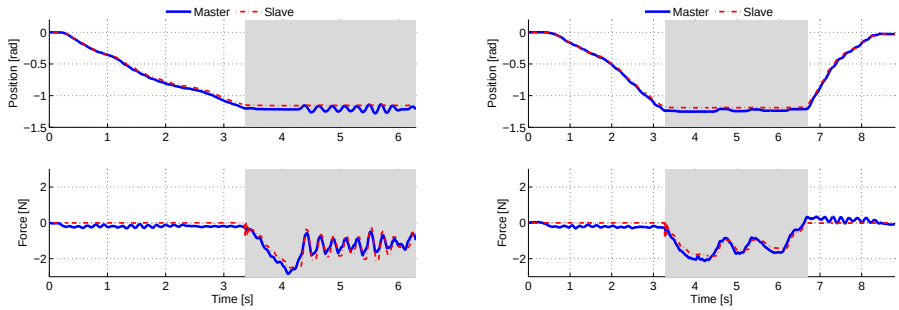


(a) $K_m = K_s = 10$, $B_m = B_s = 0.1$ and $T = 8$ ms. In this case, oscillations are clearly visible during contact with the environment.

(b) $K_m = 10$, $K_s = 2$, $B_m = B_s = 0.1$ and $T = 8$ ms. In this case the operator can exert forces on the remote environment without oscillations being present during contact.

Figure 2.13: Example response of interaction with rigid environment with different configurations which result in unstable (a) and stable (b) contacts.

## 2.5 Discussion

The results in Figures 2.9 and 2.12 show that, as in other control architectures, a higher controller damping results in a larger stability margin of the system (Figure 2.9a) and that higher controller stiffness on both the master and the slave results in less tolerance to time-delay (Figure 2.9b)[30]. The values that result in a higher stability margin are also expected to reduce the system transparency [22], thus the typical stability/transparency trade-off [22] is also visible in this analysis.

When having an impedance-type master commanding and impedance-controlled slave, the results in Figure 2.9 show that in free-air the highest stability margin is achieved when a low stiffness is configured on the master device and a high stiffness is configured on the slave. In contact with the environment, the analysis shows that reducing only the stiffness of the master doesn't contribute to increasing the stability margin of the system. Having a master with high controller stiffness commanding a slave with low stiffness provides the higher level of stability in rigid contact.

When considering the human operator influence on the system, despite its active behaviour, higher stability margins are observed due to the inclusion of the arm-hand mass and damping on the master dynamics. Similar behaviour was previously demonstrated by Hogan [75] using passivity, that, even though the human arm has an active behaviour, its impedance is passive and therefore its presence contributes to the overall stability of the system, which is confirmed by the pole-placement in Figure 2.8.

One situation that has not been analysed directly in this paper is the transition between free-air and rigid contact. Naturally, in this transition, all the high frequency modes of the system are excited, it is therefore possible that unstable situations could be triggered by the contact which are not present when only the operator interacts with the system. However, if there are no positive real poles in free-air, no unstable modes exist and the system will remain stable at all times. This doesn't mean that the "hammering" effect, in

which contact with the remote environment is achieved and removed, can't occur, but this is largely influenced by the operator input and dynamics.

The analysis is also done for constant time-delays, however, the results show that the poles of the system always move to the right with the increase of time-delay. This means that, in real situations, in which time-delay is variable and unknown, the analysis can provide a maximum limit for the delay. This boundary is often easier to determine and can be even used to, for example, buffer the messages to ensure constant delay (see e.g. [76]) and thus, stability with exactly known margin.

The experimental validation shows that the Lambert W solution can be used to determine the stability boundaries of the system based on all physical and controller parameters. Since various factors such as quantization, sampling time and friction are not modelled it is natural that some differences between theoretical and experimental results occur. Nonetheless, it is possible to observe that a constant error margin is obtained on the results in Figure 2.12.

The stability analysis is based on a numerical method, which means that the actual results are only valid for the system for which the analysis was performed. Nonetheless, the guidelines obtained in the analysis have been empirically verified in other systems and the general results hold both in one-dof and multi-dof cases. While similar results could possibly be achieved using frequency-domain techniques, these require a complex loop reshaping [22] and do not give other information than the system stability boundary. It is expected that in the future, the poles of the system can be directly related to the performance and that controllers can be designed by pole-placement or other state-space control methods. The effects of transparency on human operator task performance are an open question in the field, which remains to be studied.

## 2.6 Conclusion

The analysis presented in this paper shows that by tuning of master and slave controller parameters the 4-channel bilateral teleoperation system can be made stable for well defined amounts of time-delay. In particular, having a master device with higher controller stiffness commanding a slave with low stiffness, provides the highest stability margin in rigid contact. Configuring a low stiffness in the master and a high stiffness in the slave provides a higher stability margin in free-air motion. Increasing the controllers damping values increases increases the system robustness to time-delay in all situations.

The analysis also confirms that the human operator makes the system more stable, whereas contact with rigid environment represents the worst case-scenario regarding stability. With increasing time-delays, the system poles are placed closer to the right-half plane, which means that, once a stability boundary is determined, the system should remain stable for any time-delay value below the boundary.

The validation of the results using the experimental setup also shows that the Lambert W function provides a rather precise stability border for the bilateral teleoperation system modelled using a system of delay differential equations.

CHAPTER 3

# Performance analysis of 4-channel bilateral teleoperation under constant time-delay

J. Rebelo and A. Schiele

$17^{th}$ *International Conference on Advanced Robotics*, (accepted)

**Abstract**

*Recently developed impedance-controlled robots are better suited than conventional industrial robots for executing human-like contact tasks. However, performance of a system when using such device as a slave in time-delay bilateral teleoperation is still unknown. It is the goal of this paper to analyse the performance of a 4-channel time-delay bilateral teleoperation system with an impedance-type master device commanding an impedance-controlled slave. Using the newly introduced reflected damping in free-air criterion, it is shown that the damping felt by the human operator interacting with the system while the slave is in free-air is dependent on the local controller parameters and increases linearly with the time-delay with a factor dependent on the master and slave proportional controller gains. The transparency analysis of the system shows that, when using the transparency optimized tuning rule, a stiffness equal to that of the environment is transmitted to the operator, independently of the time-delay or controller parameters. The experimental validation, using a 1-dof master-slave teleoperation system, shows that the proposed criterion can approximate the identified damping with an accuracy of* 5% *for time-delay values up to* 30 *ms. It is also highlighted by the experimental results that, in the transition between free-air and rigid contact, the impedance rendered to the operator is lower than that of the actual environment.*

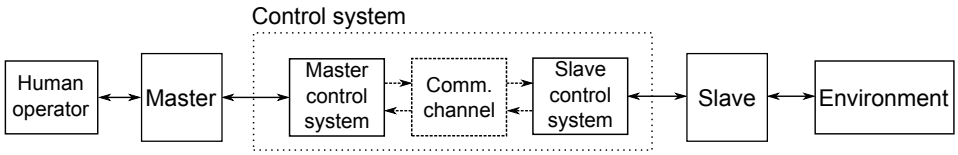


Figure 3.1: Bilateral teleoperation schematic diagram

## 3.1 Introduction

Teleoperation systems are used when human decision making capabilities are needed for executing tasks using robot manipulators in unknown and unstructured remote environments. In these cases, a human operator interacts with a master device to control a remote slave manipulator and receives feedback from the remote location. To improve the human operator task performance, not only visual but also haptic feedback has to be provided [22]. For this purpose, position, velocity and/or force information is exchanged between the master and the slave sites through the communication channel. If the two devices are placed in distant locations, the communication channel introduces delay in the signals transmitted between the master and the slave. Figure 3.1 shows the schematic diagram of a bilateral teleoperation system. This paper focuses on the performance of time-delay bilateral teleoperation control systems.

The system performance of a bilateral teleoperation system is typically assessed by a comparison of how the environment impedance relates to the impedance rendered to the operator by the master, which is defined as the system transparency [22]. In [23] the Ideal Response Conditions for a bilateral teleoperation system have been presented, which considers not only transparency but also perfect tracking in free-air motion. The 4-channel control architecture [22] has been proposed to achieve perfect transparency without time-delay. The transparency of a system with time-delay is present has been analysed in [77]. Other criteria used to evaluate the performance of a haptic system are the Z-Width [24], which represents the range of impedances that an haptic device can render in a stable fashion or the extended transparency [78] which proposed including operator perception characteristic to identify the performance of the system. The performance of a system composed of impedance- or admittance-type master and slave devices in different combinations has been studied in [26].

Typical teleoperation systems make use of commercially available master devices to control classical industrial manipulators which are designed to execute position tasks with high accuracy and velocity [9]. Using this type of manipulators to execute contact tasks in teleoperation results in large forces, both on the master and slave sides that easily make the system unstable [9]. Using impedance-controlled slave manipulators, which are designed to keep a relationship between force and position at the expense of position tracking accuracy, results in higher stability in contact situations both with and without the presence of time-delay in the communication channel [8, 13], however no performance analysis has been done so far which considers an impedance-type master device commanding impedance-controlled slave manipulators.

It is the goal of this paper to evaluate the performance of a 4-channel time-delay bilateral

teleoperation system with an impedance-type master device commanding an impedance-controlled slave under the presence of constant time-delay. The 4-channel architecture allows all common bilateral teleoperation architectures to be evaluated by adequate parameter tuning. The contact performance of the system is evaluated by computing the transparency depending on control parameters and time-delay. While contact situations are important for task execution, in bilateral teleoperation scenarios a significant amount of time is spent in free-air motion. The behaviour of the position-position architecture in free-air has been defined as "mushy" whereas the ideal 4-channel architecture has little or no damping [22]. To evaluate performance in free-air motion, the reflected damping in free-air criterion is introduced and its value is computed depending on system characteristics, controller parameters and time-delay.

## 3.2 4-channel bilateral teleoperation

For a one degree-of-freedom bilateral teleoperation system with impedance type master and slave devices (force input, velocity output) the closed-loop differential equations are represented as

$$f_m(t) + f_h = m_m \ddot{x}_m(t) + b_m \dot{x}_m(t) \tag{3.1}$$

$$f_s(t) - f_e(t) = m_s \ddot{x}_s(t) + b_s \dot{x}_s(t) \tag{3.2}$$

where $x$, $m$, $b$ are the position, mass and friction of the devices, respectively. The dot and double dot notation are used to represent the first and second derivatives and the subscripts $m$ and $s$ represent the slave and the master. The forces $f_m$ and $f_s$ are the ones applied by the master and slave and the forces $f_h$ and $f_e$ are the ones applied externally by the human operator and the environment.

For an impedance-controlled slave device [12], the slave force can be computed as

$$\begin{aligned} f_s(t) = b_s \dot{x}_s(t) - B_s \dot{x}_s(t) + K_s \left(x_{rs}(t) - x_s(t)\right) \\ + f_{\bar{s}}(t) \end{aligned} \tag{3.3}$$

where $B_s$ and $K_s$ are the user-defined damping and stiffness of the system, $x_{rs}$ the slave manipulator reference position and $f_{\bar{s}}$ the additional commanded force.

Assuming that the system interacts only with passive environments which have a spring-damper behaviour, the environment force $f_e$ can be modelled as

$$f_e(t) = -b_e \dot{x}_s(t) - k_e x_s(t) \tag{3.4}$$

where $k_e$ represents the environment stiffness and $b_e$ represents the environment damping. Replacing (3.3) and (3.4) into (3.2) results in an impedance-controlled slave with an equation of motion defined as

$$\begin{aligned} f_{\bar{s}}(t) =& m_s \ddot{x}_s(t) + B_s \dot{x}_s(t) \\ & - K_s \left(x_{rs}(t) - x_s(t)\right) + b_e \dot{x}_s(t) + k_e x_s(t). \end{aligned} \tag{3.5}$$

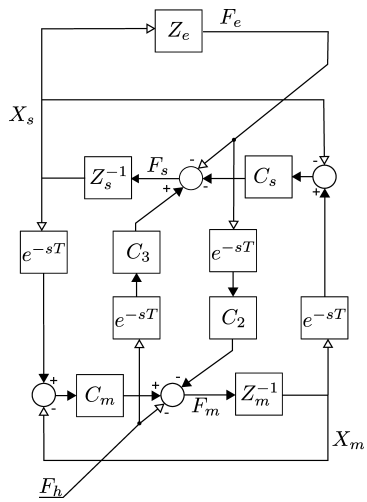


Figure 3.2: 4-channel architecture with impedance-controlled slave device. The human operator input is regarded as an external force. The hollow arrows represent physical signals and the filled arrows represent controller signals (adapted from [22]).

Independently of the mechanical type of the slave device used, i.e. impedance or admittance, Equation (3.5) is valid whenever active impedance-control is implemented [12].

In this work, the 4-channel control architecture, derived from [22], as shown in Figure 3.2, is used. This architecture is known for providing perfect transparency without time-delay and can be used to represent other common architectures such as position-position or position-force with adequate controller parameter tuning. The velocity channel controllers $C_m$ and $C_s$ are implemented as PD controllers (with the position as input), and the force channel controllers $C_2$ and $C_3$ are implemented as P controllers. The forces applied by the master and slave devices can be computed as

$$f_m(t) = -B_m \dot{x}_m(t) + K_m\left(x_s(t) - x_m(t)\right) + K_2 f_e(t) \tag{3.6}$$

$$f_{\tilde{s}}(t) = K_3 f_h(t) \tag{3.7}$$

$$x_{sr}(t) = x_m(t) \tag{3.8}$$

where $K_i$ and $B_i$ represent the proportional and derivative gains of the controller $i$ with $i = \{m, s, 2, 3\}$. In this case the human operator interaction with the system is considered an extrinsic force. The complete equations of motion of the system can be defined as

$$
\begin{aligned}
m_m \ddot{x}_m(t) + b_m \dot{x}_m(t) = \\
& - B_m \dot{x}_m(t) + K_m \left(x_s(t-T) - x_m(t)\right) \\
& - K_2 b_e \dot{x}_s(t-T) - K_2 k_e x_s(t-T) + f_h(t)
\end{aligned} \tag{3.9}
$$

$$
\begin{aligned}
m_s \ddot{x}_s(t) = \\
& - B_s \dot{x}_s(t) + K_s \left(x_m(t-T) - x_s(t)\right) \\
& - b_e \dot{x}_s(t) - k_e x_s(t)
\end{aligned} \tag{3.10}
$$

## 3.3 System performance

The performance of the teleoperation system can be evaluated by its transparency, i.e. the ratio between the real remote environment impedance and the impedance felt by the operator. However, in free-air, since the slave is not in contact with the environment, most of the forces felt by the human operator are created by damping. To evaluate this damping, the reflected damping in free-air criterion is introduced. Both criteria are computed from the frequency response of the system, therefore, all the equations in this section are in the Laplace domain, with $s$ being the Laplace argument. All the system variables presented in Section 3.2 have a upper case letter equivalent, representing the Laplace transform (e.g. $\mathcal{L}\{v_m(t)\} = V_m(s)$).

### 3.3.1 Transparency in contact

The impedance transmitted to the human operator when interacting with the master device can be computed as $V_m(s)/F_h(s)$. The Laplace transform of (3.9) and (3.10) is computed as

$$
\begin{aligned}
m_m s V_m(s) + b_m V_m(s) = \\
& - B_m V_m(s) - \frac{1}{s} K_m V_m(s) + \frac{1}{s} K_m V_s(s) e^{-sT} \\
& - K_2 b_e V_s(s) e^{-sT} - \frac{1}{s} K_2 k_e V_s(s) e^{-sT} + F_h(s)
\end{aligned} \tag{3.11}
$$

$$
\begin{aligned}
m_s s V_s(s) = & - B_s V_s(s) - \frac{1}{s} K_s V_s(s) \\
& + \frac{1}{s} K_s V_m(s) e^{-sT} + K_3 F_h(s) e^{-sT} \\
& - b_e V_s(s) - \frac{1}{s} k_e V_s(s).
\end{aligned} \tag{3.12}
$$

where $V_m(s)$, $V_s(s)$ and $F_h(s)$ are the Laplace transform of $\dot{x}_m(t)$, $\dot{x}_s(t)$ and $f_h(t)$, respectively.

From (3.11) and (3.12),

$$V_s(s) = \frac{K_s e^{-sT} V_m + sK_3 e^{-sT} F_h}{m_s s^2 + (B_s + b_e)\, s + (K_s + k_e)} \tag{3.13}$$

is derived, which allows the teleoperator impedance to be computed as

$$Y_t(s) = \frac{V_m(s)}{F_h(s)} = \frac{N_1(s)}{D_1(s)} \tag{3.14}$$

$$\begin{aligned} N_1(s) =& s(m_s s^2 + (B_s + b_e)\, s + (K_s + k_e)) \\ &+ sK_3(K_m - sK_2 b_e - K_2 k_e) e^{-2sT} \end{aligned} \tag{3.15}$$

$$\begin{aligned} D_1(s) =& (m_m s^2 + (b_m + B_m)s + K_m)\cdot \\ & (m_s s^2 + (B_s + b_e)\, s + (K_s + k_e)) \\ & - K_s(K_m - K_2 k_e - sK_2 b_e) e^{-2sT}. \end{aligned} \tag{3.16}$$

In particular, the steady-state transparency of the system can be determined by computing

$$\lim_{\omega \to 0} Z_t(j\omega) = \frac{X_m(j\omega)}{F_h(j\omega)} = \frac{K_s + k_e + K_3(K_m - K_2 k_e)}{K_m(K_s + k_e) - K_s(K_m - K_2 k_e)} \tag{3.17}$$

where $X_m(s)$ is the Laplace transform of $x_m(t)$. Steady-state transparency represents the impedance rendered to the operator by the master device once the transition between free-air and contact has settled.

### 3.3.2 Reflected damping in free-air

For the reflected damping in free-air, since the slave is not in contact with the environment, its influence is disregarded by considering $k_e = b_e = 0$. Replacing these values in (3.14), the impedance felt by the operator in free-air can be defined as

$$Y_t(s) = \frac{V_m(s)}{F_h(s)} = \frac{N_2(s)}{D_2(s)} \tag{3.18}$$

$$N_2(s) = s\left(m_s s^2 + B_s s + K_s + K_m K_3 e^{-2sT}\right) \tag{3.19}$$

$$\begin{aligned} D_2(s) =& \left(m_m s^2 + (b_m + B_m)\, s + K_m\right)\left(m_s s^2 + B_s s + K_s\right) \\ & - K_m K_s e^{-2sT}. \end{aligned} \tag{3.20}$$

Assuming that the behaviour of the system can be conveniently approximated by the that of a first order mass-damper system with a transfer function $\frac{1}{m \cdot s + b}$, the damping can be computed from the frequency response, i.e. $s = j\omega$, when $\omega \to 0$. Computing these limits for the teleoperator impedance, $\lim_{\omega \to 0} N_1(j\omega) = 0$ and $\lim_{\omega \to 0} D_1(j\omega) = K_m K_s - K_m K_s$ which corresponds to an indeterminate form of the type 0/0. Applying L'Hôpital's rule,

i.e. computing the limit of the first derivative of the numerator and the denominator with respect to $s$ to solve the indetermination, the reflected damping in free-air can be computed as

$$b_r = \frac{K_m B_s + K_s (B_m + b_m) + 2K_m K_s T}{K_s + K_3 K_m}. \tag{3.21}$$

Equation (3.21) can be used to compute how much damping a human operator feels when interacting with the master device while the slave moves in free-air.

## 3.4 Experimental setup and method

To experimentally verify the performance of the system, a setup composed by two identical single degree-of-freedom haptic devices is used. Each device consists of a Maxon brushless DC motor, gearing stage (planetary gear + capstan) and output handle. The motor is equipped with a 1024 pulses per turn encoder for position measurement and a strain-gage based force-torque sensor is mounted on the output handle. Both units are controlled by the same PC104 computer running Xenomai real-time operating system at a rate of 1kHz. The constant time delay is simulated using delay buffers for the transmission between each side. The complete setup is shown in Figure 3.3.

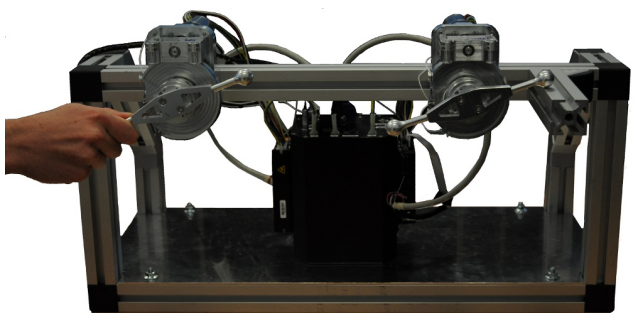

Figure 3.3: Experimental setup (master unit on the left and slave unit on the right)

Initially, the system master and slave devices are identified separately to determine the mass and damping parameters of each unit. The identification is done by applying an external force to each unit to execute a sinusoidal motion with varying speeds. Both the applied force and the resulting device velocity are recorded and the system parameters obtained using frequency-domain identification [74]. The obtained parameters for the master and slave are $m_m = 7.9 \cdot 10^{-3}\,\mathrm{kg \cdot m^2}$, $b_m = 8.44 \cdot 10^{-2}\,\mathrm{Nm \cdot rad \cdot s^{-1}}$, $m_s = 8.7 \cdot 10^{-3}\mathrm{kg \cdot m^2}$ and $b_s = 1.1 \cdot 10^{-1}\,\mathrm{Nm \cdot rad \cdot s^{-1}}$ and the identification has a Variance Accounted For (VAF) of approximately 0.94.

The bilateral teleoperation system is controlled using the 4-channel architecture with different parameters. Adapting the rules presented in [22] for perfect transparency, the force channel controller gains are always configured as $K_2 = K_3 = 1$ and the remaining controller

parameters can be freely chosen as long as their values remain positive. To identify the reflected damping in free-air the same identification method as for the individual units is used, with the operator applying a force to the master device to execute a sinusoidal motion while the slave moves in free-air. The identified damping damping $\hat{b}_r$ is compared to the predicted value computed using (3.21). The procedure is done for time-delay values from 0 up to 30 ms increasing in steps of 5 ms for two sets of controller gains. The controller gains chosen ensure that the system doesn't become unstable for the delay values used. The system contact transparency is determined by computing the stiffness rendered to the operator, using the position and force measurements, when the master device is used to command the slave into contact with a rigid remote environment.

## 3.5 Results and analysis

Using the 4-channel architecture transparency-optimized controller rules, defined in Section 3.4, the system steady-state transparency is defined as

$$\lim_{\omega \to 0} Y_t(j\omega)\Big|_{\text{4-channel}} = \frac{K_s + k_e + (K_m - k_e)}{K_m(K_s + k_e) - K_s(K_m - k_e)} \tag{3.22}$$

$$= \frac{1}{k_e} \tag{3.23}$$

with the reflected damping in free-air being

$$b_r\Big|_{\text{4-channel}} = \frac{K_m B_s + K_s\,(B_m + b_m) + 2K_m K_s T}{K_s + K_m}\,. \tag{3.24}$$

Equation (3.23) shows that the steady-state transparency corresponds to the stiffness of the environment. For this control architecture, Equation (3.24) shows that the reflected damping of the system depends on the controller proportional gains, the communication delay and master and slave damping and that the reflected damping should increase in a linear manner with time-delay.

To verify that the system response can be approximated by that of a first-order mass-damper system for frequencies within the range of human operator motion, Figure 3.4 shows a comparison between the frequency response of the system, computed using (3.14), and the first-order approximation with a damping of $b_r$ and a mass equal to that of the master device, i.e. $m_m$, both with $T = 0$ ms and $T = 30$ ms.

It is visible from 3.4(a) that, when no time-delay is present in the system, the first-order approximation is very accurate in the whole range of frequencies of closed-loop human operation. For the case with a time-delay of 30 ms, shown in Figure 3.4(b), it is visible that the damping approximation is still valid within the range of frequencies in which the human operates. Differences appear in the higher frequencies due to the changes in the cut-off frequency of the system, which suggests that the inertia felt by the human can also altered due to time-delay and controller effects.

Figure 3.5 shows an example of a system response using $K_m = K_s = 10$, $B_m = B_s = 0.3$ and time-delay values of $T = 0$ ms and $T = 30$ ms. The figure shows that, to reach

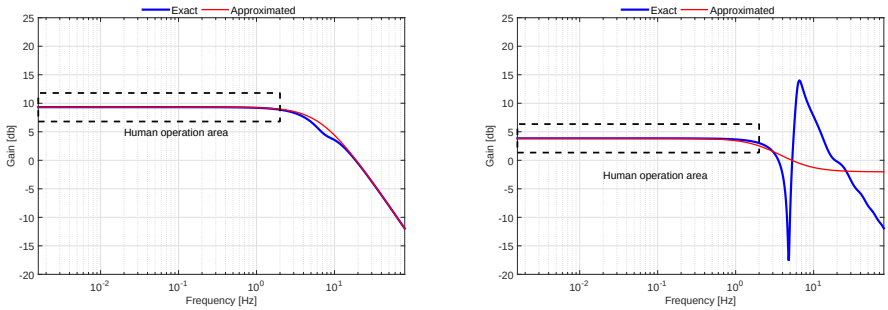


(a) No time-delay ($T = 0$ ms)

(b) 30 ms time-delay ($T = 30$ ms)

Figure 3.4: Comparison between teleoperator frequency response (in blue) and mass-damper frequency response approximation(in red) for $K_m = K_s = 10$, $B_m = B_s = 0.3$ with $T = 0$ ms and $T = 30$ ms in free-air motion.

velocities of about 2 rad/s a force of 0.8 N is applied (at $t = 4.5$ s) when there is no time-delay whereas an applied force of 1 N results in speed of just over 1 rad/s (at $t = 4.5$ s) when a constant communication delay of $T = 30$ ms is present in the system. This shows that, in this case, the system is perceived by the operator as having approximately a 60% larger damping due to time-delay effects.

In rigid contact, both without time-delay and with 30 ms delay, a stiffness equal to that of the environment is transmitted to the operator. However, in the transition between free-air and rigid contact the high frequencies are not transmitted to the operator, as visible by comparing the master and slave forces, for example at $t = 7$ s in Figure 3.5 (a), which means that, at the moment in which contact is reached, less stiffness is rendered to the operator than that of the actual contact. This happens in both test scenarios, with a larger effect when time-delay is present in the communication channel.

Following the procedure described in Section 3.4, the comparison between the predicted and identified reflected free-air damping the two sets of controller parameters is shown in Figure 3.6. The VAF for the identified values is, in all cases, between 0.8 and 0.9.

The results show that the difference between the theoretical and the measured value is never larger than approximately 5% of the measured damping. This indicates that the theoretical approximation gives an accurate prediction of the system damping transmitted to the human operator. It is not shown in this paper that, for large time-delay values, the damping approximation remains valid. However, for the control methods analysed, robustness to large time-delay is also limited, which makes the approximation valid in the working range. Comparing the results from Figure 3.5 with the damping values of Figure 3.6(a) it is visible that there is an approximately 60% increase in the damping between the no-delay and 30 ms delay cases.

Comparing these results to the stability analysis done by the authors in [79] it is clear that the parameter choices which result in larger stability of the system will typically results in a higher free-air damping being transmitted to the operator in free-air motion. However, no effect is visible on the steady-state transparency in rigid contact, which should remain

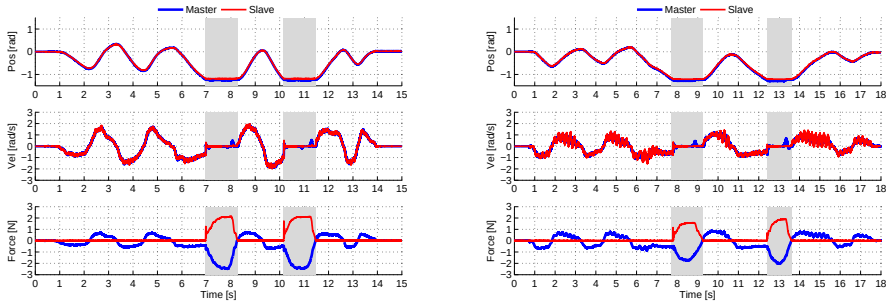


(a) No time-delay (b) 30 ms time-delay

Figure 3.5: Measured system response for $K_m = K_s = 10$, $B_m = B_s = 0.3$ with $T = 0$ and $T = 0.03$. The shaded areas represent moments in which the slave is in contact with the environment.

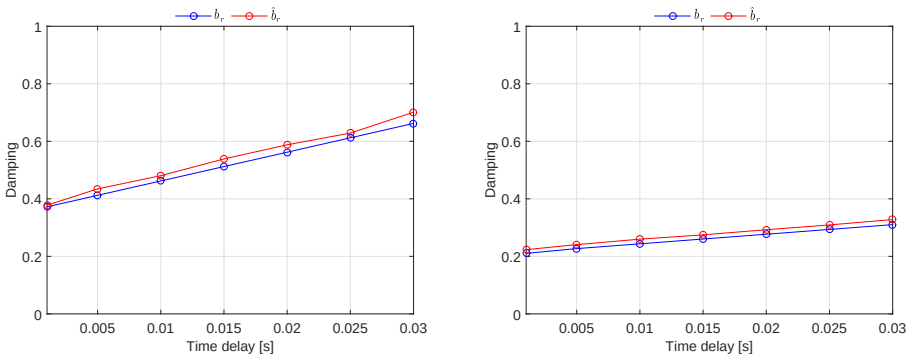


(a) $K_m = K_s = 10$, $B_m = B_s = 0.3$ (b) $K_m = 2, K_s = 10, B_m = 0.1$, $B_s = 0.3$

Figure 3.6: Theoretical and estimated reflected damping values. The points marked with a circle are the ones for which the test was performed.

very high independently of time-delay, as long as the system stability is kept.

## 3.6 Conclusions

The performance analysis done in this paper shows that, using the 4-channel architecture for an impedance-type master device commanding an impedance-controlled slave, perfect steady-state transparency can be achieved, with the stiffness of the environment being exactly rendered to the operator. In the transition between free-air and contact some additional dynamics which make the transition be perceived as softer than in reality are introduced by the system.

In free-air motion, the newly introduced reflected damping in free-air criterion shows

that the damping felt by the operator increases linearly with time-delay with a factor dependent on the proportional gains of the controllers. The experimental validation shows that the proposed criterion is valid for the frequency range of the human operator motion.

# Part II

# Time-delay robust stability

CHAPTER 4

# Time domain passivity controller for 4-channel time-delay bilateral teleoperation

J. Rebelo and A. Schiele
*IEEE Transactions on Haptics*, 2014 (in press)

**Abstract**

*Time-domain passivity control has been used successfully to stabilize teleoperation system with position-force and position-position controllers, however the performance with these control architectures is sub-optimal both with and without time-delay. This work extends the network representation of the time-domain passivity controller to the 4-channel architecture which reaches perfect transparency to the user without time-delay. The proposed architecture is based on the previously presented time-delay power network concept and modelling all the controllers as dependent voltage sources and using only series passivity controllers. The obtained results on a one degree-of-freedom setup show that, using this method, the system can be made stable for time-delays up to 1s as well as in the presence of data losses and complete data blackouts in the communication channel. Using the 4-channel time-domain passivity framework, a better performance in terms of transparency, when compared to other time-domain passivity architectures, is obtained both with and without time delay.*

## 4.1 Introduction

Teleoperation is an important field of research since it allows combining the planning and decision capabilities of human operators with the usability of robot manipulators located in remote, potentially inaccessible, or dangerous locations. However, in bilateral control scenarios, there is an inevitable time delay in the communication channel, which can render the system unstable [28].

Anderson and Spong [28] and Niemeyer [30] have proposed the use of passivity as the criterion to stabilize the system by placing a damping element that dissipates the energy generated by the delay in the communication channel. However, even though the proposed methods ensure stability for a constant delay, they are very conservative and reduce the transparency of the system.

To address these issues in the control of haptic interfaces exploring virtual environments, Hannaford and Ryu [34] have introduced a time-domain passivity controller, in which the passivity of the system is monitored in real-time and the damping is applied only when instability occurs. This framework was later extended by Artigas *et al.* [80] for use in bilateral teleoperation with time delay. In the proposed solution, the energy input at each side is measured and transmitted over the communication channel to the opposite side. If the output energy is higher than the input energy, this means that the communication channel is generating energy, and thus potentially making the system unstable.

This framework was first presented for the position-force architecture [81], which has a clear power network representation. Artigas *et al.* [36, 82] later introduced the concept of Time Delay Power Network (TDPN), which allowed the extension of the framework to the position-position architecture [36] and provided a higher level of abstraction. Nonetheless, both the position-force and position-position architectures have been shown to have suboptimal performance in terms of transparency both with and without time delay [22]. Also, the modelling of the position controllers as current sources and the use of parallel passivity controllers causes position drifts over time [35], which is undesirable in many teleoperation scenarios.

The goal of this work is to extend the time-domain passivity controller framework to achieve stable operation using a 4-channel architecture [22] under time delay. This control architecture provides perfect transparency to the user when no communication delay is present and can also be used to model any of the formerly mentioned control schemes. The proposed solution is analogous to the TDPN but all the controllers are modelled as voltage-dependent sources and only series passivity controllers are used, which ensures that no position drift occurs over time.

This paper is organized as follows: Section 4.2 reviews the previously introduced time-domain passivity control. Section 4.3 introduces the proposed model for the 4-channel architecture. The experimental results are presented and discussed in Section 4.4 and the conclusions are stated in Section 4.5.

## 4.2 A review of time-domain passivity control

Passivity is a widely used criterion to ensure the stability of teleoperation systems [28]. However, when a system is designed to be passive in every situation, the results can be too

conservative and lead to low levels of transparency [22]. To address this issue in haptic interfaces interacting with virtual environments, Hannaford and Ryu [34] proposed a time-domain passivity controller, which consists of monitoring the system's energy in real-time and dissipating it only when the system presents an active behaviour.

To measure the system's energy, the output of the one-port operator is instrumented with a Passivity Observer (PO) which computes the energy as

$$E_{\text{obs}}(n) = \Delta T \sum_{k=0}^{n} f(k)v(k) \tag{4.1}$$

where $\Delta T$ is the sampling time, $f(k)$ and $v(k)$ are the force and velocity at instant $k$. Using the voltage and current convention shown in Figure 4.1, when the measured energy is negative (i.e., energy is flowing out of the network block), the network presents an active behaviour which can make the system unstable. A variable dissipation element called the Passivity Controller (PC) can be used to dissipate this excess energy. Depending on the causality of the one-port network (impedance or admittance), the PC can be either series (computing a force to be dissipated) or parallel (computing a velocity to be dissipated). Figure 4.1 shows an electrical diagram example of a series and a parallel PC.

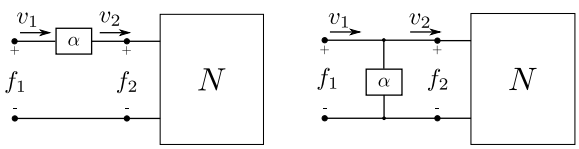


(a) Series PC (b) Parallel PC

Figure 4.1: Series and parallel passivity controller (adapted from [34])

For the series PC, the value of the dissipation element $\alpha$ can be computed as

$$\alpha(n) = \begin{cases} -E_{\text{obs}}(n)/(\Delta T \cdot v_2(n)^2) & \text{if } E_{obs} < 0 \\ 0 & \text{if } E_{obs} \geq 0 \end{cases} \tag{4.2}$$

causing the force rendered at the haptic device to be

$$f_1(n) = f_2(n) + \alpha(n)v_2(n). \tag{4.3}$$

The parallel passivity controller works in an analogous manner, but changing the velocity set-point instead of the force. A detailed description of the parallel passivity controller and a proof of passivity using this controller is given in [34].

Considering a bilateral teleoperation system, such as the one shown in Figure 4.2, and assuming that the system has been designed to have a passive, i.e. stable, behaviour when no time delay is present in the communication channel, it can be shown that the instability that appears when time delay is present is due to energy injected by the active behaviour of the communication channel [30].

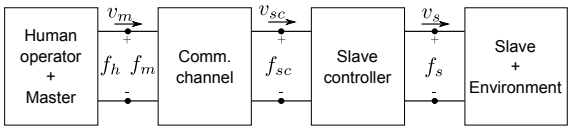


Figure 4.2: Time delay bilateral teleoperation system

When monitoring the passivity of a communication channel instead of a haptic device, the communication channel two-port network as shown in Figure 4.2 has to be considered. The passivity observer of a two-port is defined as

$$E_{\text{obs}}(n) = \Delta T \sum_{k=0}^{n} [f_m(k)v_m(k) - f_{sc}(k)v_{sc}(k)]. \tag{4.4}$$

From (4.4) it is clear that the energy has to be monitored simultaneously on both sides of the two-port, which is impossible due to the unavoidable time delay introduced by the communication channel. A solution to this problem was proposed by Artigas *et al.* [80, 83] and Ryu *et al.* [35], where the energy on each side of the channel is monitored and transmitted over the communication channel to the opposite side.

For the communication channel two-port network, the energy can be separated into the input energy $E_{\text{in}}$ and the output energy $E_{\text{out}}$ at the master and slave sides, and can be computed at each port as

$$E_M^{\text{in}}(n) = \begin{cases} E_M^{\text{in}}(n-1) + \Delta T \cdot P_m(n) & \text{if } P_m(n) > 0 \\ E_M^{\text{in}}(n-1) & \text{if } P_m(n) \leq 0 \end{cases} \tag{4.5}$$

$$E_S^{\text{in}}(n) = \begin{cases} E_S^{\text{in}}(n-1) + \Delta T \cdot P_s(n) & \text{if } P_s(n) > 0 \\ E_S^{\text{in}}(n-1) & \text{if } P_s(n) \leq 0 \end{cases} \tag{4.6}$$

$$E_M^{\text{out}}(n) = \begin{cases} E_M^{\text{out}}(n-1) & \text{if } P_m(n) \geq 0 \\ E_M^{\text{out}}(n-1) - \Delta T \cdot P_m(n) & \text{if } P_m(n) < 0 \end{cases} \tag{4.7}$$

$$E_S^{\text{out}}(n) = \begin{cases} E_S^{\text{out}}(n-1) & \text{if } P_s(n) \geq 0 \\ E_S^{\text{out}}(n-1) - \Delta T \cdot P_s(n) & \text{if } P_s(n) < 0 \end{cases} \tag{4.8}$$

where $P(n) = f(n)v(n)$ is the power generated at instant $n$.

To ensure the passivity of the whole block, it is sufficient to guarantee that the energy output at the master and slave ports is always smaller than or equal to the energy input at the slave and master ports [80]. Even though in this situation it is still necessary to monitor both ports simultaneously, using Eqs. (4.5)–(4.8) results in a monotonic increase of all the monitored energies. This means that if the energy measured at the input side is sent to the output side over the delayed communication channel, the only consequence is that the energy will be limited to a value which is less than or equal to the one strictly needed. Thus, no violation of passivity occurs, but more energy than required will be dissipated.

Given these passivity conditions, the series passivity controller on the master side can be calculated as

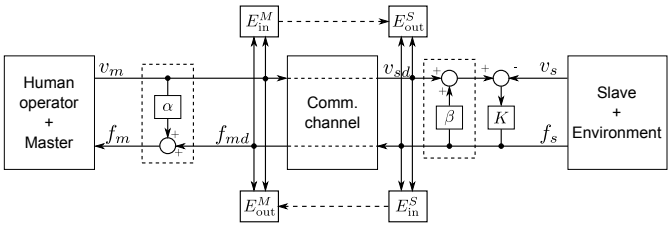


Figure 4.3: Time delay bilateral teleoperation control diagram with passivity observer and passivity controller

$$\alpha(n) = \begin{cases} \frac{E_M^{\text{out}}(n) - E_S^{\text{in}}(n-T)}{\Delta T \cdot v_m^2(n)} & \text{if } E_M^{\text{out}}(n) > E_S^{\text{in}}(n-T) \text{ and } v_m(n) \neq 0 \\ 0 & \text{if } E_M^{\text{out}}(n) \leq E_S^{\text{in}}(n-T) \end{cases} \tag{4.9}$$

and the parallel passivity controller on the slave side as

$$\beta(n) = \begin{cases} \frac{E_S^{\text{out}}(n) - E_M^{\text{in}}(n-T)}{\Delta T \cdot f_s^2(n)} & \text{if } E_S^{\text{out}}(n) > E_M^{\text{in}}(n-T) \text{ and } f_s(n) \neq 0 \\ 0 & \text{if } E_M^{\text{out}}(n) \leq E_S^{\text{in}}(n-T). \end{cases} \tag{4.10}$$

An overview of this architecture, including the passivity observers and the passivity controllers, is shown in Figure 4.3.

This time-domain passivity controller method was originally proposed for the position-force architecture, since in this case the power representation of the system is clearly determined by the velocity-force combination. When using a position-position (P-P) control architecture, there are only positions (or equivalently velocities) being transmitted in each direction, and therefore there is no direct power representation of the system. Figure 4.4 shows a circuit representation of the P-P architecture. Artigas *et al.* [36] extended this framework by introducing the Time-Domain Power Network (TDPN) concept and presenting its application to the P-P architecture. The TDPN can be represented as a two-port network with force flowing in one direction and velocity flowing in the opposite direction. The TDPN equivalent of a communication channel is depicted in Figure 4.5.

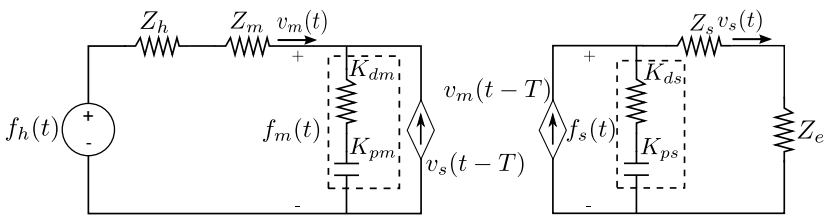

Figure 4.4: Electrical representation of the P-P architecture (adapted from [36])

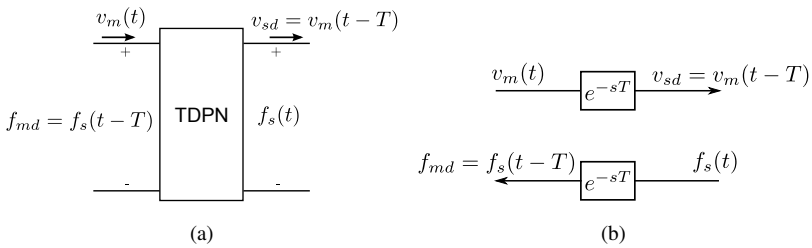


Figure 4.5: Time-Delay Power Network equivalent (a) of a position-force communication channel (b)

Using the currently proposed time-domain passivity frameworks, passivation of time delay teleoperation using the position-force and the P-P architectures has been demonstrated. However, the performance of this architecture in terms of transparency has been shown to be sub-optimal even without time delay [22]. Additionally, when using parallel passivity controllers, the velocity set-point is modified to ensure that the system remains stable. The modified set-point is then integrated by the velocity controller to determine the force to be applied to the master or slave device. The integration of a modified velocity causes the position between the slave and the master to drift. This position offset that builds up between the master and the slave is unacceptable in many teleoperation applications, for which the master and the slave are prefered to be always aligned.

## 4.3 4-channel time-domain passivity

In this section, an extension of the time-domain passivity framework for use with the 4-channel architecture with time delay in the communication channel [22], as illustrated in Figure 4.6, is presented. The proposed extension makes use of the TDPN methodology [82] but with the behaviour of all the controllers modelled as that of dependent voltage sources. Using series passivity controllers, the force output of the controller is modified to ensure stability. This means that the position integration is always done on the unmodified velocity signal, which will result in no position drift due to energy dissipated using the PC. In the remainder of this section, a TDPN model for the 4-channel architecture is presented and passivity conditions for the system are determined. From this model, the passivity observers with an energy tracking mechanism and passivity controllers for the master and slave sides are defined and implemented.

### 4.3.1 4-channel TDPN modelling

Consider the bilateral teleoperation system represented in Figure 4.6. In this system, a human operator, modelled as an extrinsic force $f_h^*$ and a passive impedance behaviour $Z_h$, interacts with a master device with admittance causality, i.e., force input velocity output, $Z_m^{-1}$. On the remote side, an admittance causality slave $Z_s^{-1}$ interacts with an environment with impedance $Z_e$, which is assumed to be passive. The proposed method is independ-

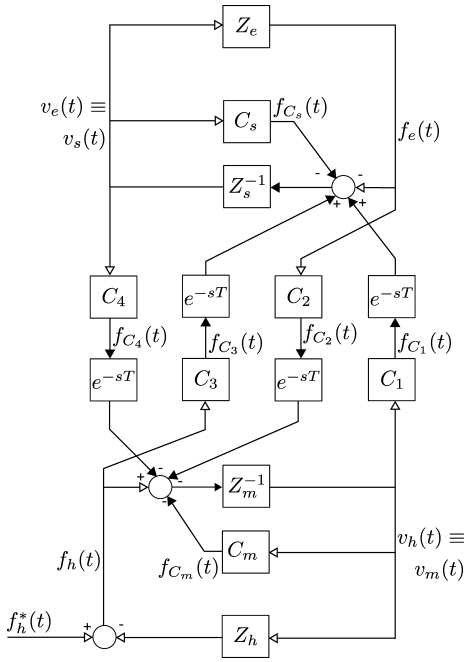


Figure 4.6: 4-channel architecture (adapted from [22]). The hollow arrows represents physical signals and the filled arrows, controller signals.

ent of the dynamics of the master, slave, operator and environment, therefore these can be assumed to be generic functions. The system controllers are tuned following the transparency optimized rules presented in [22] and such that when no time delay is present in the communication channel, the overall system is passive, i.e., stable.

In the 4-channel architecture, both velocity and force information is transmitted between the master and the slave. The velocity channel controllers $C_m$, $C_s$, $C_1$ and $C_4$ are implemented as PI controllers with velocity as an input. This implementation is equivalent to a PD controller with position as an input. In practice, using a PD controller prevents numerical drift problems which can appear due to the non-ideal numerical integrator of the PI controller. Independently of the used implementation, this controller ensures that there is both a position and a velocity coupling, which emulates the physical behaviour of a spring–damper system connecting the master and the slave. In the electrical domain, this can be modelled as a series resistor-capacitor circuit. In previous works, passivity controllers were implemented as a variable resistor element in parallel with the current supply (see e.g. [36]). From an input–output perspective, the complete controller can be regarded as a current dependent voltage source, as illustrated in Figure 4.7(a). Equivalently, the force channel controllers $C_2$ and $C_3$, which are implemented as P controllers, can be modelled as a simple gain which is equivalent to a voltage dependent voltage source, as shown in Figure 4.7(b).

Assuming each of the controllers to be a dependent voltage source, the equivalent elec-

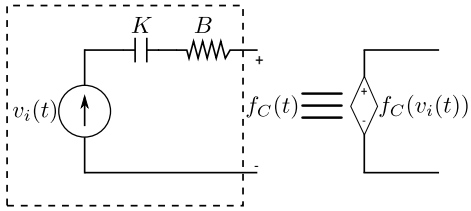


(a) Velocity channel controller

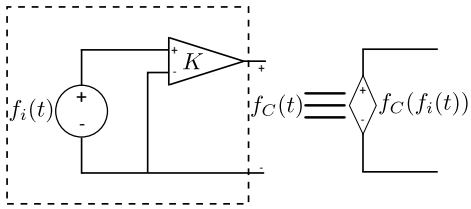


(b) Force channel controller

Figure 4.7: Electrical domain representation of the velocity and force channel controllers

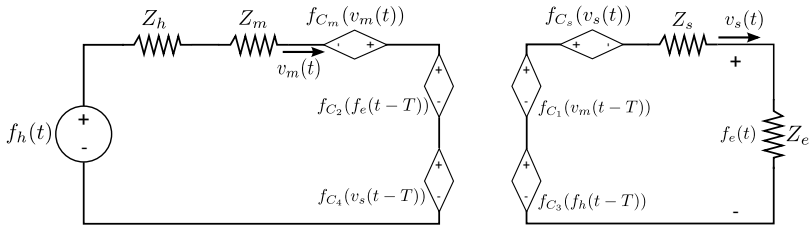


Figure 4.8: Electrical equivalent of the 4-channel architecture

trical scheme of the 4-channel architecture can be represented as in Figure 4.8. It is clear that controllers $C_1$ to $C_4$ suffer the effects of time delay, however there has not been, up to now, a clear network representation that would allow us to define passivity observers that could be used to monitor whether energy is being generated in the system or not. In a manner analogous to [82], the energy of the communications channel can be computed as

$$\begin{aligned} E_{N_z}(n) =& \Delta T \sum_{k=0}^{n} v_m(k) \left[ f_{C_2}(k-T) + f_{C_4}(k-T) \right] \\ &+ v_s(k) \left[ f_{C_1}(k-T) + f_{C_3}(k-T) \right] \end{aligned} \tag{4.11}$$

which can be divided into its components

$$E_{N_z}(n) = E_{N_m}(n) + E_{C_{rm}}(n) + E_{N_s}(n) + E_{C_{rs}}(n) \tag{4.12}$$

where $E_{N_m}$ and $E_{N_s}$ are the energies in the master and slave networks and $E_{C_{rm}}$ and $E_{C_{rs}}$ are the energies in the remote master and slave controllers. Each of these energies can be represented as

$$E_{N_m}(n) = \Delta T \sum_{k=0}^{n} \Big[ v_m(k)[f_{C_2}(k-T) + f_{C_4}(k-T)] + v_m(k-T)[f_{C_2}(k) + f_{C_4}(k)] \Big] \tag{4.13}$$

$$E_{N_s}(n) = \Delta T \sum_{k=0}^{n} \Big[ v_s(k)[f_{C_1}(k-T) + f_{C_3}(k-T)] + v_s(k-T)[f_{C_1}(k) + f_{C_3}(k)] \Big] \tag{4.14}$$

$$E_{C_{rm}}(n) = \Delta T \sum_{k=0}^{n} \Big[ - v_m(k-T)[f_{C_2}(k) + f_{C_4}(k)] \Big] \tag{4.15}$$

$$E_{C_{rs}}(n) = \Delta T \sum_{k=0}^{n} \Big[ - v_s(k-T)[f_{C_1}(k) + f_{C_3}(k)] \Big]. \tag{4.16}$$

In this case, the system, including the communication channel, can be represented as shown in Figure 4.9. The remote master and slave controllers $C_{rm}$ and $C_{rs}$ are responsible for the motion and force feedback of the system, therefore they are expected to behave in an active manner. The $N_m$ and $N_s$ networks are responsible for the energy transmission between the master and the slave and should therefore have a passive behaviour, thus not injecting energy into the system, so that the passivity of the communication channel is ensured.

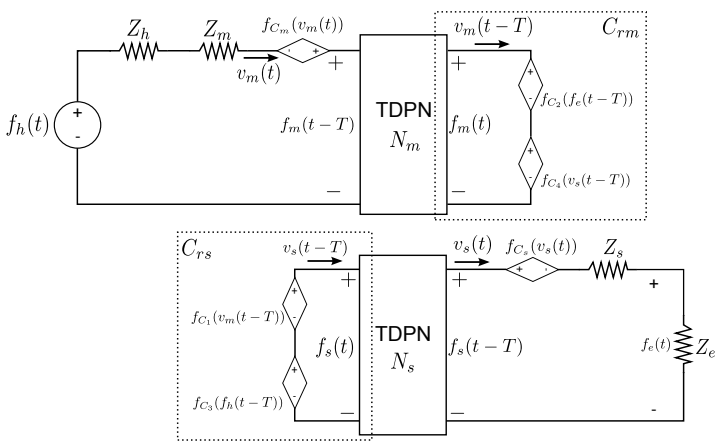


Figure 4.9: 4-channel architecture representation with TDPN

Since the system is designed for passivity when there is no time delay, we assume that the local controllers $C_m$ and $C_s$ are always passive, i.e., $E_{C_m}(n) \geq 0$ and $E_{C_s}(n) \geq 0$ at

any time instant $n$.

Therefore, for the system to remain passive, both the $N_m$ and $N_s$ networks have to remain passive. The energy of each of the networks can be defined as

$$E_{N_m}(n) = E_{N_m}^{L_{in}}(n) + E_{N_m}^{L_{out}}(n) + E_{N_m}^{R_{in}}(n) + E_{N_m}^{R_{out}}(n) \tag{4.17}$$

$$E_{N_s}(n) = E_{N_s}^{L_{in}}(n) + E_{N_s}^{L_{out}}(n) + E_{N_s}^{R_{in}}(n) + E_{N_s}^{R_{out}}(n) \tag{4.18}$$

where the superscripts $R$ and $L$ represent the left and right side of the network block, referring to Figure 4.9.

As the voltage controllers are assumed to be ideal, the voltage generated by the controller is independent of the current across it and the internal resistance has a value of 0. This means that the current is completely determined by the circuit to which the supply is connected, thus supplying and absorbing unlimited power. This implies that all the energy that is input from the master side towards $N_m$ and from the slave side towards $N_s$ will be absorbed by the voltage supplies $C_{rm}$ and $C_{rs}$ respectively. Following this rationale, the Lemma presented in [36] can be extended to Lemma 1.

**Lemma 1** *In a system composed of a TDPN connected to an ideal voltage/current supply, energy is transmitted only from the source to the TDPN.*

Therefore the passivity conditions for the system can be defined as

$$\begin{aligned} E_{N_m}^{R_{in}}(n) &\geq E_{N_m}^{L_{out}}(n) \\ E_{N_s}^{L_{in}}(n) &\geq E_{N_s}^{R_{out}}(n). \end{aligned} \tag{4.19}$$

With this representation, the network relations between the different controllers and the communication channel become explicit, allowing the passivity of the communication channel to be monitored using passivity observers and the passivity conditions to be maintained using passivity controllers. Since only energy flows from the sources to the TDPN are considered, the superscripts $R$ and $L$ are dropped in the remaining analysis for simplicity.

### 4.3.2 4-channel passivity observer

Eq. (4.19) shows that the system becomes unstable when there is more energy output from the TDPN than input by the corresponding controllers on the opposite side. Thus, instrumenting each side of the TDPN with a PO, the output and input energies can be computed using Eqs. (4.5)–(4.8).

However, the communication channel can not only generate but also dissipate energy, i.e., $E_{\text{out}}(n) \leq E_{\text{in}}(n-T)$. Even though this has no impact on the stability of the system, it can allow an offset to build up between the input and output energies monitored by the PO. This offset results in a slowing down of the PC's response when the system becomes active. To address this problem, an energy tracking mechanism is integrated in the output-side PO. The energy tracking can be implemented on both the master and slave sides by

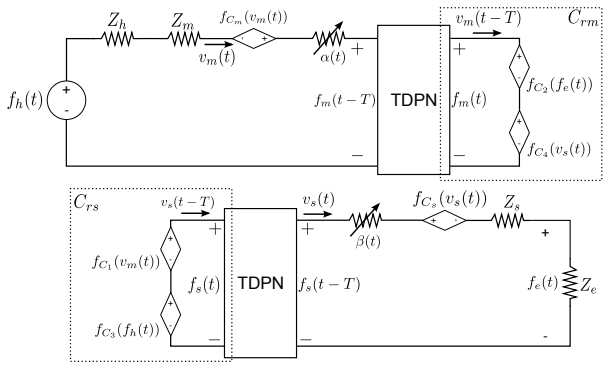


Figure 4.10: 4-channel architecture representation with TDPN and PC.

$$E_{\text{out}}(n) = \begin{cases} E_{\text{out}}(n) + \Delta E(n) & \text{if } \Delta E(n) > 0 \\ E_{\text{out}}(n) & \text{if } \Delta E(n) \leq 0 \end{cases} \tag{4.20}$$

where $\Delta E(n) = E_{\text{in}}(n-T) - E_{\text{out}}(n)$ represents the energy difference between the input and the output side. When $\Delta E(n) \leq 0$ the excess energy will be dissipated using a PC.

### 4.3.3 4-channel passivity control

Assuming that the voltage sources are ideal, i.e., that they can absorb infinite energy, a PC is only needed at the master and slave output sides to dissipate the excess energy generated by the communication channel. Taking the master side as an example, the energy that must be dissipated by the passivity controller can be calculated as

$$E_M^{\text{diss}}(n) = E_M^{\text{out}}(n) - E_M^{\text{in}}(n-T) - E_M^{\text{diss}}(n-1). \tag{4.21}$$

This means that the passivity controller must determine a force that dissipates this energy as in (4.2) and (4.3). An identical calculation can be done to implement the slave side passivity controller. This ensures that the communication channel remains passive and therefore the system is stable. The complete system in the electrical domain can be represented as shown in Figure 4.10.

Using the proposed PO/PC combination, the energies in the TDPN are restricted such that

$$E_M^{\text{out}}(n) = E_M^{\text{in}}(n-T) \tag{4.22}$$

$$E_S^{\text{out}}(n) = E_S^{\text{in}}(n-T). \tag{4.23}$$

From the definitions (4.5)–(4.8), it is clear that $E_{out}(n) \leq E_{in}(n-T)$, therefore the passivity condition (4.19) is always satisfied. This is valid also for asymmetric and varying time delays, as well as data loss and total communication link blackouts, as will be experimentally demonstrated in Section 4.4.4.

The overall architecture including the PC can be implemented as in Figure 4.11. Note that the two slave controllers $C_1$ and $C_3$ are computed at the master side and the two master controllers $C_2$ and $C_4$ computed at the slave side, and the resulting forces summed and transmitted over the delayed communication channel. Even though only two communication channels are effectively used, the effects of both force and velocity channels are combined in the transmitted force signal.

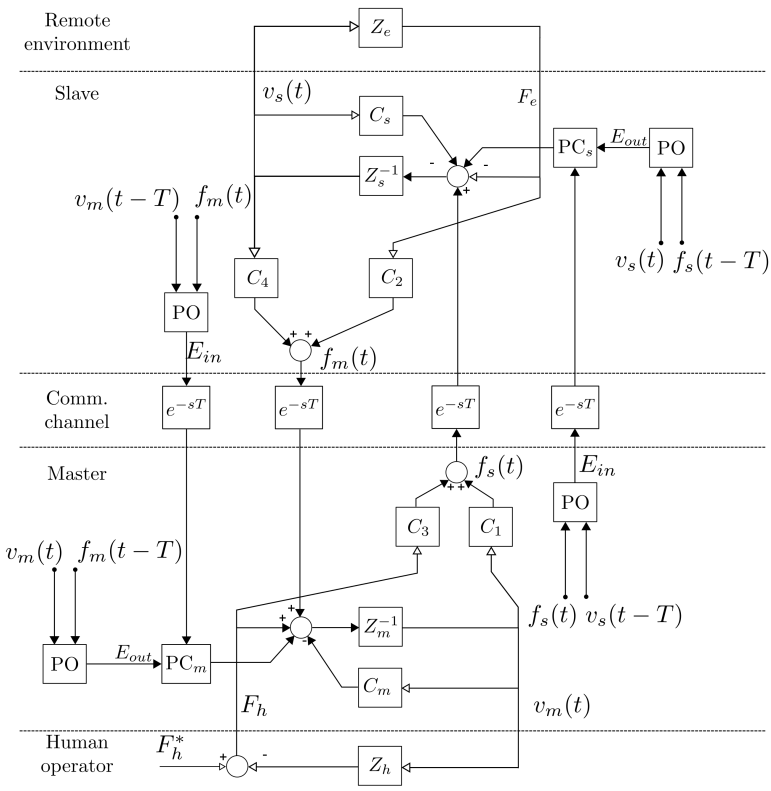


Figure 4.11: 4-channel architecture implementation with time-domain passivity controller. Note that master and slave velocities which are also transmitted to the opposite side are not explicitly represented in the diagram for simplicity.

Considering the controllers as voltage sources and using only series passivity controllers avoids problems with position drift previously reported with parallel passivity controllers [35]. As explained in [80], one of the issues with this architecture is that the energy needs to be transmitted to each side through a delayed communication. This does not affect the stability, but more energy than is strictly needed will be dissipated, which will result either in lower stiffness being rendered to the operator while in contact or larger damping while in free-air motion.

## 4.4 Experimental results

To validate the proposed architecture, this section presents the results of teleoperation under different time delays.

### 4.4.1 Experimental setup and method

The experimental setup consists of two identical one degree of freedom joints. Each joint is composed of a Maxon brushless DC motor, a gearing stage (planetary gear + capstan), and an output handle. The motor is equipped with a 1024 pulses per turn encoder and the output shaft has a strain-gauge based force/torque sensor for output torque measurement. Both units are controlled by the same PC104 computer running Xenomai real-time operating system at a rate of 1kHz. The time delay is simulated using delay buffers for the data transmission between each side. Figure 4.12 shows the one degree-of-freedom setup with the master on the left and the slave on the right, including the aluminium bar used to render the hard contacts.

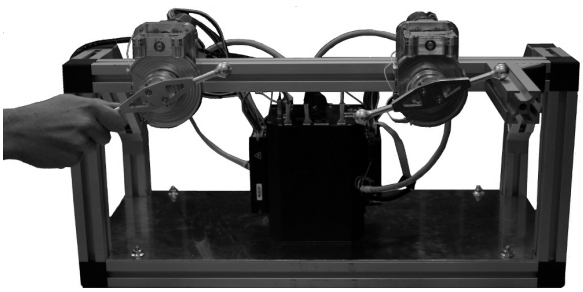

Figure 4.12: Experimental setup (master unit on the left and slave unit on the right)

The controllers are tuned following the tuning rules for ideal transparency without time delay demonstrated by Lawrence [22]. The proportional gain of the force channel controllers $C_2$ and $C_3$ is set to 1. The velocity channel controllers must obey $C_m = C_4$ and $C_s = C_1$. This tuning does not compensate for the inertia and damping of the devices, therefore a small force is expected to be felt in free-air motion. In this research, the derivative gain of $C_m$ was set to 0.4 and the proportional gain to 7. For the case of $C_s$, these gains were defined as 0.4 and 4 for the derivative and proportional parts, respectively. The controller values have been observed to have an effect on the stability of the system, however, as long as the tuning rules are respected, the transparency behaviour without time delay should remain identical [22]. In this case, the values were selected so that the system would be stable for time delays up to 30 ms without additional passivity control stabilization. The same controller values were kept for all the tests performed.

In the presented experimental scenario, the operator moves the master handle until the slave contacts with the environment, keeps the contact for a few seconds, then returns to the origin and repeats the procedure. After two contacts, the operator makes some motion in free-air to analyse the position tracking behaviour of the system. The operator keeps a soft

grip on the master device so that any unstable situation is easily visible. Soft contacts were not tested since their behaviour is naturally more stable than that of rigid contacts.

### 4.4.2 Teleoperation without time delay

For this test, no time delay was present, so that the performance of the system under the tuning conditions could be evaluated. Figure 4.13(a) shows the master and slave positions and forces during the test. The contacts with the environment occur approximately between 2.5 and 3.5 seconds and 5 and 6.5 seconds. At these moments, the forces applied by the slave on the environment are almost identically reflected to the human operator, whereas in free-air motion, the operator applies a force of approximately 0.2 N to move the device. The positions of the master and the slave are identical throughout the whole experiment. From Figure 4.13(b) it can be seen that for both the master and the slave sides, the observed input and output energy flows are identical.

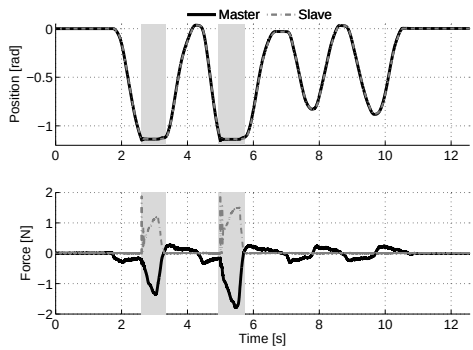


(a) Position and force

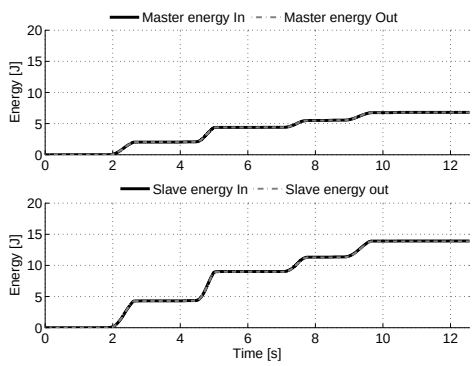


(b) Energy flows

Figure 4.13: Master–slave behaviour in teleoperation without time delay. In all figures the shaded area represents the time at which the slave is in contact with the environment.

### 4.4.3 Teleoperation with 100 ms round-trip delay

For the tests in this section a round-trip delay of 100 ms in the communication channel was used. The system is first tested without the passivity controller to evaluate the stability of the architecture. In the second test the passivity controller without the energy tracking is tested to verify the effects of not correcting for the passive energy offset. In the third test the complete proposed passivity control architecture is implemented and tested.

***Teleoperation without passivity controller***

Without a passivity controller, and with a 100 ms round-trip time delay in the communication channel, some oscillations occur in contact situations, as shown in Figure 4.14(a). From the energy flows in Figure 4.14(b) it can also be seen that there is a deviation between the input and the output energies: the master output energy is larger than the input energy after four seconds and the input energy in the slave is larger than the output energy after two seconds.

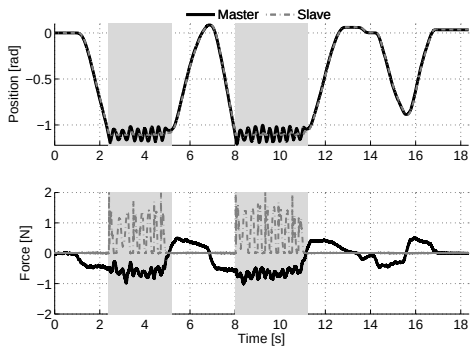


(a) Position and force

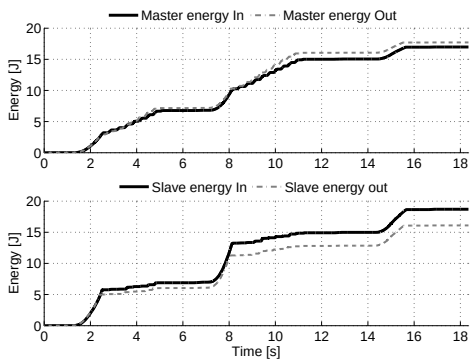


(b) Energy flows

Figure 4.14: Master–slave behaviour in teleoperation with 100 ms round trip delay without passivity controller.

***Teleoperation with passivity controller without energy tracking***

The position and force behaviour of the system applying only the passivity controller without the energy tracking is shown in Figure 4.15(a). As can be observed, the system has no oscillation behaviour after the first contact, however some initial bounces occur on the second contact for about two seconds before the system becomes stable.

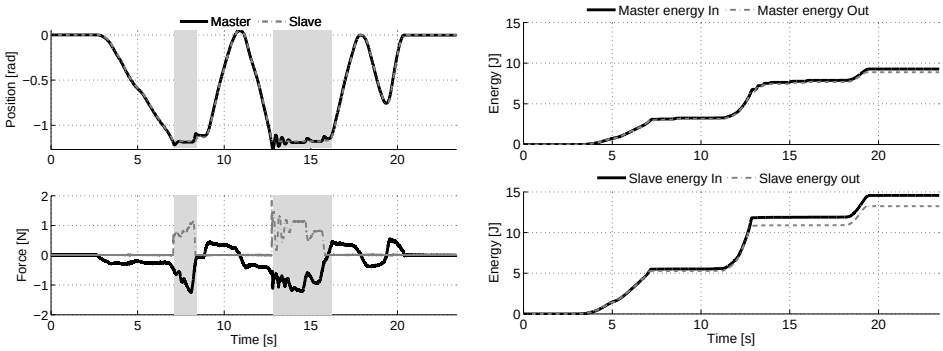


(a) Position and force

(b) Energy flows

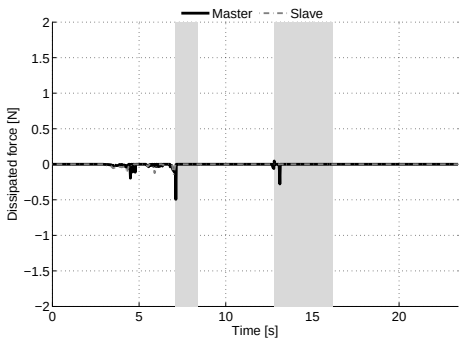


(c) PC forces

Figure 4.15: Master–slave behaviour in teleoperation with 100 ms round trip delay using passivity controller without energy tracking.

Analysing the master and slave energy flows from Figure 4.15(b) it can be seen that an offset appears between the input and output energy of the slave. This situation is visible, for example, between seconds 7 and 11 and from second 13 to the end of the experiment on the slave side.

It can be seen in Figure 4.15(c) that the PC acts mainly on the master side with a maximum force of about -0.5 N. After the second contact the PC action is about 1 s after the occurrence of contact.

***Teleoperation with passivity controller and energy tracking***

The position and force response when applying the proposed passivity controller with energy tracking is depicted in Figure 4.16(a). In this case no oscillation behaviour is visible on either the first or the second contact. From Figure 4.16(b) it can be observed that on both the master and slave sides, the energy input and output track each other perfectly.

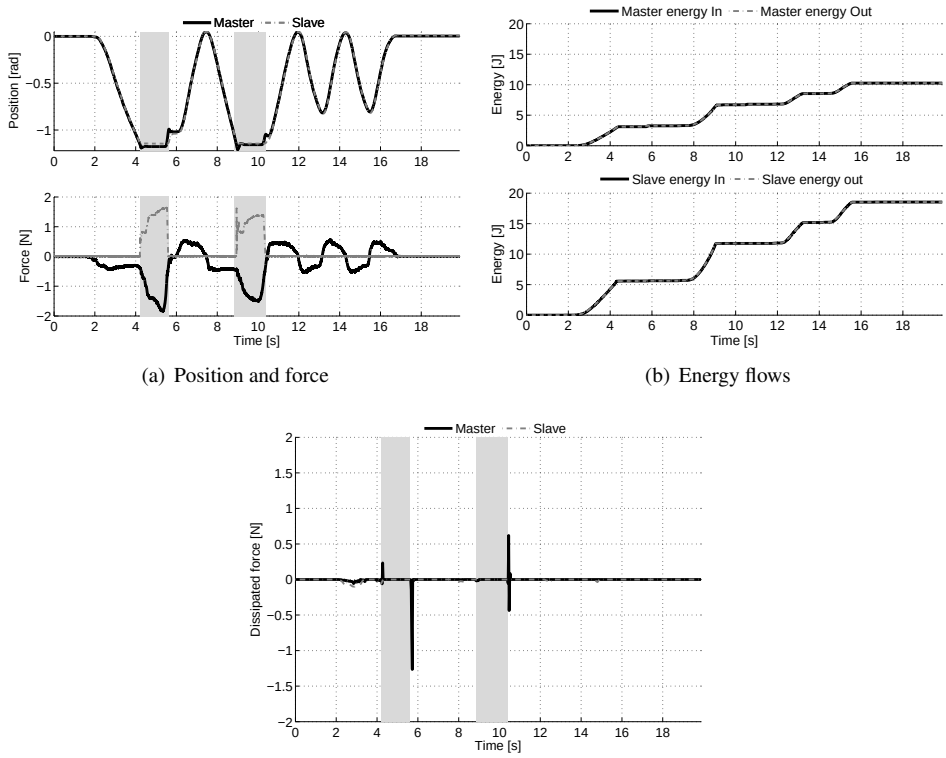


(a) Position and force

(b) Energy flows

(c) PC forces

Figure 4.16: Master–slave response in teleoperation with 100 ms round trip delay using passivity controller.

Figure 4.16(c) shows that most of the dissipation force command is on the master side with a maximum absolute value of 1.25 N. To move the master in free-air, the operator applies a force of approximately 0.3 N in all cases. The transparency behaviour of the system when using the PC is very similar to that of the scenario without time delay.

### 4.4.4 Teleoperation with asymmetric 1 s round trip delay and data loss

For larger time delays, it is expected that the system has an unstable behaviour both in free-air motion and in contact. For this test, a communication channel with an asymmetric 1 s round-trip delay, with 400 ms delay between the master and the slave and 600 ms between

the slave and the master, and a data loss of 10% was used. When a packet is lost, the values received from the previous packet are kept.

### *Teleoperation without passivity controller*

From the position and force behaviour shown in Figure 4.17(a) it is possible to see that with these communication channel characteristics, the system has an unstable oscillatory behaviour while in free-air motion. Once the contact is reached the oscillations increase and cannot be stopped by the operator. As in the case with a 100 ms round-trip delay, the energy flows in Figure 4.17(b) show offsets between the input and output energies on both sides.

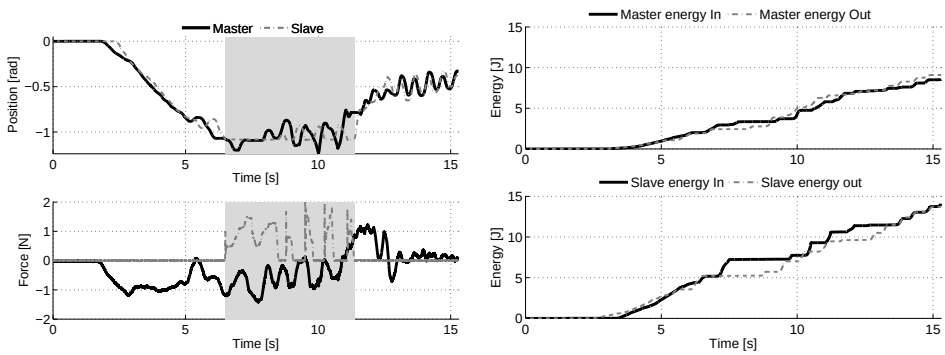


(a) Position and force (b) Energy flows

Figure 4.17: Master–slave response in teleoperation with 1 s asymmetric round-trip delay without passivity controller.

### *Teleoperation with passivity controller and energy tracking*

Applying the PC to the system results in the position and force behaviour shown in Figure 4.18(a). As can be seen, the operator can move the master in free-air with a force of approximately 1 N and the contact is rendered on the master side one second after it is reached by the slave. During the data blackout, between 12 s and 14 s, energy is dissipated on the master side and no motion is visible on the slave side. Once the communication is restored the system recovers and operations continue normally. It can also be seen that after the two contacts and data blackout, the positions of the master and the slave in free-air motion are still identical. The input and output energy flows are always equal, as seen in Figure 4.18(b). From Figure 4.18(c) it is clear that the PC acts for several seconds with forces up to 1.5 N on both the master and slave sides and both in free-air and contact situations.

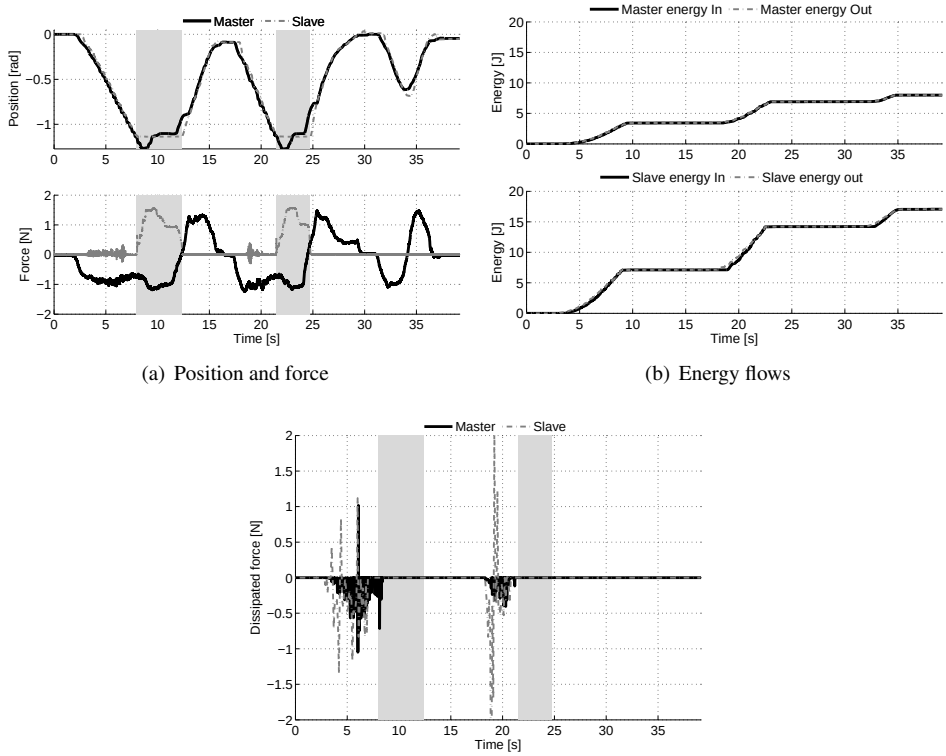


(a) Position and force

(b) Energy flows

(c) PC forces

Figure 4.18: Master–slave behaviour in teleoperation with 1 s asymmetric round-trip delay, 10% data loss and 2 s data blackout, using passivity controller.

### 4.4.5 Analysis and discussion

As can be seen from the positions and forces in Figure 4.13(a), the system using the 4-channel architecture has a high degree of transparency, with the reflected inertia in free-air motion being very low, the contact forces identically reflected to the user, and very accurate position tracking between the master and the slave. The only force that is not transmitted to the human operator is the very high frequency at impact, which is expected given the bandwidth of the master mechanics. However the effect on the rigid contact rendering is very minimal, as seen in the position transition of the master device from free-air to contact. It can be seen in Figure 4.13(b) that the input and output energy for both the master and slave channels are identical, which is as expected since without time delay, the communication channel has no influence on the data transmission.

When a time delay of 100 ms is present in the communication channel, the system presents an unstable behaviour in contact situations, as seen in Figure 4.14(a). Figure 4.14(b) shows that this instability can be traced to the energy output of the communica-

tion channel's being larger than the input energy. When the PC is used to dissipate this excess energy, the system becomes stable and the user can render the contact as shown both in Figures 4.15(a) and 4.16(a). If the proposed energy tracking is not used, the system is only stable after a few initial bounces, as can be seen in the second contact in the situation in Figure 4.15(a). From Figure 4.15(b), it can be seen that when moving in free-air between second 5 and 7 of the experiment, an offset appears between the input and output energy on the slave side. Once the system reaches contact, the output energy starts increasing, but it takes about two seconds for it to reach the output energy level, a time during which the system allows for some instability. This behaviour can also be observed, for example, in the results of [36], but negative effects were not reported, possibly due to the different nature of the proposed controller. Using the proposed energy tracking mechanism on the output PO, the energy flows between the input and the output track each other perfectly, as seen in Figure 4.16(b). In terms of transparency, the system still renders a very stiff contact to the master with only a small difference perceived in the contact instant. In free-air, the operator feels a large damping due to the effects of the time delay on the controllers and the position tracking remains accurate independently of the use of the PC.

For the 1 s asymmetric time delay, the system shows a very unstable behaviour, both in free-air motion and in contact, with increasing oscillations which cannot be easily controlled by the human operator, as shown in Figure 4.18(a). Once the PC is used the system is stable but the large forces required to dissipate the excess energy cause some vibrations which feel unnatural to the operator. As reported earlier [35], the series PC presents a noisier behaviour which can be clearly felt by the user. This is especially clear in the phase immediately after the data blackout. Nonetheless, the authors believe that position tracking is an important requirement for teleoperation and the noise could be reduced using, for example, the technique presented in [35]. Even though the contact is rendered to the operator in a stable manner, this happens only after 1 s, which means that the current master position can potentially be far from the actual contact point. Once the contact is rendered, the master side is pushed by the effect of force feedback to the place where the actual contact is located. This behaviour is dependent on the human operator's reaction, but is particularly visible in the first contact (at $t = 9\,\mathrm{s}$) in Figure 4.18(a). The contact always feels softer which means that transparency of the system has been reduced due to the time delay. Analysing the master forces in free-air motion for this level of delay, it can also be seen that the damping felt is much higher than in the non-delayed scenario, requiring a force about five times higher from the operator to move the master in free-air.

## 4.5 Conclusion

The proposed time-domain passivity framework is able to stabilize a time-delay teleoperation system using a 4-channel architecture. The framework stabilizes the teleoperation system for different constant time delays as well as in the presence of data losses and complete data blackouts in the communication channel.

By modelling all the controllers as dependent voltage sources and using only series passivity controllers, any position drift between the master and the slave is avoided. The disadvantage of this approach, when compared to the parallel passivity control, is that the

dissipation behaviour introduces some noise in the form of vibrations and can at some moments feel slightly unnatural to the operator.

Using the 4-channel time-domain passivity framework, a better performance in terms of transparency, when compared to other time-domain passivity architectures, is obtained both with and without time delay.

CHAPTER 5

# Time-domain passivity control in 4-channel multi-dof bilateral teleoperation

J. Rebelo and A. Schiele

*IEEE International Conference on Intelligent Robots and Systems (IROS) 2015*,
(submitted)

**Abstract**

*Time-domain passivity control teleoperation has been shown to stabilize highly transparent one-dof time-delay bilateral teleoperation systems using the 4-channel architecture. However, multiple degrees-of-freedom are typically needed to execute meaningful tasks in teleoperation. This paper extends the 4-channel time-domain passivity control architecture to multi-dof. To dissipate the excess energy generated by the time-delay in the communication channel, two methods are analysed: uniform dissipation in all directions and dissipation in the direction of maximum velocity. The experimental results, using the Sensoric Arm Master arm exoskeleton controlling a Kuka Lightweight Robot in Cartesian space with a round-trip communication delay of 300 ms, demonstrate that the proposed multi-dof 4-channel time-domain passivity control framework is able to stabilize the system while retaining a high level of transparency. The results also show that, while different energy dissipation methods change the forces being transmitted to the operator by the passivity controller, neither stability nor transparency are affected.*

Figure 5.1: Bilateral teleoperation system with master exoskeleton device (on left) commanding an impedance-controlled Kuka Lightweight Robot (on right)

Teleoperation systems allow human operators to apply their planning and decision making capabilities on a remote location where a robotic system is operating. For human-like manipulation tasks to be executed, multiple degrees-of-freedom (DOF) have to be simultaneously controlled. However, in bilateral teleoperation, there is an inevitable time delay in the communication channel, which can easily make the system unstable [28] if no additional control measures are taken.

The use of passivity as a solution for this problem was originally proposed by Anderson and Spong [28] and Niemeyer [30], with the system being designed to be passive independent of the amount of delay in the communication channel. However, even though the proposed methods ensure stability for any constant delay, they are very conservative and reduce the transparency of the system. Time-domain passivity control [34], in which the passivity of the system is monitored in real-time and a variable damping element is used to dissipate energy when instability occurs, was introduced to address these issues. This framework was initially proposed for haptic interfaces exploring virtual environments and was later extended by Artigas *et al.* [80] for use in bilateral teleoperation with time delay. In the proposed solution, the energy input at each side is measured and transmitted over the communication channel to the opposite side. If the output energy is higher than the input energy, this means that the communication channel is generating energy, and thus potentially making the system unstable.

The time-domain passivity controller framework was first presented for the position-force architecture [81], which has a clear power network representation. Artigas *et al.* [36, 82] later introduced the concept of Time Delay Power Network (TDPN), which allowed the extension of the framework to the position-position architecture [36] and provided a higher level of abstraction. In [84] the authors have recently extended the framework for the 4-channel architecture [22], which has a better performance in terms of transparency both without and with time delay in the communication channel. The proposed solution made use of the TDPN concept while modelling all the controllers as voltage sources to avoid problems with position drift previously reported [35].

While these works have focused on the improvement of the time-domain passivity control functionality, most of the results have only been demonstrated and analysed on setups with 1 DOF. An extension to the time-domain passivity to multi-dof was presented by

Preusche *et al.* [37] for stable interaction with virtual environments. In [85], Ott *et al.* analysed the position-force time-domain passivity and proposed dissipating the energy in the nullspace direction with the results presented on a simulation.

It is the goal of this work to research how a multi-dof bilateral teleoperation system can be kept stable when using the 4-channel architecture with time-delay in the communication channel while keeping the highest possible transparency. This is achieved by extending the 4-channel time-domain passivity control method, presented by the authors in [84], to a generic multi-DOF scenario and exploring different energy dissipation strategies.

## 5.1 Multi-dof 4-channel bilateral control

The bilateral teleoperation control in this work is implemented using the 4-channel architecture [22] for all the Cartesian degrees-of-freedom of the system. The presented implementation considers using an impedance-type master to command an impedance-controlled slave. Using this architecture, the master sends both the position and orientation commands, as well as the actual force and torque exerted by the operator, to the impedance-controlled slave manipulator. The measured force and pose of the slave manipulator are sent back to the master device and used to compute the amount of force/torque that is rendered by the master device to the operator. A generic diagram of the complete teleoperation control architecture is shown in Figure 5.2.

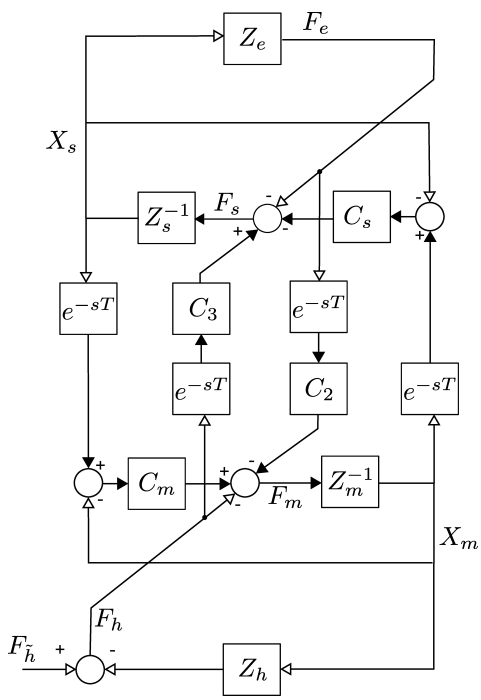


Figure 5.2: Bilateral teleoperation 4-channel control architecture

In multi-dof, the master joint torques resulting from the force-feedback commands can be calculated at each instant using the principle of virtual work as

$$\tau_m(t) = \mathbf{J}_m^T(\mathbf{q}(t))\Big[\underbrace{\mathbf{K}_2(\mathbf{q}(t))\mathbf{f}_e(t-T(t))}_{\mathbf{f}_{C_2}(t)} + \underbrace{\mathbf{K}_m(\mathbf{x}_s(t-T(t)) - \mathbf{x}_m(t))}_{\mathbf{f}_{Cm}(t)}\Big] \tag{5.1}$$

where $\tau_f$ is the master commanded joint torque vector, $\mathbf{K}_2$ is the master force channel diagonal gain matrix, $\mathbf{f}_e$ is the force-torque vector measured by the force-torque sensor mounted on the slave device, $T$ is the time delay measured at each time instant $t$, $\mathbf{K}_m$ is the master position channel diagonal gain matrix, $\mathbf{x}_s$ is the actual slave manipulator position and $\mathbf{x}_m$ the actual master position which corresponds to the slave manipulator reference.

On the slave side, both the stiffness $\mathbf{K}_s$ and damping $\mathbf{B}_s$ of the manipulator can be configured independently in each Cartesian direction. The joint torque commands for the slave manipulator are computed as

$$\tau_s(t) = \mathbf{J}_s^T(\mathbf{q}(t))\Big[\underbrace{\mathbf{K}_s(\mathbf{x}_m(t-T(t)) - \mathbf{x}_s(t))}_{\mathbf{f}_{Cs}(t)} + \underbrace{\mathbf{K}_3\mathbf{f}_h(t-T(t))}_{\mathbf{f}_{C_3}(t)} + \mathbf{B}_s(\dot{\mathbf{x}}_s(t))\Big] \tag{5.2}$$

where $\tau_s$ is the slave commanded joint torque vector, $\mathbf{K}_s$ is the slave Cartesian stiffness diagonal matrix, $\mathbf{K}_3$ is the slave force channel diagonal gain matrix and $\mathbf{f}_h$ is the force-torque vector measured by the force-torque sensor mounted on the slave device. Gravity, friction and other dynamic effects on the slave manipulator are considered to be compensated and, since the user has no control over them, they are explicitly left out of the computation.

## 5.2 Multi-dof 4-channel passivity control

To ensure system stability when time-delay is present in the communication channel, the 4-channel time-domain passivity control presented by the authors in [84] is used. This section descibes the multi-dof extension of the 4-channel passivity control. The method is based on monitoring the input and output energies at each side of the communication channel and it is therefore independent of the mechanical and control system parameters.

Assuming each of the controllers to be a dependent voltage source [84], the equivalent electrical scheme of the 4-channel architecture can be represented as shown in Figure 5.3.

Considering a multi-dof two-port, such as for example the $N_m$ network shown in Figure 5.4, the observed energy can be computed as

$$\begin{aligned} E_{obs}(n) &= \Delta T \sum_{k=0}^{n} [\mathbf{v}_l(k)\cdot\mathbf{f}_l(k) + \mathbf{v}_r(k)\cdot\mathbf{f}_r(k)] \\ &= \Delta T \sum_{k=0}^{n} [P_l(k) - P_r(k)], \end{aligned} \tag{5.3}$$

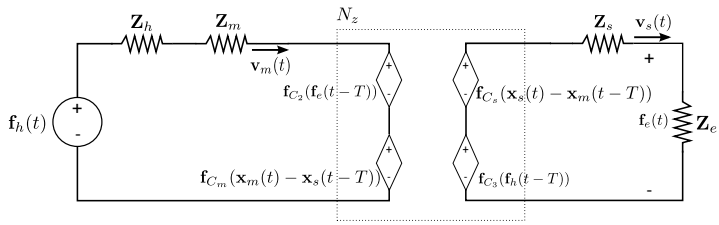


Figure 5.3: Electrical model of the multi-dof 4-channel bilateral teleoperation system

where $\mathbf{v}$ is the velocity, $\mathbf{f}$ is the force, $P$ is the power, the operator $\cdot$ is the dot product and the subscripts $l$ and $r$ represent the left and right sides of the operator, respectively. In this derivation it is assumed that the system sample time is much smaller than the system mechanical time-constants. The energy of the system can be divided in input and output energy for each side by computing

$$E_l^{\text{in}}(n) = \begin{cases} E_l^{\text{in}}(n-1) + \Delta T \cdot P_l(n) & \text{if } P_l(n) > 0 \\ E_l^{\text{in}}(n-1) & \text{if } P_l(n) \leq 0 \end{cases} \tag{5.4}$$

$$E_r^{\text{in}}(n) = \begin{cases} E_r^{\text{in}}(n-1) + \Delta T \cdot P_r(n) & \text{if } P_r(n) > 0 \\ E_r^{\text{in}}(n-1) & \text{if } P_r(n) \leq 0 \end{cases} \tag{5.5}$$

$$E_l^{\text{out}}(n) = \begin{cases} E_l^{\text{out}}(n-1) & \text{if } P_l(n) \geq 0 \\ E_l^{\text{out}}(n-1) - \Delta T \cdot P_l(n) & \text{if } P_l(n) < 0 \end{cases} \tag{5.6}$$

$$E_r^{\text{out}}(n) = \begin{cases} E_r^{\text{out}}(n-1) & \text{if } P_r(n) \geq 0 \\ E_r^{\text{out}}(n-1) - \Delta T \cdot P_r(n) & \text{if } P_r(n) < 0. \end{cases} \tag{5.7}$$

As shown in [80], a two-port operator is passive as long as the energy output at the left and right sides is always smaller than or equal to the energy input at the right and left sides, respectively. The energy in the communications two-port network is computed as

$$\begin{aligned} E_{N_z}(n) =& \Delta T \sum_{k=0}^{n} \mathbf{v}_m(k) \cdot \left[\mathbf{f}_{C_2}(k-T) + \mathbf{f}_{C_m}(k-T)\right] \\ &+ \mathbf{v}_s(k) \cdot \left[\mathbf{f}_{C_s}(k-T) + \mathbf{f}_{C_3}(k-T)\right], \end{aligned} \tag{5.8}$$

which can be divided into its components

$$E_{N_z}(n) = E_{N_m}(n) + E_{C_{rm}}(n) + E_{N_s}(n) + E_{C_{rs}}(n) \tag{5.9}$$

where $E_{N_m}$ and $E_{N_s}$ are the energies in the master and slave networks and $E_{C_{rm}}$ and $E_{C_{rs}}$ are the energies in the remote master and slave controllers. Each of these energies can be represented as

$$E_{N_m}(n) = \Delta T \sum_{k=0}^{n} \Big[ \mathbf{v}_m(k) \cdot [\mathbf{f}_{C_2}(k-T) + \mathbf{f}_{C_m}(k-T)] + \mathbf{v}_m(k-T) \cdot [\mathbf{f}_{C_2}(k) + \mathbf{f}_{C_m}(k)] \Big] \tag{5.10}$$

$$E_{N_s}(n) = \Delta T \sum_{k=0}^{n} \Big[ \mathbf{v}_s(k) \cdot [\mathbf{f}_{C_s}(k-T) + \mathbf{f}_{C_3}(k-T)] + \mathbf{v}_s(k-T) \cdot [\mathbf{f}_{C_s}(k) + \mathbf{f}_{C_3}(k)] \Big] \tag{5.11}$$

$$E_{C_{rm}}(n) = \Delta T \sum_{k=0}^{n} \Big[ -\mathbf{v}_m(k-T) \cdot [\mathbf{f}_{C_2}(k) + \mathbf{f}_{C_m}(k)] \Big] \tag{5.12}$$

$$E_{C_{rs}}(n) = \Delta T \sum_{k=0}^{n} \Big[ -\mathbf{v}_s(k-T) \cdot [\mathbf{f}_{C_s}(k) + \mathbf{f}_{C_3}(k)] \Big]. \tag{5.13}$$

Considering these energy separations the system can be represented using TDPN. Since each TDPN is a multi-dof two-port network, the passivity observers for the input and output energies can be implemented in the same manner as (5.4) to (5.7). When the energy output is larger than the energy input on the opposite side, the communication channel has an active behaviour, thus injecting energy into the system, which can make it potentially unstable. To ensure stability this excess energy has to be dissipated by means of a passivity controller. As shown by the authors in [84], it is sufficient to place passivity controllers on the master and slave output sides of the TDPN, since the voltage sources are assumed ideal, meaning they can both generate and absorb an infinite amount of energy. The system representation with TDPN and passivity controllers is shown in Figure 5.4.

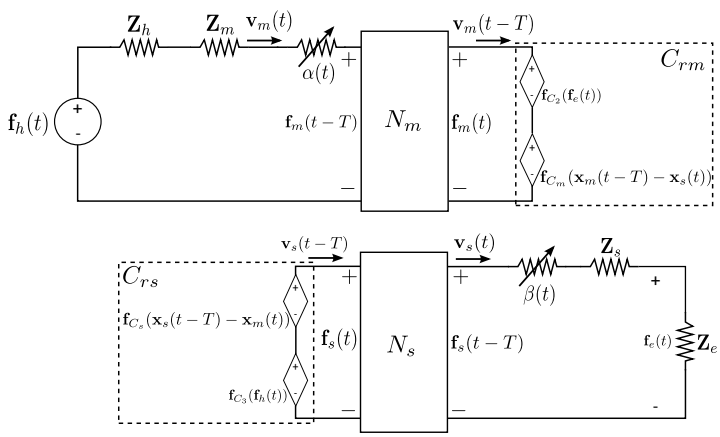


Figure 5.4: Electrical model of the multi-dof 4-channel bilateral teleoperation system with TDPN and passivity controller elements

In multi-dof excess energy can be dissipated in different manners. Independently of the

energy dissipation strategy, it is expected that using the proposed combination of passivity observers and controllers the multi-dof 4-channel can be made passive when time-delay is present on the communication channel.

## 5.3 Energy dissipation strategies

In this section two different methods for dissipating the excess energy introduced by the communication channel are presented. These methods are uniform energy dissipation and dissipation in the direction of maximum velocity. These two methods are chosen since they allow simple implementation but have significantly different behaviour. The computations done for the passivity controller elements using each of the principles are detailed in this section.

### 5.3.1 Uniform energy dissipation

In the uniform energy dissipation method, the energy to be dissipated is distributed in every direction for which the absolute velocity is above zero. The energy is dissipated equally in every direction which is expected to minimize its effect on the operator motion. Taking the master side as an example, the value of the series passivity controller for each Cartesian direction can be computed as

$$\alpha_i(n) = \begin{cases} \frac{\left(E_M^{\text{out}}(n) - E_M^{\text{in}}(n-T)\right)/d}{\Delta T \cdot v_{m_i}^2(n)} & \text{if } E_M^{\text{out}}(n) > E_M^{\text{in}}(n-T) \text{ and } v_{m_i}(n) \neq 0 \\ 0 & \text{otherwise,} \end{cases} \tag{5.14}$$

where $d$ is the number of directions in which energy is to be dissipated, and where the subscript $i$ is the actual direction for which the dissipation element is being calculated. The same calculation can be done for the slave side PC element $\beta$ by replacing the master energy and velocity values by the corresponding slave values.

### 5.3.2 Direction of maximum velocity

In the direction of maximum direction method, all the energy is dissipated in the direction for which the velocity is largest. A larger velocity means that more energy can be dissipated in one time step. This method is expected to reduce the amount of time during which the passivity controller is enabled, thus minimized the disturbances to the operator. In this case, the value of the series passivity controller for each Cartesian direction can be computed as

$$\alpha_i(n) = \begin{cases} \frac{\left(E_M^{\text{out}}(n) - E_M^{\text{in}}(n-T)\right)}{\Delta T \cdot v_{m_i}^2(n)} & \text{if } E_M^{\text{out}}(n) > E_M^{\text{in}}(n-T) \text{ and } v_{m_i}(n) \neq 0 \text{ and } i \Rightarrow \max \mathbf{v}_m \\ 0 & \text{otherwise,} \end{cases} \tag{5.15}$$

## 5.4 Experimental setup

An experimental setup composed of the Sensoric Arm Master (SAM) exoskeleton [86], used as a master device, controlling a 7-DOF Kuka Lightweight Robot (LWR) in impedance-control mode is used to evaluate the performance of the proposed passivity controller methods.

The SAM is a 7-DOF serial arm exoskeleton with each joint equipped with an incremental encoder and current-controlled locally using commercially available ELMO servo drives. The control algorithms are executed on a master control PC and the communication with the local controllers is done via an EtherCAT communication bus running at 1 kHz. To measure the end-effector force and torques between the operator and the exoskeleton an ATI Gamma 6 DOF force-torque sensor with a resolution of 0.01 N and 0.0005 Nm is mounted at the base of the joystick handle. The force-torque sensor readouts are sampled via UDP at the same frequency as the EtherCAT network.

The LWR, used as the slave device in this setup, is a commercially available 7 DOF lightweight robot which can be used directly in impedance-controlled mode using the Kuka Fast Research Interface (FRI) [87] at a frequency of 1 kHz. The Cartesian impedance can be configured in values ranging, approximately, from 200 N/m to 2000 N/m for translations and 2 Nm/deg to 500 Nm/deg for rotations. An ATI Gamma 6 DOF force-torque sensor with a resolution of 0.01 N and 0.0005 Nm is mounted on the robot tool to measure the actual contact forces and torques. Both the master and slave force-torque sensor readings are set to 0 when operation is started. The controllers for the two devices run on different computers which communicate with each other over UDP sockets with time-delay simulated using constant delay buffers. Figure 5.5 shows the master and slave devices with the respective Cartesian axis mapping. Further details on the system implementation can be found in [88].

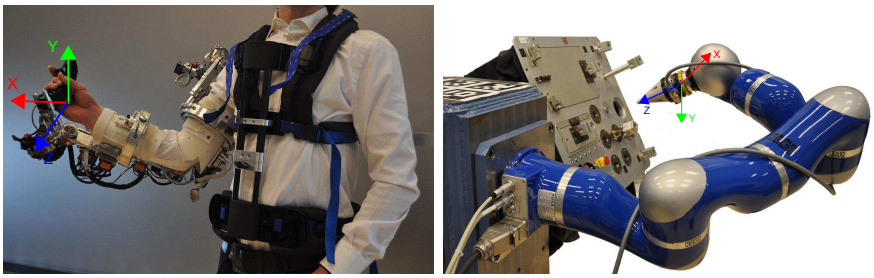


(a) SAM exoskeleton (b) Kuka Lightweight Robot

Figure 5.5: Master (a) and slave (b) devices and reference frames. The axis on the figure illustrate the mapping between the master and the slave devices.

In the presented experimental scenario, the operator is instructed to use the master device to command the slave into contact with a rigid environment, keep the contact for a few seconds, then release from contact and repeat the procedure. After two contacts, the operator makes some motion in free-air to analyse the position tracking behaviour of the system. The environment used in this experiment has a stiffness of approximately 5000 N/m.

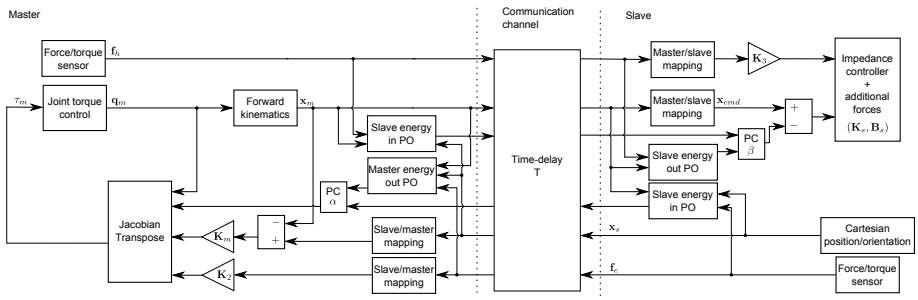


Figure 5.6: 4-channel bilateral teleoperation control architecture with communication time-delay.

The system is tested both with and without time-delay. The controllers parameters have been tuned to allow hard contacts to be rendered in a stable manner with time-delay up to 50 ms and have values of $\mathbf{K}_2 = \mathbf{K}_3 = \mathbf{I}_{6\times6}$, $\mathbf{K}_m = \mathbf{I}_{3\times3} \cdot 250$ N/m for translations and $\mathbf{I}_{3\times3} \cdot 2$ Nm/deg for rotational motions and $\mathbf{K}_s = \mathbf{I}_{3\times3} \cdot 800$ N/m for translations and $\mathbf{I}_{3\times3} \cdot 25$ Nm/deg for rotational motions. The rotational motion values are intentionally kept low since these motions do not play any role in the presented task. To evaluate the system behaviour, positions, forces and energy flows for both the master and the slave are recorded. The stored positions are the master actual position, corresponding to the slave command, and the slave actual position. In terms of forces, both the interaction force between the human and the master as well as the contact force between the slave and the environment are recorded. The input and output energy flows for each of the TDPN are also stored as well as the passivity controller force responses, when relevant. All the values refer to the LWR reference axes.

## 5.5 Results

In this section, the results obtained during teleoperation with the proposed control architecture are presented and analysed.

### 5.5.1 Teleoperation with 300 ms round-trip time-delay without passivity control

The performance of the system with a round-trip time-delay of 300 ms without passivity control is shown in this section. Figure 5.7 shows the position and force behaviour of the system. In free-air motion the position of the slave tracks the master position with errors up to approximately 20 mm and 0.02 rad. When contact occurs, at $t = 9$ s, the forces transmitted to the operator do not allow the contact with the remote environment to be kept. The motion observed between $t = 4$ s and $t = 9$ s is involuntary and caused by the system instability. The instability can be related to the excess of output energy on the master side, as shown in Figure 5.8.

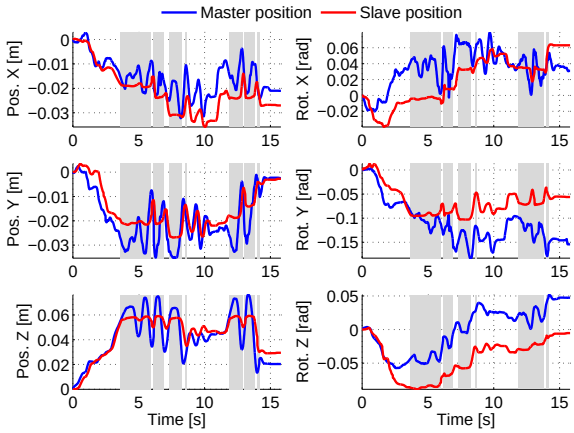


(a) Position response

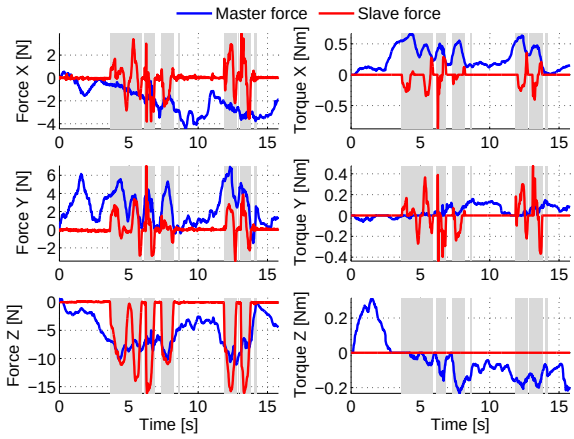


(b) Force response

Figure 5.7: Master and slave position and force behaviour in teleoperation with 300 ms round-trip time delay without passivity control. The grey areas represent moments in which the slave is in contact with the environment. The environment is placed normal to the Z direction of motion.

### 5.5.2 Teleoperation with 300 ms round-trip time-delay with passivity control

Using the passivity controller with uniform energy dissipation, with a communication round-trip time-delay of 300 ms, results in the position and force behaviour shown in Figure 5.9. Before the first contact occurs, the system remains stable without any effect from the passivity controller. In contact with the environment the system remains stable, with most of the PC effects happening when the operator is moving away from the contact ($t = 5$ s and $t = 11$ s). Using the uniform energy dissipation strategy, the PC generates forces of up

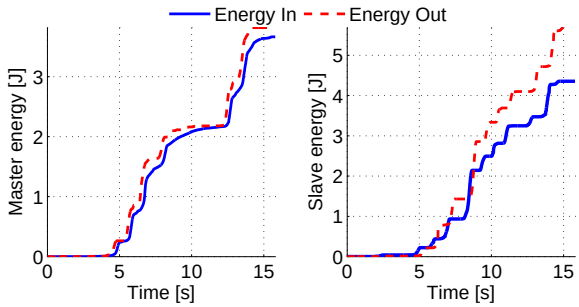


Figure 5.8: Master and slave energy flows in teleoperation with 250 ms round-trip time delay without passivity control.

to 2 N and torques of up to 1.5 Nm.

Using the passivity controller with dissipation in the direction of maximum velocity, results in a similar force and position behaviour of the system, as shown in Figure 5.10. In this case, the PC dissipates most of the energy with torque commands up to 8 Nm.

Analysing the master and slave input and output energies shown in Figure 5.11 it can be seen that, using the passivity controller, the input and output energies are always approximately equal, independently of the energy dissipation strategy.

### 5.5.3 Analysis and discussion

When a 300 ms time delay is present in the communication channel the operator is still able to control the system in a stable manner in free-air, however, as shown in Figure 5.7, once the rigid contact is touched by the slave, the operator is unable to remain in contact. This instability would prevent the operator from executing any task since it is not possible to interact with the remote environment. The instability can be related to the large difference between the output and input energies visible in Figure 5.8.

As shown both in Figure 5.9 and 5.10, using the 4-channel passivity control scheme, the system remains stable independently of the energy dissipation method, with the operator able to stably interact with the environment. When using the uniform energy dissipation method, the operator feels small forces applied to every direction of motion, which cause only small disturbances. Using the dissipation in the direction of maximum velocity results in larger forces being applied in a single direction which are sometimes more complicated for the operator to handle. In all cases, the PC forces behave in a oscillatory manner and introduces some vibrations in the structure which can be clearly felt by the operator. The overall behaviour of the system is highly dependent on how the human operator interacts with the master device, on the characteristics of the remote environment and on the controller parameter settings. Further studies are needed to understand how these combined effects influence the human operator task performance.

Table 5.1 shows the stiffness rendered to the operator computed from the force and position values reported. As it can be seen, for both energy dissipation methods the system renders a transparency of approximately 80%. This shows that the 4-channel time-domain

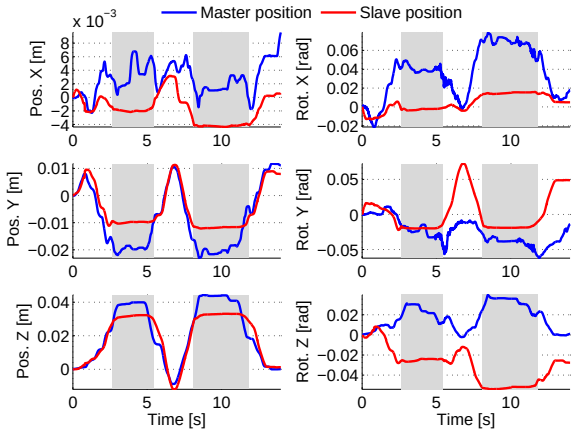


(a) Position response

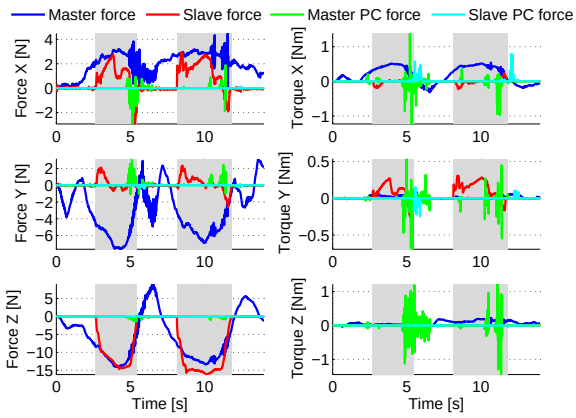


(b) Force response

Figure 5.9: Master and slave position and force behaviour in teleoperation with 300 ms round-trip time delay with passivity control and uniform energy dissipation.

Table 5.1: Stiffness rendered to the operator in contact with 5000 N/m environment with 300 ms round-trip time-delay

| | No PC | PC with uniform energy diss. | PC dissipation max. vel. |
|---|---|---|---|
| Rendered stiffness [N/m] | Unstable | 4000 | 3800 |

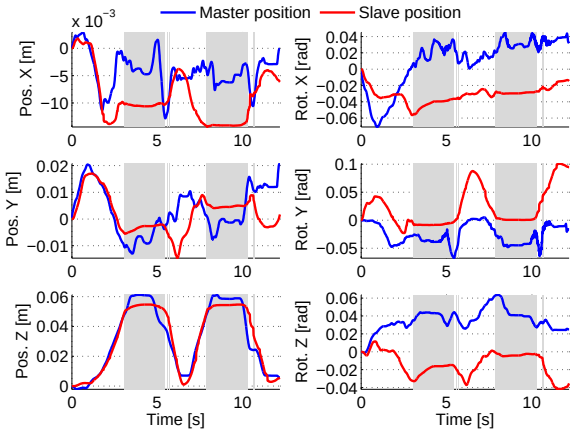


(a) Position response

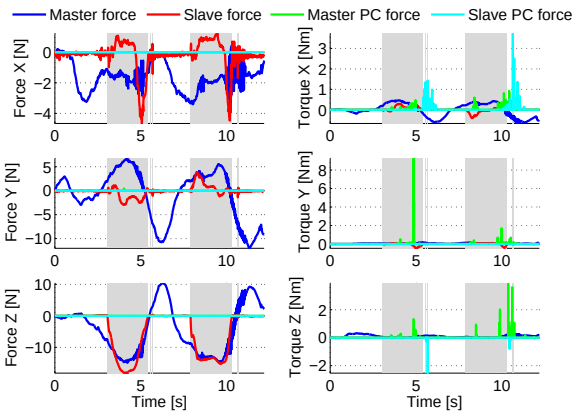


(b) Force response

Figure 5.10: Master and slave position and force behaviour in teleoperation with 300 ms round-trip time delay with passivity control and dissipation in the direction of maximum velocity.

passivity control can be used to ensure high transparency in time-delay bilateral teleoperation.

## 5.6 Conclusions

The proposed time-domain passivity method is able to stabilize a multi-dof bilateral system being controlled using the 4-channel architecture. This system provides a high level of transparency while still ensuring stability for the presence of time delay in the communication channel.

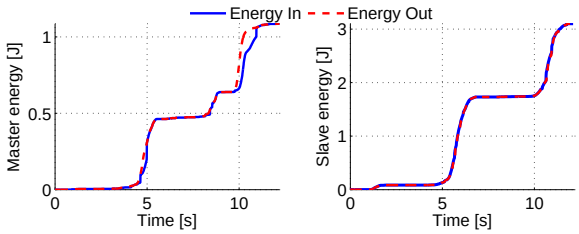


(a) Uniform energy dissipation

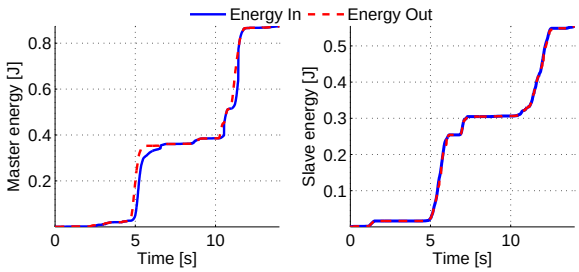


(b) Dissipation direction max. velocity

Figure 5.11: Master and slave energy flows in teleoperation with 300 ms round-trip time delay with passivity control.

The effects of the PC on the operator are highly dependent on the energy dissipation method. However, as long as all energy is dissipated, both the stability and high transparency performance of the system are guaranteed using this system.

# Part III

# Multi-dof bilateral teleoperation

CHAPTER 6

# An intuitive and portable haptic arm exoskeleton workstation for bilateral robot teleoperation

J. Rebelo [1], T. Sednaoui, E. Den Exter, T. Krueger and A. Schiele
*IEEE Robotics and Automation Magazine, vol. 21, no.4*, December 2014

**Abstract**

*Currently existing state-of-the-art haptic master devices with human-like workspaces are based on heavy robotic manipulators which are not wearable and not easily portable. In many applications, in particular in space teleoperation, portable lightweight master devices are needed. It is the goal of this work to develop a complete end-to-end teleoperation system using a portable arm exoskeleton to control a 7-DOF slave manipulator with transparent force-reflection to the operator. The proposed master device architecture makes use of local joint controller communicating over an EtherCAT bus for high performance and using a tablet computer for a high-level Graphical User Interface. The results show that using the developed exoskeleton haptic device as the controller for the 7-DOF Kuka Lightweight robot in impedance-mode, with a system control frequency of* 1 *kHz, contact with surfaces of different stiffness are able to be accurately rendered to the operator.*

[1] In this work, the author was responsible for the mapping between the master and slave devices and the control algorithms implementation and partially responsible for the hardware implementation

## 6.1 Introduction

Teleoperation systems are used when the human planning and decision-making capability is needed during robotic remote operations. To execute meaningful tasks remotely, the operator has to be able to simultaneously control multiple degrees-of-freedom of the slave robot and to efficiently receive information from the remote site. In these cases, haptic feedback has been shown to improve the operator task execution performance [1].

The potential applications of teleoperation systems are in areas so diverse as remote handling of hazardous materials [89], underwater maintenance and repairing tasks [90] or space exploration scenarios [59]. In all these applications the tasks occur in a remote location at which, due to accessibility, cost and/or safety reasons, a robotic system is better suited to operate than a human.

In many cases the remote teleoperation of robot manipulators is done using joystick interfaces and multiple screens with complex user interfaces [91]. These type of systems are not intuitive and a large amount of training hours is required for an operator to achieve a reasonable performance level. In this scope a system composed of a wearable haptic device, combined with a single touch-screen user interface can provide a much more intuitive interface for the user to teleoperate full remote robotic systems. In particular, when the system is to be used in space teleoperation the device must be both light and portable such that it can be easily worn and adapted to differential operational scenarios.

Currently existing state-of-the-art haptic master devices with human-like workspaces such as the ViSHaRD10 [92] or the DLR bimanual interface [93] are based on heavy robotic manipulators which are not wearable and not easily portable. A haptic exoskeleton for interaction with virtual environments was presented in [94] however the device is also not portable and is limited to 5 DOF. Under the scope of European Space Agency programmes, both the Sensoric Arm Master [86] and the X-Arm2 [58] haptic exoskeletons for teleoperation were developed. While the mechanics of both devices are lightweight, the portability is limited by the lack of body orthosis and dependence on desktop computers and large external hardware for control of the system. Other types of exoskeletons have been presented in literature for different applications such as power augmentation [95], which focus on allowing the user to transport heavy loads rather than on accurate force rendering, or rehabilitation [96] where the goal is typically to allow the user to exercise certain joints for physical recovery. This distinct set of requirements makes these types of exoskeletons unsuitable for teleoperation. A recent review of different upper limb exoskeleton devices can be found, for example, in [97].

In terms of performance, it was shown in [22] that perfect transparency in 1 DOF can be achieved by using a 4-channel control architecture. The devices presented in [94] and [86] have shown good capabilities for rendering virtual environments however no performance while controlling robotic manipulators was reported. The position-force architecture using the ViSHaRD10 [92] to control a 7 DOF manipulator allows executing a stiffness discrimination and a screwing task in teleoperation, however a low level of transparency, which is typical in this architecture, is reported in the results.

It is the goal of this work to develop a complete end-to-end teleoperation system using the modified Sensoric Arm Master (SAM) exoskeleton as a haptic master device to control a 7-DOF Kuka Lightweight Robot (LWR) with transparent force-reflection to the operator.

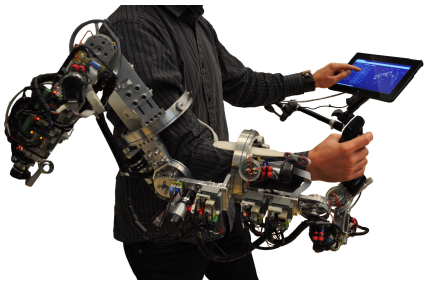

Figure 6.1: Sensoric Arm Master exoskeleton being worn by an operator

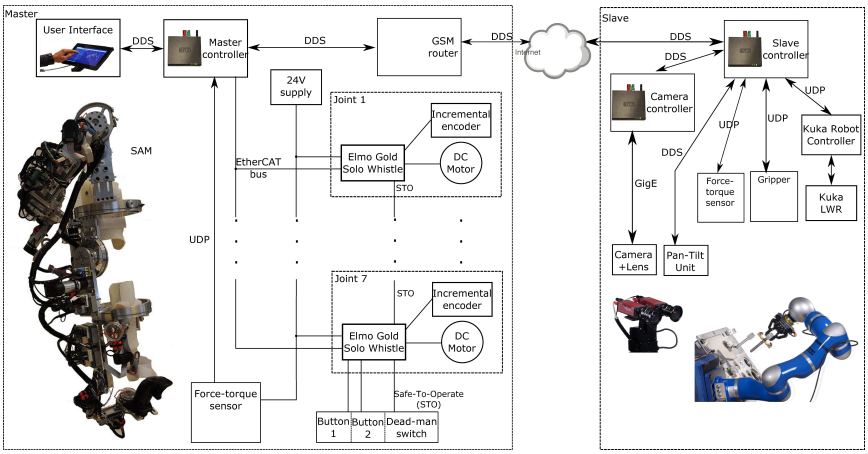


Figure 6.2: System architecture overview

The new master implementation allows having, for the first time, a completely portable wearable master exoskeleton featuring an intuitive user interface both in terms of robot control and system operation. A Cartesian multi-dof 4-channel architecture [22] which provides a high level of transparency to the operator is implemented and validated using the setup. This system can be used to perform generic teleoperation tasks and provides a first step towards a technology demonstration experiment that will be carried out on-board the International Space Station in the coming years [59]. While the system used is very specific, the discussion aims to be as generic as possible regarding the implementation of multi-dof bilateral teleoperators using wearable haptic master devices.

## 6.2 System architecture

The bilateral teleoperation system presented in this article consists of a 7 DOF exoskeleton arm master used by a human operator to control a 7 DOF slave robot. The local joint control of the master device is implemented using distributed servo drives communicating

using a state-of-the-art EtherCAT network, while the communication between the master and the slave devices is achieved using User Datagram Protocol (UDP) communication. The high-level control of the system by the operator is performed via a web-based Graphical User Interface (GUI) on a tablet computer which communicates with the remaining components of the system using the Data Distribution Service (DDS) communication middleware. The master device being worn by an operator is shown in Figure 6.1, with the system architecture depicted in Figure 6.2. The remaining of this section explains each of the components in this architecture in detail.

### 6.2.1 Sensoric Arm Master

***Exoskeleton***

The Sensoric Arm Master (SAM) [86] is a serial kinematics exoskeleton, isomorphic to the human arm. It has 7 DOFs from the shoulder to the wrist, as shown in Figure 6.3. The link lengths between joint 3 and 4, joint 5 and 6 and joint 7 and the joystick handle are adaptable using sliding mechanisms and have to be adjusted depending on the operator dimensions to allow adequate alignment with the human arm joints. The kinematics have been implemented such that singularities of the mechanism are placed outside the human operator reachable workspace. All the joints are actuated using a combination of DC motors and capstan gears for low friction and backdrivability. The joint torques were initially designed to be 1/20th of maximum human torque with additional torque included in joints 3 and 5 to allow for friction compensation of the open bearings. Given the fact that only commercially available DC motors are used and gear ratio limitations these torques do not correspond exactly to the design target. Table 6.1 gives a summary of the actual exoskeleton torques and typical and maximum human torques for each joint. More details on the mechanical design of the device can be found in [86].

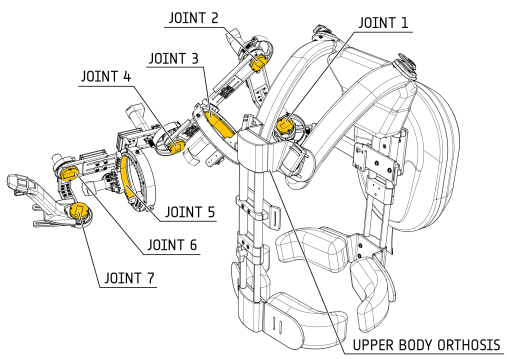


Figure 6.3: SAM joint configuration and upper body orthosis

Every joint is equipped with an incremental encoder and is current-controlled using commercially available ELMO servo drives. The exoskeleton control algorithms are executed on a master control PC and the communication with the individual ELMO drives

Table 6.1: SAM joint torque output

| Joint | SAM continuous/stall torque [Nm] | Typical human torque in daily life [Nm] [98] | Max. human arm torque [Nm] [98] |
|---|---|---|---|
| 1 | 4.4 / 19.7 | 10 | 134 |
| 2 | 4.4 / 19.7 | 9.6 | 115 |
| 3 | 6 / 27 | 3.1 | 60 |
| 4 | 3.6/16.4 | 3.8 | 72 |
| 5 | 2.2 / 7.7 | 0.4 | 9 |
| 6 | 0.4/1.7 | 0.38 | 21 |
| 7 | 0.4/1.7 | 0.25 | 20 |

installed throughout the arm is done via an EtherCAT communication bus [99]. Each of the 7 EtherCAT slaves has a local current control loop which is driven by the EtherCAT bus. The communication runs over the Ethernet physical medium, implementing a specific summation process and logical addressing system that optimizes the bandwidth usage and ensures real-time communication. The architecture requires a master device which addresses the slaves in the network. The implementation of the EtherCAT master used in this work is based on the open source SOEM master [100] for its low level protocols and runs on any computer with the Linux operating system. Additionally, the protocol provides means for using a distributed clock which ensures that all the devices in the bus run in a synchronous manner.

To measure the end-effector force and torques between the operator and the exoskeleton an ATI Gamma 6 DOF force-torque sensor with a resolution of 0.01 N and 0.0005 Nm is mounted at the base of the joystick handle. The force-torque sensor readouts are sampled via UDP at the same frequency as the EtherCAT network.

As a safety mechanism, a dead-man switch is present on the operator joystick and the drive electronics hardware is only enabled when this button is pressed by the user. The Safe-To-Operate (STO) signal of the ELMO drives is used for this purpose. Two additional multi-purpose digital inputs, corresponding to buttons 1 and 2 in Figure 6.2, are available.

To minimize the hardware footprint and keep the system portable, all the control algorithms and the EtherCAT master are executed on a FitPC2 ($10 \times 10 \times 3$ cm) running Xenomai real-time Linux. The whole system is powered from a Lithium Polymer battery pack. Using this configuration, a maximum achievable control bandwidth of 1 kHz was reached over the full exoskeleton system. The same embedded PC is also used to handle the connection to the LWR through UDP and the DDS interface to the GUI.

### *Graphical User Interface*

The high level system state control and user interaction is done by using a GUI on a touch-screen. For the implementation, a state-of-the-art cross platform approach using HTML, CSS and JavaScript has been chosen. Using these languages, the GUI can be ported to any platform which has a compatible web browser or even converted to a native app. The data communication between the master controller and the GUI is done using the

DDS communication middleware [101]. The middleware provides a loosely coupled data-centric publisher-subscriber system featuring a broad number of Quality of Service (QoS) settings. To define the data that is published or subscribed only a single data interface file needs to be created by the developers. The middleware takes care of all the connectivity and delivery within different networks and eases the development and portability as well as the possibility to extend the system by connecting other devices.

The GUI runs on a tablet computer which the user can operate while wearing the exoskeleton. This means that all the controls are accessible during operation. The interface is currently used for initial joint calibration and for starting and stopping the teleoperation. Since DDS messages can't currently be read directly by Javascript, a custom made DDS/Websocket bridge runs on a machine in the same network. This bridge reduces the maximum data update rate to approximately 40 to 60 Hz, which is nonetheless sufficient for typical GUI purposes. Figure 6.4 shows an example of the user interface screen during operation.

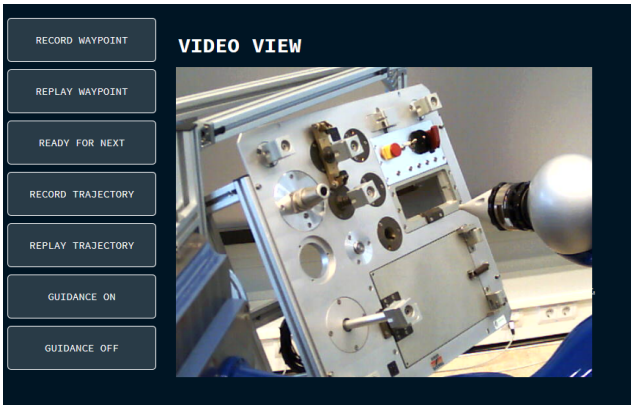


Figure 6.4: GUI during operation phase. The GUI provides the remote site video feed to the operator as well as additional information on the master and slave status and access to all the high level control of the system.

### *Upper body orthosis*

To make the exoskeleton portable, a dedicated upper body orthosis was built. The design consists of a vest that can be strapped to the operator's body in order to transfer load away from the arm and onto the body. During development, static and dynamic anthropometric factors were taken into account to ensure a close and comfortable fit to operators of different statures and body sizes. In addition, the vest includes design features present in most mountaineering backpacks to ensure maximum load transfer to the hips of the operator.

Figure 6.5 shows the prototype of the vest with the SAM exoskeleton mounted to the back. On the front and back of the vest a telescopic frame was implemented to provide adjustability to fit different operator statures in addition to being a generic mounting interface for exoskeletons.

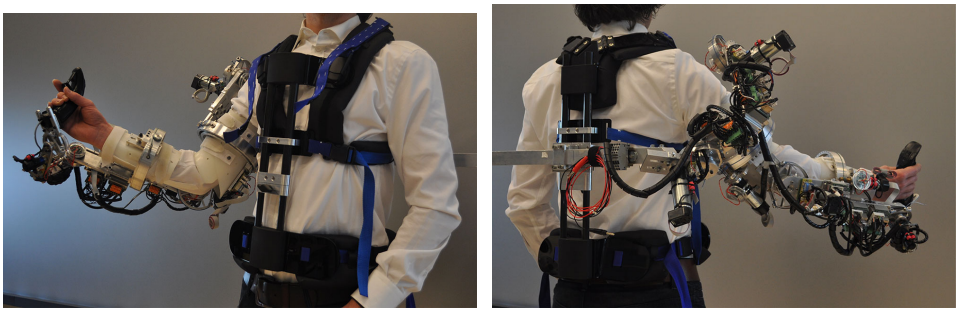

(a) Front view (b) Back view

Figure 6.5: Operator wearing the SAM exoskeleton with the upper body orthosis. The telescopic frames implemented in the front and the back to provide adjustability to operators with different statures are visible in the figures.

### 6.2.2 Kuka Lightweight Robot

The LWR, used as the slave device in this setup, is a commercially available 7 DOF lightweight robot which can be used directly in impedance-controlled mode. The Cartesian impedance can be configured in values ranging, approximately, from 500 N/m to 2000 N/m for translations and 10 Nm/deg and 500 Nm/deg for rotations. The damping can be configured at joint level between $0.1\,\mathrm{Nm}\cdot\mathrm{rad}^{-1}\cdot\mathrm{s}$ and $2\,\mathrm{Nm}\cdot\mathrm{rad}^{-1}\cdot\mathrm{s}$. An ATI Gamma 6 DOF force-torque sensor with a resolution of 0.01 N and 0.0005 Nm is mounted on the robot tool to measure the actual contact forces and torques. Both the master and slave force torque sensor are set to 0 when operation is started. The manipulator is controlled using the Kuka Fast Research Interface (FRI) [87] at a frequency of 1 kHz. Using this interface it is possible to control both the tool Cartesian pose and forces/torques as well as the stiffness and damping of the robot.

## 6.3 Control architecture

This section describes the control structure of the bilateral teleoperation system. The first part gives a brief description of the Cartesian mapping between the master and the slave devices and the second part describes the 4-channel bilateral control architecture.

### 6.3.1 Master/slave mapping

In typical teleoperation scenarios two types of mapping between master device and slave robots are used, either *indexed*, i.e. the operator moves to an arbitrary position and the control starts relative to this initial point or *absolute*, in which the master and slave devices are aligned before starting the operation according to a predefined mapping.

In this work, a 6 DOF indexed Cartesian mapping, between the master and the slave device is used. The end-effector pose of the master device is computed using its forward

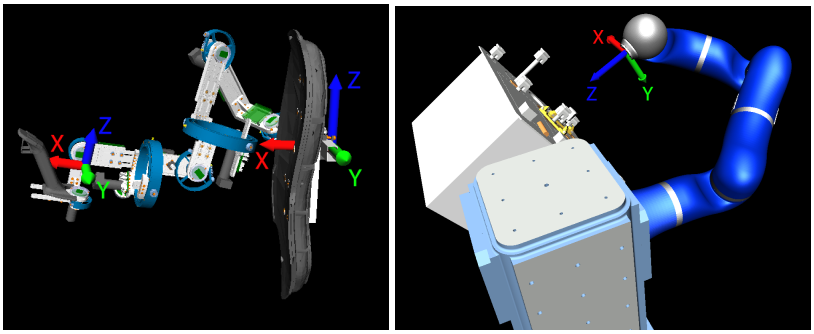


Figure 6.6: Master-slave initial mapping and reference frames. The LWR world frame is not explicitly shown since all the motion happens relative to the initial tool frame. The X, Y and Z axis of the SAM are mapped to the X, Z and -Y axis of the LWR, respectively.

kinematics and the difference between the actual and the start pose is computed and converted to a pose command to the LWR. There is no scaling between the measured and the commanded motion, i.e. a 1 cm motion at the master side corresponds to a 1 cm motion command at the slave side. Figure 6.6 shows a typical initial configuration mapping and reference frames for both the master and the slave. Given the orientation of the two devices and the camera image angle, the X, Y and Z axis of the SAM are mapped to the X, Z and -Y axis of the LWR, respectively. This transformation corresponds to a rotation which can be defined in matrix format as

$$\mathbf{R}_{\text{SAM}}^{\text{LWR}} = \begin{bmatrix} 1 & 0 & 0 \\ 0 & 0 & 1 \\ 0 & -1 & 0 \end{bmatrix} \tag{6.1}$$

### 6.3.2 4-channel bilateral teleoperation control

The bilateral teleoperation control is done using the 4-channel architecture [22] implemented for all the Cartesian degrees-of-freedom of the system. Using this architecture the master sends both position commands and the actual force the operator is exerting to the impedance-controlled slave manipulator. The measured force and position of the slave manipulator are sent back to the master device and used to compute the amount of force that is transmitted to the operator. Additionally, the weight of the master device felt by the operator can be reduced by a gravity compensation algorithm. The complete teleoperation control architecture is shown in Figure 6.7.

The master joint torques resulting from the force-feedback commands can be calculated at each instant using the principle of virtual work as

$$\tau_f(t) = \mathbf{J}_m^T(\mathbf{q}) \left[ \mathbf{K}_2(\mathbf{q}(t))\mathbf{f}_e(t) + \mathbf{K}_m(\mathbf{x}_s(t) - \mathbf{x}_m(t)) \right] \tag{6.2}$$

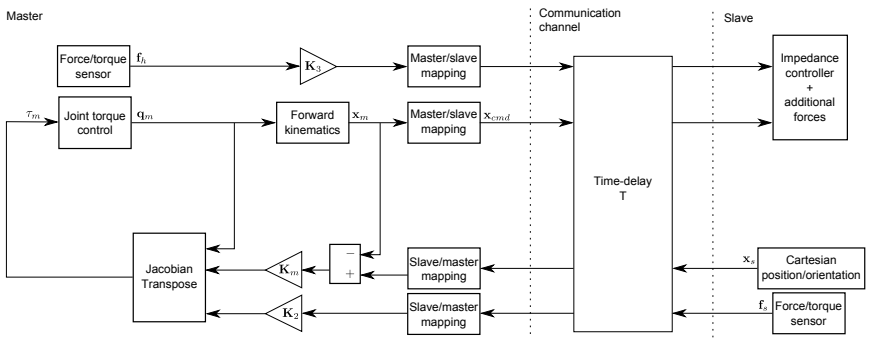


Figure 6.7: Teleoperation 4-channel control architecture.

where $\tau_f$ is the master commanded joint torque vector, $\mathbf{K}_2$ is the master force channel diagonal gain matrix, $\mathbf{f}_s$ is the force-torque vector measured by the force-torque sensor mounted on the slave device, $\mathbf{K}_m$ is the master position channel diagonal gain matrix, $\mathbf{x}_s$ is the actual slave manipulator position and $\mathbf{x}_m$ the actual master position which corresponds to the slave manipulator reference. The gravity compensation algorithm is implemented to compute the torque caused by gravity on each link $i$ as detailed in, for example, [102].

On the slave side, both the stiffness $\mathbf{K}_s$ and damping $\mathbf{B}_s$ of the manipulator can be configured independently in each Cartesian direction using the FRI interface. The joint torque commands in the slave manipulator are computed as

$$\tau_s(t) = \mathbf{J}_s^T(\mathbf{q}) \left[ \mathbf{K}_s (\mathbf{x}_m(t) - \mathbf{x}_s(t)) + \mathbf{K}_3 \mathbf{f}_h(t) + \mathbf{B}_s (\dot{\mathbf{x}}_s(t)) \right] \tag{6.3}$$

where $\tau_s$ is the slave commanded joint torque vector, $\mathbf{K}_s$ is the slave Cartesian stiffness diagonal matrix, $\mathbf{K}_3$ is the slave force channel diagonal gain matrix and $\mathbf{f}_m$ is the force-torque vector measured by the force-torque sensor mounted on the slave device. The LWR controller internally compensates for gravity, friction and other dynamic effects of the manipulator, however since the user has no control over these parameters they are explicitly left out of computation.

Following the tuning rules given in [22], using this control architecture and making $\mathbf{K}_2 = \mathbf{K}_3 = \mathbf{I}$ is expected to provide the user with perfect contact transparency. However, in this case, since the joint friction and other dynamic effects of the master device are not compensated, the operator will feel additional force in free-air, which deviates from perfect transparency in this condition.

## 6.4 Bilateral teleoperation performance

This section shows the performance of the complete bilateral teleoperation system when using the SAM exoskeleton to command the LWR, both in free-air and contact. In the presented experimental scenario the operator is instructed to drive the slave manipulator into contact with three surfaces with a different stiffness, keeping the contact with it for a

couple of seconds. The surfaces are a soft foam, a hard foam and a rigid metal plate. This is a typical stiffness discrimination task which is common in many teleoperation scenarios. To facilitate the analysis, the results presented correspond only to Cartesian positions. Since rotational motion is not required to execute this task, they are not commanded and their stiffness setting is kept at maximum to prevent motion. Nonetheless, end-effector rotations can also be controlled by the setup, with a motion and force behaviour similar to that of the Cartesian positions.

Figure 6.8 shows the Cartesian position and force performance of the system in bilateral teleoperation with $K_s = 1000\,\mathrm{N/m}$, $B_s = 0.7$, $K_m = 150\,\mathrm{N/m}$ and $K_2 = K_3 = 1$ with all the values identical in every Cartesian direction and 30% gravity compensation. The parameters were tuned following the transparency rules detailed in Section 6.3. Additionally, the position channel gains were chosen such that a satisfactory position tracking behaviour of the slave was achieved. The plotted forces correspond to the commanded and force/torque sensor measurements at the master and to the force/torque sensor measurements at the slave.

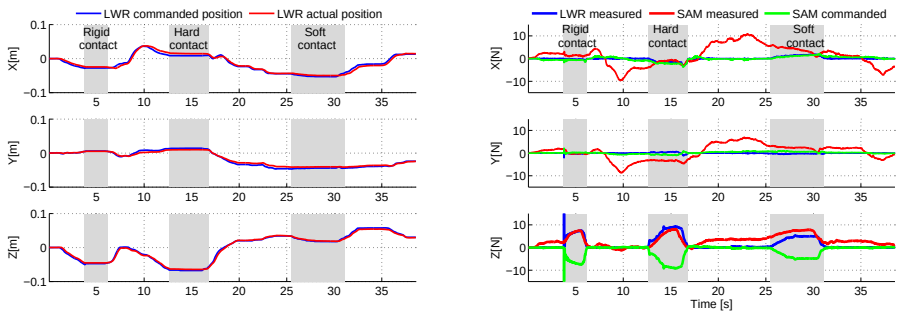


(a) Master and slave positions

(b) Master and slave forces

Figure 6.8: Master-slave position and force behaviour during the stiffness discrimination task with $K_s = 1000\,\mathrm{N/m}$, $B_s = 0.7\,\mathrm{N \cdot m^{-1} \cdot s}$, $K_m = 150\,\mathrm{N/m}$ and $K_2 = K_3 = 1$ with all the values identical in every Cartesian direction. The shadowed areas represent the moments in which the manipulator is in contact with the environment. The SAM commanded force does not include the gravity compensation commands.

As shown in Figure 6.8, the robot manipulator follows the master trajectory in each Cartesian direction with negligible errors. In free-air motion, even though there are no forces commanded to the operator, the interaction force measured at the master has a value of up to 10 N in the X direction and 5 N in both the Y and Z directions.

The contacts with the rigid, hard and soft surfaces occur in the Z direction between 3 and 6 seconds, 12 and 16 seconds and 25 and 31 seconds, respectively. In both the rigid and the hard contact, the forces rendered to the operator accurately follow those measured at the slave end-effector. In the soft contact there is a deviation of approximately 2 N between the force rendered to the operator and the force exerted by the slave on its environment. At impact between the slave and the rigid surface ($t = 3\,\mathrm{s}$) a force peak of more than 10 N

Table 6.2: Comparison between actual and rendered stiffness for different surfaces

| Surface | Actual [N/m] | Rendered [N/m] |
|---|---|---|
| Rigid | $5.2 \cdot 10^5$ | $4.5 \cdot 10^4$ |
| Hard | 4910 | 4620 |
| Soft | 250 | 400 |

occurs which is not transmitted to the operator. Throughout the entire operation the system is stable, showing no oscillations and no involuntary losses of contact.

Table 6.2 shows the actual and rendered stiffness for each of the surfaces, estimated from the position and force data of the master and slave, respectively. The rigidity of the surface rendered to the operator is one order of magnitude smaller than that of the actual surface whereas the hard and soft surfaces have very approximate values.

## 6.5 Discussion

In this section both the system implementation and control advantages and disadvantages are discussed in regard to design decisions and possible future improvements.

### 6.5.1 System implementation

The system hardware presented is a fully integrated solution for a portable bilateral teleoperation workstation. The developed orthosis is of particular importance since it allows the user to carry the whole mass of the exoskeleton (approximately 7 Kg) in a backpack-like fashion. During tests, in which several operators carried the exoskeleton on their body, many positive reactions were observed and demonstrated the feasibility of a comfortable portable exoskeleton.

Using the EtherCAT protocol allowed reaching high performance control bandwidths while keeping a reduced hardware size and weight. The downside of the protocol is its complexity, especially the fact that each slave in the network needs to be configured individually at start-up and multiple algorithms are necessary on the master to handle the distributed clock of the system.

Having the GUI running on a tablet allows the user to view the video feed and execute high-level control of the system (e.g. start/stop commands or online parameter adaptation) while still being able to control the robot using the exoskeleton. The multi-platform nature of the interface and the use of DDS is also advantageous since the GUI can easily be deployed on other machines, thus allowing easy reconfiguration of the system according to the operation needs.

Two fundamentally different communication approaches exist intentionally within the system. A message-centric approach using UDP is implemented for the master-slave communication that takes place in real-time, while a data-centric approach has been chosen for the GUI for its flexibility and easy reconfiguration. In the future, DDS, with its multiple QoS options can also be used on the real-time links.

### 6.5.2 Teleoperation control and performance

From the system performance results presented in Section 6.4, it can be seen that using the 4-channel architecture with the SAM exoskeleton controlling the LWR in impedance-control mode achieves a high level of transparency in both free-air and contact. The stiffness rendered to the operator for different surfaces allows a clear distinction to be felt between them.

Analysing the impact with rigid contact in Figure 6.8 at $t = 3$ s it can be observed that the high frequency components of the force are not transmitted to the operator. Nonetheless the transition between free-air and contact feels very crisp and is clearly distinguishable from the transition between free-air and hard contact.

In free-air motion the dynamics of the master device are felt by the operator, in particular the effects of gravity and friction in the joints. Given the mass of the device, the used DC motors are not able to fully compensate for gravity while still having enough power to generate force feedback to the operator. With 30% gravity compensation the user can operate the device more comfortably while the motors can still provide sufficient torque for accurate force-feedback rendering. Since the force/torque sensors are reset to 0 at the start of the operation, to prevent the uncompensated effects of gravity on the master side to be transmitted to the slave, these effect are not visible in the measured SAM forces. The forces caused by friction are always below 10 N and are therefore causing little effect to the operator. It was shown in [86] that these values could be further reduced using model-based compensation.

As shown in Figure 6.8, the commanded forces are not exactly rendered to the operator, which is expected given the open loop control of the joint torque controller. Nonetheless, the stiffness rendered to the operator has enough accuracy to clearly distinguish between the different types of contact. The effects of different controllers with local force and torque control loops should be studied in the future. Additionally, how the accuracy of the environment rendered to the operator affects task performance is a continuous research question in the field. This system provides the means to investigate this in more depth.

## 6.6 Conclusion

The system presented in this paper allows 6 DOF bilateral teleoperation with a high level of transparency. Using the SAM haptic device as the controller for the Kuka LWR in impedance-mode, with a system control frequency of 1 kHz, contact with surfaces of different stiffness are able to be accurately rendered to the operator.

Making use of the EtherCAT bus enables the high performance haptic master to have a modular architecture with a very small, distributed hardware footprint. This modular design combined with the adjustable body orthosis and the tablet interface makes the SAM workstation a fully portable teleoperation master with a human-like workspace.

CHAPTER 7

# Multiple degree-of-freedom bilateral teleoperation over mobile Internet network

J. Rebelo, S. Kimmer, E. Matheson and A. Schiele
*International Journal of Field Robotics*, (submitted)

**Abstract**

*Currently existing bilateral teleoperation systems do not allow task execution with a high level of transparency over low bandwidth communication networks with time-delay. The goal of this work is to develop a complete teleoperation system which can be used to execute 6-DOF tasks with force-feedback over an uncertain delayed communication link. The system implementation is based on the Sensoric Arm Master portable exoskeleton as the master device commanding an impedance-controlled Kuka Lightweight manipulator. The bilateral control is implemented using the 4-channel architecture with time-domain passivity control to ensure stability independently of the communication network characteristics. Video and data communication between the master and the slave side occurs over a bandwidth limited mobile Internet connection with an average* 100 *ms delay and* 17% *data loss. To handle the network limitations, video is compressed to keep the bandwidth usage to 96kbits/s. The results for a contact task with different environments show that the system remains stable at all time and that soft environments are accurately rendered but limited transparency is achieved for hard and rigid environments. In free-air, since weight and friction of the master device are not compensated, the operator feels forces up to 10N. The capabilities of the system to execute a 6-DOF activities are demonstrated by executing a complex peg removal task.*

## 7.1 Introduction

Robots are particularly well suited for executing tasks that occur in locations that are too dangerous for or inaccessible by human operators. However, for robot manipulators executing complex activities in unknown, unstructured environments - despite the recent increases in computation power - human input is still required for task planning and execution. To execute meaningful tasks remotely, the operator has to be able to simultaneously control multiple degrees-of-freedom of a slave robot and to efficiently receive information from the remote site. In these cases, haptic feedback has been shown to improve the operator task execution performance [1]. Such bilateral teleoperation systems can be used for applications in space exploration [58], nuclear material handling [1] and robotic surgery [2].

Current existing state-of-the-art teleoperation systems, such as the Da Vinci surgical system, [2], allow controlling robots in multi-dof, however no force-feedback is provided to the operator. While the system enables various surgical tasks to be executed, operations require a large amount of training and complex activities are limited to a few, very skilled operators [4]. It is generally agreed that force-feedback could allow simpler and more efficient task execution using the system [5]. Most of the existing bilateral teleoperation systems make use of commercially available master devices, such as the Geomagic Touch[1] [6] or the sigma.7 [7], to control industrial slave manipulators [8, 9, 10]. These bilateral teleoperation systems often show at least one of three main limitations: instability on contact with stiff environments, reduced force-feedback performance to the operator and limited master workspaces.

In the particular case of space-to-ground teleoperation, which is the main focus of this research, the teleoperation system must provide a high level of transparency, be stable for any communications time-delay conditions and use a lightweight and portable master device. At present, the transmission links available for space-ground communication have limited bandwidths and variable delays in the order of tens or hundreds of milliseconds with data loss up to 30%. These characteristics place constraints both on data transmission, in particular for video [103], and on the performance in terms of the achievable transparency [22] and stability [28]. Due to these constraints, teleoperation in space environments has so far been limited to teleoperation without force-feedback relying in local autonomy [104] and bilateral teleoperation of two degrees-of-freedom devices with limited force-feedback performance [3]. Under the scope of European Space Agency programmes, the portable Sensoric Arm Master (SAM) [84] has been developed as a portable and intuitive interface for bilateral teleoperation.

The goal of this work is to present the development of a complete teleoperation system which can be used to execute 6-DOF tasks with force-feedback over an uncertain delayed communication link. For this purpose the portable 7-DOF SAM exoskeleton is used as the master device and a 7-DOF Kuka Lightweight robot is used as the slave manipulator. Communication occurs over the Internet using a GSM connection on the master side and a land-line connection on the slave side. This situation is analogous to the one corresponding to communications from space to ground over an S-band link [59] and is also proves the feasibility of the technology for ground teleoperation.

[1] formerly known as Sensable Phantom Omni

## 7.2 System architecture

The bilateral teleoperation system used in this work consists of a master side composed of the 7 DOF SAM exoskeleton arm master and a tablet computer running the GUI. The slave side consists of a 7 DOF Kuka Lightweight robot equipped with a Robotiq Gripper and an ATI force-torque sensor. A separate camera system is mounted on a pan-and-tilt unit for visual feedback from the slave side. The communication between the master and the slave side occurs over the internet using a land-based connection on the slave side and a mobile WAN router on the master side. The system architecture is depicted in Figure 7.1. The remaining of this section explains each of the components of this architecture in detail.

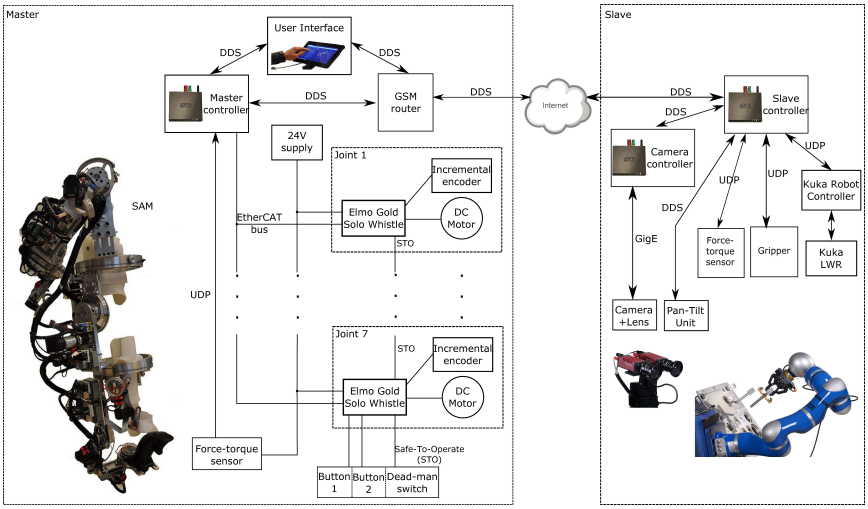


Figure 7.1: System architecture diagram

### 7.2.1 Master-slave communications

Communication between the master and slave occurs over the Internet with a Conel LR7 GSM router on the master side and a regular high-speed internet connection on the slave side. To connect the GSM router to the slave network a Virtual Private Network (VPN) connection is established. To minimise the complexity of interconnecting systems with different addresses and to ensure that the received messages fulfil the required quality-of-service (QoS), the RTI Data Distribution Service (DDS) middleware [101] is used. All communication in this work makes use of best effort transmission (UDP) with no deadline for message arrival and reading always the most recent packet. This type of QoS ensures the most consistent behaviour for real-time systems when using unreliable communication channels such as the Internet.

To identify the characteristics of the connection, a test was performed, in which a ramp with unitary slope was sent from the master to the slave and echoed back to the master is performed. With this test, the amount of round-trip time-delay and data loss can be

identified. Figure 7.2 shows the characteristics of the communication link between the master and the slave using DDS with the same QoS as in the teleoperation system. The connection shows an average round-trip time-delay of approximately 0.1 s and a data loss of 17%. These characteristics can vary depending on the network usage and the amount of data transmitted over the link; however, they were observed to be the most typical characteristics of the link.

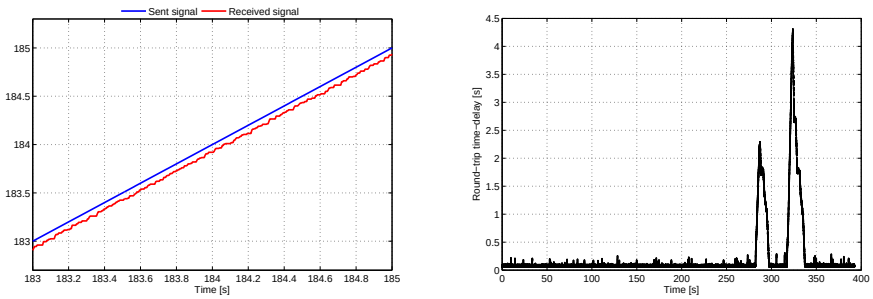


(a) Signal sample (b) Network characteristics

Figure 7.2: Connection test between the master and the slave using DDS with the same QoS setting used in the teleoperation system

### 7.2.2 Master side

The portable Sensoric Arm Master (SAM) is a 7-DOF serial arm exoskeleton with each joint equipped with an incremental encoder and DC motors that are current-controlled locally using commercially available ELMO servo drives. A master control PC executes the control algorithm and the communication with the local joint controllers is done via an EtherCAT communication bus at 1 kHz. Table 7.1 shows the maximum torques provided for each joint. To measure the end-effector force and torques between the operator and the exoskeleton an ATI Gamma 6 DOF force-torque sensor with a resolution of 0.01 N and 0.0005 Nm is mounted at the base of the joystick handle. The force-torque sensor readouts are sampled via UDP a frequency equal to that of the EtherCAT network. As a safety mechanism, a dead-man switch is present on the operator joystick and the drive electronics hardware is only enabled when this button is pressed by the user. More detailed information on the system implementation can be found in [88].

Higher-level control of the system, such as start and stop commands or joint calibration, is performed using a Graphical User Interface (GUI) by the operator on a 10inch diameter Dell Latitude touch screen tablet computer running Windows 8.1. Visual feedback from the remote location to the operator is provided using the same interface. Both video and command communication with the remaining components of the system make use of the Data Distribution Service (DDS) communication middleware. The software receives DDS packages with H.264 network abstraction layer (NAL) units as the payload which is pushed into an H.264 decoder on the tablet. As soon as enough NAL units to decode a video frame

Table 7.1: SAM exoskeleton maximum torque per joint

| Joint | Max. torque (Nm) |
|---|---|
| 1 | 4.4 |
| 2 | 4.4 |
| 3 | 6 |
| 4 | 3.6 |
| 5 | 2.2 |
| 6 | 0.4 |
| 7 | 0.4 |

arrive, the data is decoded and drawn on the screen. The encoding and displaying of one frame takes approximately 8ms. Swipe functions from the touch interface can be used to send pan and tilt commands to the remote pan and tilt unit. With a 2 finger pinching motion the zoom of the camera can be altered. Figure 7.3 shows an example of the calibration screen and camera view on the GUI running on the tablet.

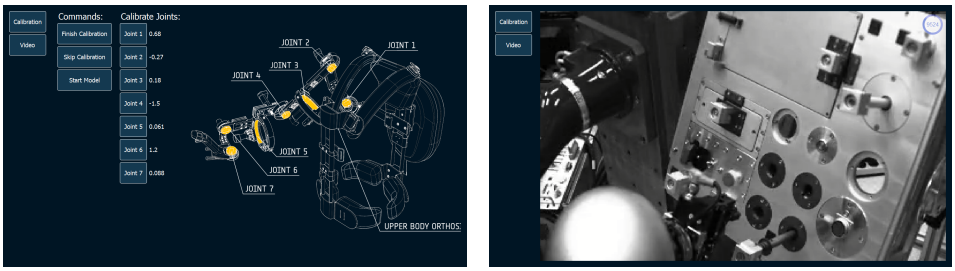


(a) Calibration interface (b) Camera view

Figure 7.3: Screen captures of the calibration screen and camera view on the Graphical User Interface running on the tablet. The calibration views also shows the joint numbers for the master device. The camera image shows the robot manipulator and the taskboard and peg used when executing peg-in-a-hole type of tasks.

### 7.2.3 Slave side

The Kuka Lightweight Robot (LWR), used as the slave device in this setup, is a commercially available 7 DOF lightweight robot which can be used directly in impedance-control mode. The Cartesian impedance can be configured in values ranging, approximately, from 200 N/m to 2000 N/m for translations and 2Nm/deg and 500 Nm/deg for rotations. The damping can be configured at the joint level between $0.1\,\mathrm{Nm}\cdot\mathrm{rad}^{-1}\cdot\mathrm{s}$ and $2\,\mathrm{Nm}\cdot\mathrm{rad}^{-1}\cdot\mathrm{s}$. An ATI Gamma 6 DOF force-torque sensor with a resolution of 0.01 N and 0.0005 Nm is mounted on the robot tool to measure the actual contact forces and torques. Both the master and slave force torque sensor are set to 0 when the operation is started. The manipulator is controlled using the Kuka Fast Research Interface (FRI) [87] at a frequency of 1 kHz.

Using this interface it is possible to control both the tool Cartesian pose and forces/torques as well as the Cartesian stiffness and damping of the manipulator.

An Allied Vision Technology Prosillica GX2000C colour camera with an attached motorised zoom (8 mm to 48 mm) lens is used for capturing motion pictures. The camera is connected via a GigE vision interface to an encoding computer. As soon as a raw frame from the camera arrives at the camera controller it is resized to 352x288, transformed to monochrome and encoded with an H.264 encoder. In [103] a description is given on how the encoder parameters for a packeted network should be set. The encoder packs the data into NAL units which are sent via DDS to the slave. The encoder is set to use 84kbit/s on average, has a hypothetical reference decoder (HRD) set to 100ms, uses only 1 slice per frame and sends a P-slice every 4s. A P-slice is a slice of a frame which can be decoded without dependency on previous frames. The exposing of a frame takes 40ms and the encoding approximately 16ms. The HRD ensures a maximum delay for a bandwidth limited transport with the consequence of quality reduction of the P-slices.

## 7.3 Control architecture

For the bilateral teleoperation control, the 4-channel architecture is implemented. To ensure that the system remains stable at all times, the 4-channel time-domain passivity control presented by the authors in [84] is used. These controllers are expected to provide a high-level of transparency while making the system remain stable at all times, independently of the communication channel characteristics. This section details the implementation of the 4-channel architecture and the time-domain passivity controller used in this work.

### 7.3.1 4-channel bilateral teleoperation control

The bilateral teleoperation control is designed using the 4-channel architecture [22] implemented on all the Cartesian degrees-of-freedom of the system. Using this architecture, the master sends both the position and orientation commands, as well as the actual force and torque exerted by the operator, to the impedance-controlled slave manipulator. The measured force and pose of the slave manipulator are sent back to the master device and used to compute the amount of force/torque that is rendered by the master device to the operator. The complete teleoperation control architecture is shown in Figure 7.4.

The master joint torques resulting from the force-feedback commands can be calculated at each instant using the principle of virtual work as

$$\boldsymbol{\tau}_m(t) = \mathbf{J}_m^T(\mathbf{q}(t))\left[\mathbf{K}_2(\mathbf{q}(t))\mathbf{f}_e(t-T(t)) + \mathbf{K}_m(\mathbf{x}_s(t-T(t)) - \mathbf{x}_m(t))\right] \tag{7.1}$$

where $\boldsymbol{\tau}_f$ is the master commanded joint torque vector, $\mathbf{K}_2$ is the master force channel diagonal gain matrix, $\mathbf{f}_s$ is the force-torque vector measured by the force-torque sensor mounted on the slave device, $T$ is the time delay measured at each time instant $t$, $\mathbf{K}_m$ is the master position channel diagonal gain matrix, $\mathbf{x}_s$ is the actual slave manipulator position and $\mathbf{x}_m$ the actual master position which corresponds to the slave manipulator reference.

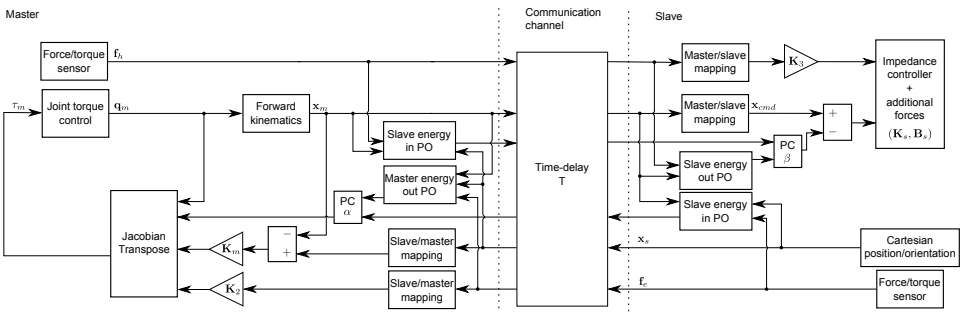


Figure 7.4: Bilateral teleoperation control architecture

On the slave side, both the stiffness $\mathbf{K}_s$ and damping $\mathbf{B}_s$ of the manipulator can be configured independently in each Cartesian direction using the FRI interface. The joint torque commands for the slave manipulator are computed as

$$\boldsymbol{\tau}_s(t) = \mathbf{J}_s^T(\mathbf{q}(t))\left[\mathbf{K}_s(\mathbf{x}_m(t-T(t)) - \mathbf{x}_s(t)) + \mathbf{K}_3\mathbf{f}_h(t-T(t)) + \mathbf{B}_s(\dot{\mathbf{x}}_s(t))\right] \tag{7.2}$$

where $\boldsymbol{\tau}_s$ is the slave commanded joint torque vector, $\mathbf{K}_s$ is the slave Cartesian stiffness diagonal matrix, $\mathbf{K}_3$ is the slave force channel diagonal gain matrix and $\mathbf{f}_m$ is the force-torque vector measured by the force-torque sensor mounted on the slave device. The LWR controller internally compensates for gravity, friction and other dynamic effects of the manipulator; however, since the user has no control over these parameters, they are explicitly left out of the computation.

### 7.3.2 Multi-dof time-domain passivity control

To ensure that the system remains stable independently of the communication channel characteristics, the 4-channel time-domain passivity control is used [105]. This method is based on monitoring the input and output energies at each side of the communication channel and dissipating the excess energy. The method is therefore independent of the mechanical and control system parameters settings.

Considering a multi-dof two-port, the observed energy can be computed as

$$\begin{aligned} E_{obs}(n) &= \Delta T \sum_{k=0}^{n} [\mathbf{v}_l(k)\cdot\mathbf{f}_l(k) + \mathbf{v}_r(k)\cdot\mathbf{f}_r(k)] \\ &= \Delta T \sum_{k=0}^{n} [P_l(k) - P_r(k)], \end{aligned} \tag{7.3}$$

where $\mathbf{v}$ is the velocity, $\mathbf{f}$ is the force, $P$ is the power, the operator $\cdot$ is the dot product and the subscripts $l$ and $r$ represent the left and right sides, respectively. In this derivation it is

assumed that the system sample time $k$ is much smaller than the system mechanical time-constants. The energy of the system can be divided in input and output energy for each side by computing

$$E_l^{\text{in}}(n) = \begin{cases} E_l^{\text{in}}(n-1) + \Delta T \cdot P_l(n) & \text{if } P_l(n) > 0 \\ E_l^{\text{in}}(n-1) & \text{if } P_l(n) \leq 0 \end{cases} \tag{7.4}$$

$$E_r^{\text{in}}(n) = \begin{cases} E_r^{\text{in}}(n-1) + \Delta T \cdot P_r(n) & \text{if } P_r(n) > 0 \\ E_r^{\text{in}}(n-1) & \text{if } P_r(n) \leq 0 \end{cases} \tag{7.5}$$

$$E_l^{\text{out}}(n) = \begin{cases} E_l^{\text{out}}(n-1) & \text{if } P_l(n) \geq 0 \\ E_l^{\text{out}}(n-1) - \Delta T \cdot P_l(n) & \text{if } P_l(n) < 0 \end{cases} \tag{7.6}$$

$$E_r^{\text{out}}(n) = \begin{cases} E_r^{\text{out}}(n-1) & \text{if } P_r(n) \geq 0 \\ E_r^{\text{out}}(n-1) - \Delta T \cdot P_r(n) & \text{if } P_r(n) < 0. \end{cases} \tag{7.7}$$

When the energy output is larger than the energy input on the opposite side, the communication channel has an active behaviour, thus injecting energy into the system, which can make it potentially unstable. To ensure stability, this excess energy has to be dissipated by means of a passivity controller. As shown by the authors in [84], it is sufficient to place passivity controllers on the master and slave output sides of the TDPN, since the voltage sources are assumed ideal, meaning they can both generate and absorb an infinite amount of energy.

In multi-dof systems excess energy can be dissipated in different manners. For example, the energy could be dissipated in the Cartesian direction with higher velocity, in the motion nullspace or equally distributed in every direction. The method used in this paper consists of dissipating the energy equally in every direction. The effects of uniformly distributing the energy is expected to minimise the effects on task performance execution. Taking the master side as an example, the force output of the series passivity controller for each Cartesian direction can be computed as

$$f_{M_i}^{PC}(n) = \begin{cases} \frac{\left(E_M^{\text{out}}(n) - E_M^{\text{in}}(n-T)\right)/d}{\Delta T \cdot v_{m_i}^2(n)} & \text{if } E_M^{\text{out}}(n) > E_M^{\text{in}}(n-T) \text{ and } v_{m_i}(n) \neq 0 \\ 0 & \text{otherwise,} \end{cases} \tag{7.8}$$

where $d$ is the number of directions in which energy is to be dissipated, and where the subscript $i$ is the actual direction for which the dissipation element is being calculated. Using the proposed combination of passivity observers and controllers, the multi-dof 4-channel can be made passive when time-delay is present on the communication channel.

## 7.4 Control implementation and tuning

Following the tuning rules given in [22], using this control architecture and making $\mathbf{K}_2 = \mathbf{K}_3 = \mathbf{I}$ is expected to provide the user with perfect contact transparency. However,

in this case, due to the presence of time-delay in the communication channel and since the joint friction and other dynamic effects of the master device are not compensated, the operator will feel additional forces in free-air, which deviate from perfect transparency.

The values measured by the slave force/torque sensor are compensated to remove the gravity effect of the 1 kg gripper and filtered using a low-pass filter with a 100 Hz cut-off frequency to remove the vibration noise introduced by the slave manipulator motors during motion.

In all cases the system control parameters were tuned such that the system remains stable with time-delay values up to 20 ms for fixed round-trip time-delay occurring during contact with a rigid surface. The control parameters are configured for XYZ translations and rotations as $\mathbf{K}_m = \text{diag}([20, 20, 20, 2, 2, 2])$, $\mathbf{K}_s = \text{diag}([700, 700, 700, 10, 15, 5])$, $\mathbf{K}_2 = \text{diag}([1, 1, 1, 0.4, 0.6, 0.2])$ and $\mathbf{K}_3 = \text{diag}([1, 1, 1, 1, 1, 1])$. The gains on matrix $\mathbf{K}_2$ have to be kept below 1 since the uncompensated inertial torques caused by the gripper are sufficient to make the system unstable, even when no time-delay is present in the communication channel.

## 7.5 System performance

This section shows the performance of the complete bilateral teleoperation system when using the SAM exoskeleton to command the LWR, both in free-air and contact. The first experimental scenario is a contact task with different environments and the second a peg removal task. This section presents the teleoperation performance results for each of these tasks.

### 7.5.1 Contact task

For the contact task, the operator is instructed to drive the slave manipulator into contact with three surfaces of different stiffness, keeping in contact with each for a couple of seconds. The surfaces used are soft foam, hard foam and a rigid metal plate. The first test is performed without the passivity controller and the second test with the passivity controller.

#### *System behaviour without passivity control*

The behaviour of the system during the contact task without passivity control is shown in Figure 7.5. In free-air motion the system is stable, with the slave manipulator following the commanded pose of the master device with an accuracy of approximately 0.02 m. The lag between the master command and the slave response appears due to the communication delay introduced by the communication channel. Once the slave device makes contact with the hard environment, approximately at $t = 57$ s, involuntary oscillations appear, not only in the contact direction X, but also in the Y and Z directions. These oscillations prevent the operator from keeping continuous contact with the environment.

#### *System behaviour with passivity control*

The behaviour of the system during the contact task with passivity control is shown in Figure 7.6. The results show that the system allows probing of all three environments

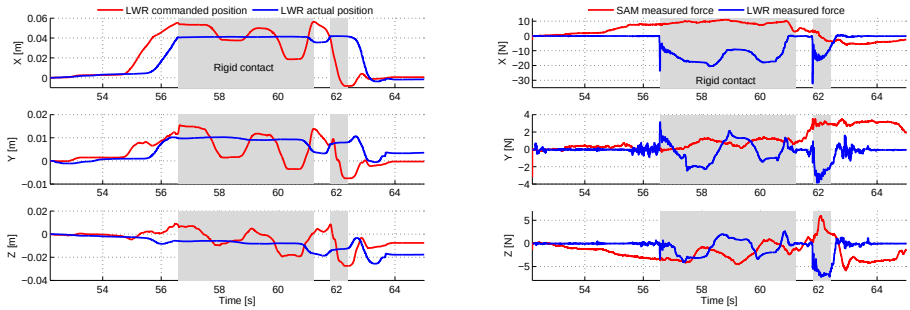


(a) Position response (b) Force response

Figure 7.5: System position and force response as viewed from the master side during the contact task without using time-domain passivity control. Contact with the environment occurs mainly in the X direction. The areas marked in grey correspond to moments in which the slave is in contact with the environment. The oscillations observed during contact are involuntary motions caused by system instability.

without the existence of involuntary oscillations. From Figure 7.7 it can be observed that the passivity controller acts with small force commands just after contact with the environment is established, and acts with forces of up to 1.5 N on the master side and 2 N on the slave side when contact with the environment is released.

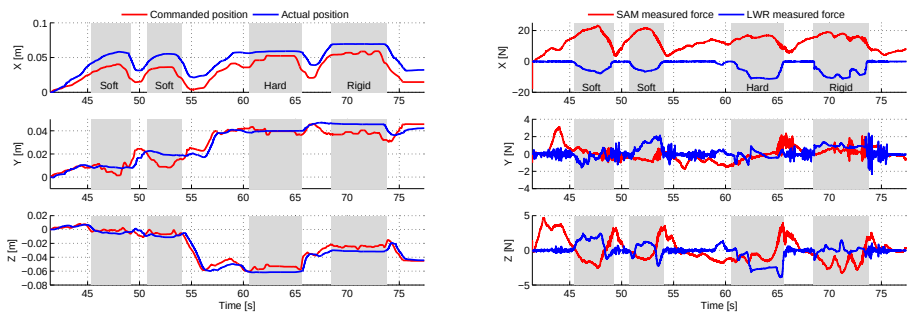


(a) Position response (b) Force response

Figure 7.6: System position and force response as viewed from the master side during the contact task using time-domain passivity control. Contact with the environment occurs mainly in the X direction. The areas marked in grey correspond to moments in which the slave is in contact with the environment.

Table 7.2 shows the measured stiffness on the slave side and rendered stiffness of the environment computed from the ratio between the distance from the environment start and the measured force, averaged throughout the entire contact duration.

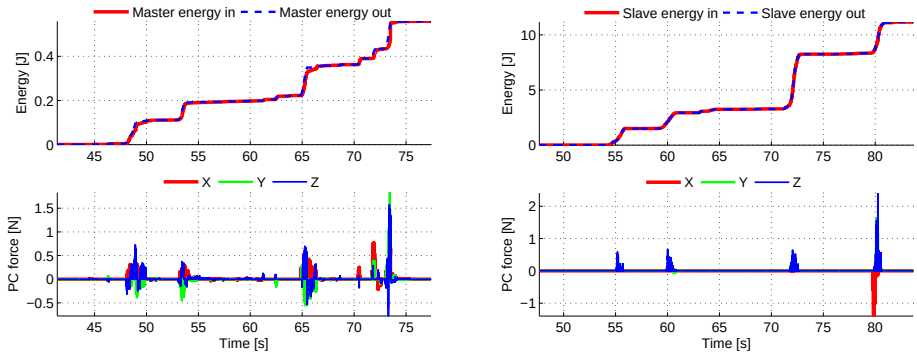


(a) Master side (b) Slave side

Figure 7.7: Master and slave time-domain passivity control response during the contact task

Table 7.2: Comparison between actual environment stiffness and reflected stiffness to the operator

| Environment | Measured stiffness [N/m] | Reflected stiffness [N/m] |
|---|---|---|
| Soft | 450 | 620 |
| Hard | 3700 | 1600 |
| Rigid | 10750 | 4500 |

### 7.5.2 Peg removal task

For the peg removal task, the operator is instructed to use the master device to command the slave manipulator to grasp a peg and remove it from the hole in which it is inserted. Both peg and the hole are metallic with a diameter difference between them of approximately 0.9 mm and a total peg length of 2 cm. The behaviour of the system and of the passivity controller during the execution of this task is shown in Figures 7.8 and 7.9, respectively.

During the approach phase, in which the operator aligns the gripper with the peg, the motion occurs only in free-air and no signs of instability are visible. The slave manipulator follows the master position with errors of 0.01 m for translational motion and up to 0.1 rad for rotational motion. In free-air motion, even though no forces or torques are measured on the slave side, there are forces of just below 10 N and torque of up to 1 Nm being measured on the master side. These forces and torques are both due to the uncompensated weight and friction of the master device and the forces due to the position difference between the master and the slave.

Once the gripper closes, at $t = 56$ s, the peg is grasped and the operator executes a motion in the $X$ direction to remove the peg from the hole. In this phase, there are forces of up to 20 N being transmitted to the operator and executed on the slave side. During this phase there are small actions of the passivity controller up to 1 N that ensures that the system remains stable.

After the peg is removed from the hole, the operator motion speed increases and the

passivity controller releases the accumulated energy during the force task. During this period, the passivity controller commands force and torque values up to 5 N and 5 Nm, respectively. The passivity controller effects are visible on the measured forces and torques on both the master and slave sides; however, its only effect on the position and orientation motion is a reduction of the speed. The high frequency vibrations are clearly felt by the operator but do no affect the motion in an uncontrolled manner.

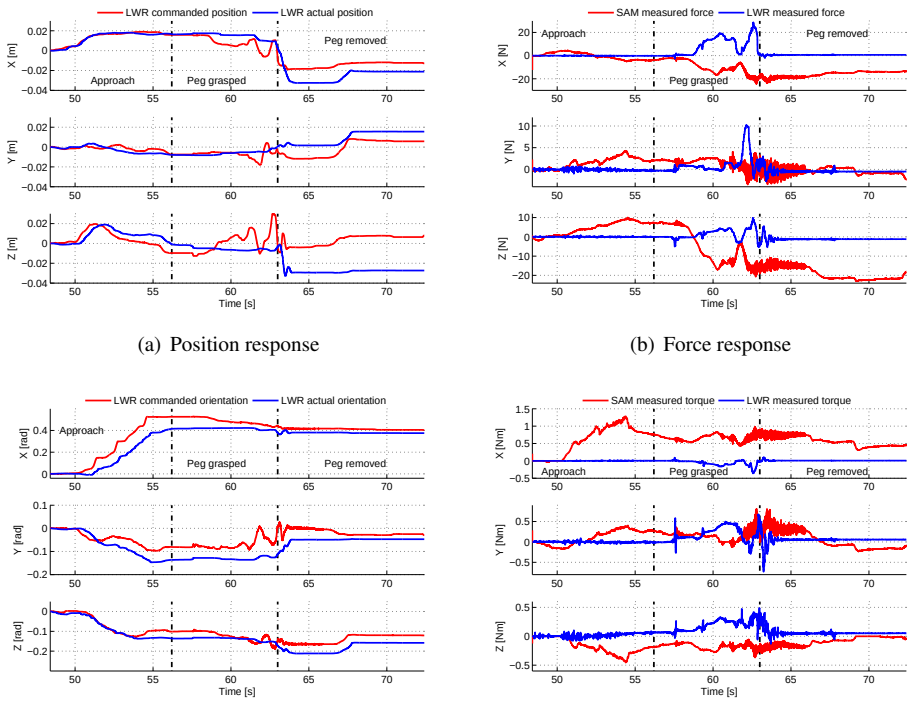


(a) Position response

(b) Force response

(c) Orientation response

(d) Torque response

Figure 7.8: System position/orientation and force/torque response as viewed from the master side during peg removal task

## 7.6 Discussion

Using the presented teleoperation system, it is possible to execute 6-DOF tasks in bilateral teleoperation over a mobile internet network with variable time-delay. In terms of transparency for translational motion, the system provides a ratio between the measured and reflected environment of 1 for soft environments, a ratio of 0.5 for hard environments and a ratio of 0.2 for rigid environments. For rigid environments, the currently used DC motors do not provide enough torque to render higher stiffness to the operator. Despite the reduced transparency, the stiffness rendered to the operator by the master device is different for each

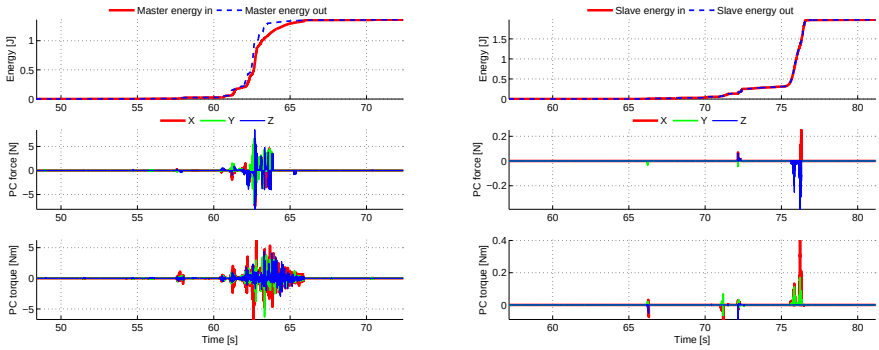


(a) Master side

(b) Slave side

Figure 7.9: Master and slave time-domain passivity control response during the contact task

of the three environments. In free-air motion, since the effects of friction and gravity are not compensated, the operator has to interact with forces different from 0. While these forces are within an acceptable range for human operators, long-term operations can be limited by these effects due to fatigue.

For rotational motions, the system transparency has not been measured; however, the gains of the control parameters have to be reduced due to the uncompensated effects of the gripper inertial forces. If the tuning rules for perfect transparency are followed, the system becomes unstable even in situations without time-delay. In the future, an inertial estimator should be used to avoid these effects and allow an increase of the gain parameters. The low-pass filter used to remove the vibration effects of the slave manipulator is also required to ensure that the operator can interact with the system without feeling these vibrations, which can be otherwise clearly perceived.

In terms of stability, the passivity controller ensures that the system remains stable at all times as shown in the results reported in Figures 7.6 and 7.8. To ensure stability of the system, the passivity controller issues force commands that prevent unstable oscillation from occurring. As observed in Figures 7.7 and 7.9, the passivity controller force commands result in high frequency noise, however no influence on operator motion is observed. Without time-domain passivity control, the system is not usable since involuntary oscillations are introduced when the slave is in contact with the remote environment.

Since the bandwidth for video transmission is limited to 90kbit/s, the video sent to the operator is black and white, and the quality, when objects move in the image is seriously reduced due to the compression algorithm characteristics. The ability to change the zoom and control the pan-and-tilt of the camera is very useful for observing different details of the taskboard during operations. This gives the operator the possibility of having a broader view during large range motions and a detailed image of the place in which more precise tasks need to be executed. During this experiment, different camera placements were tried which, combined with the kinematic mapping between the master and the slave, seemed to influence the performance of the operator during the experiment. A more detailed analysis

of these effects should be completed to determine the ideal camera placement to maximise the task performance.

Task executing performance was not explicitly studied during this work, however different operators have been able to execute the proposed tasks. Operators were successfully able to qualitatively determine the stiffness of each tested surface and could successfully remove the peg from the hole on the taskboard. Further user studies need to be performed to determine how different system parameter tuning affect the ability of the operators to execute different tasks.

## 7.7 Conclusions

The teleoperation system presented in this paper allows the execution of complex contact and peg removal tasks in bilateral teleoperation over a mobile Internet communication network with variable time-delays whilst maintaining system stability. Despite the existence of a delay, the operator can feel an impedance transmitted through the master device which results in the rendering of different stiffness values for different environments. In free-air motion, since the device is not capable of compensating its own weight and no friction compensation was implemented, the operator feels a force of up to 10N which does not prevent task execution but can reduce the amount of time the system can be used due to fatigue.

The combined force-feedback with the low bandwidth video transmission makes this system usable also in real-life situations in which high-speed cable internet connections are not available. Using this system it should be possible to investigate the relationships between transparency, video quality and master/slave mapping with the operator task performance in order to determine the best conditions for executing tasks remotely in an intuitive and efficient manner.

CHAPTER 8

# Master-slave mapping and slave base placement optimization for intuitive and kinematically robust direct teleoperation

J. Rebelo and A. Schiele

*12th International Conference on Control, Automation and Systems (ICCAS)*, 2012

**Abstract**

*Combining redundant slave manipulators with suitable master devices in teleoperation systems, allows human operator to plan and execute complex handling tasks in unknown, remote environments. However, the existence of singularities, joint limits and manipulator redundancies can lead to instability, causing loss of control and potentially leading to dangerous situations. It is the goal of this work is to study how to optimally map kinematically dissimilar master-slave devices with similar, human-like workspaces for telemanipulation tasks. The proposed mapping strategy proposes using only a part of the slave workspace which is reachable by the human operator during teleoperation. With convenient scaling and slave base placement using a genetic algorithm, the reachable area is placed such that singularities and joint limits are always avoided during real-time teleoperation. Combining the slave mounting optimization with an elbow angle redundancy mapping for configuration control is shown to ensure geometrical correspondence between the operator and the slave manipulator. The proposed mapping is demonstrated using a full arm master exoskeleton to command a 7-DOF slave manipulator.*

## 8.1 Introduction

Redundant manipulators, i.e. manipulators with more degrees of freedom (DOF) than the ones required for executing a given task, have increased dexterity which allows them to manoeuvre in constrained and complex environments. In particular, the recent human-like 7-dof manipulators, such as the DLR Lightweight Robot (LWR) series [14] or the Robonaut arms [15], besides having dimensions similar to those of humans, allow dexterous and flexible manipulation with precise force and torque control. If combined with suitable master devices, thus enabling human planning and decision capabilities, such robots are ideal for executing human-like handling tasks in unknown environments through teleoperation.

Nonetheless, most of the current commercially available haptic devices, such as the Phantom® or the Falcon®, have small workspaces which makes it necessary to use workspace indexing or rate control techniques in such scenarios. This becomes unnatural and seriously reduces the task execution capabilities of the operator. Some researchers use identical master and slave devices [106], however, this is a very inflexible solution since only one type of slave manipulator can be used at a time and there is no guarantee that the master device provides an ideal human-machine interface (HMI).

Using distinct master and slave devices with similarly large workspaces allows generic control of various slaves if a convenient kinematic interface can be implemented for position and orientation tracking in real-time. If an operator is free to command the slave into arbitrary areas outside the slave usable workspace, the manipulator can easily be driven into singularities or joint limits. In these areas small Cartesian commands can result in large joint speeds or instability [107], causing loss of control by the operator and potentially leading to dangerous situations.

The Damped Least-Squares (DLS) [107] and gradient projection [108] methods have been successfully used to avoid numerical instability respectively in singularities and joint limits. However, in both cases, the solution of the problem results in end-effector or null-space trajectory deviations which are unpredictable for the operator and therefore difficult to handle in direct bilateral control scenarios. Tsumaki *et al.* [109] proposed a singularity-consistent method which realizes the motion only along feasible directions without deviation, neglecting the need for joint-limit handling and geometric match between master and slave for goal tracking predictability.

When an absolute mapping between the master and the slave manipulator is used, the slave manipulator base can be placed in a way that allows all the commanded poses to be place outside areas with singularities. The problem of robot base placement optimization was previously studied for increasing the performance of industrial workcells or placing a mobile base. Panames and Zeghloul [110] presented an optimization which combines the Jacobian condition number and distance to joint limits criteria for optimizing the path of a manipulator. Tian *et al.* [111] use a genetic algorithm with a fitness function based on the manipulability measure to optimize the placement of a manipulator with only two degrees-of-freedom. These works focused on optimization for predefined tasks with paths that were previously known or could be computed and not on arbitrary motions which are determined in real-time.

To the authors' knowledge, the only teleoperation related optimization was done by Zacharias *et al.* [112] who previously introduced the capability map concept to compare the

usability of two configurations of the DLR bimanual haptic interface [106] and determine the optimal operator position for maximum workspace coverage. Since equal master-slave devices were used, the problems with joint limits, singularities and unmatched workspaces were not considered.

The goal of this work is to study how to optimally map kinematically dissimilar master-slave devices with similar, human-like workspaces for telemanipulation tasks in unstructured remote environments. The purpose of the mapping is to ensure full geometrical correspondence between the operator and the slave manipulator configuration and guarantee operation in areas which are always sufficiently away from singularities and joint limits. In this research, as the path planning is done in real-time by the human operator, the slave workcell mounting is optimized such that every point of the reachable area is in a zone of good manipulability of the slave manipulator workspace. The geometrical correspondence together with releasing the operator from considering control issues is expected to lead to more intuitive and robust direct teleoperation. While the following method aims to be generic it will be applied to an exoskeleton-based master controlling a redundant slave manipulator.

## 8.2 Master-slave mapping

To achieve geometrical correspondence between an operator and a slave manipulator while avoiding problems with singularities and joint limits, the approach followed in this work can be divided in four steps: 1) workspace offset and scaling; 2) optimized end-effector mounting; 3) redundancy mapping for configuration control and 4) slave workcell mounting optimization. For this analysis the EXARM exoskeleton [113] and the Kuka LWR IV based on [14] are used as master and slave devices, respectively.

The EXARM exoskeleton is a 16-DOF exoskeleton, which allows a large range of human arm motion while not requiring mechanical adjustments for different operators in the $5^{th}$ to the $95^{th}$ percentile of male population. The operator is attached to the device at the upper arm and the forearm using inflatable air cushions and the palm is attached using an orthopaedic glove. The EXARM measures the position of the human arm indirectly through potentiometers mounted on each axis. In the laboratory environment the exoskeleton is suspended using a counter-weight system, such that the operator does not feel the weight of the device. The exoskeleton being worn by the operator and the most relevant frame assignments are shown in Figure 8.1

The DLR Lightweight Robot (LWR) is a 7-DOF anthropomorphic arm described by the Denavit-Hartenberg (D-H) parameters (using the convention of [102]) and joint limits shown in Table 8.1. The LWR standard mounting and frame assignments are shown in Figure 8.2.

### 8.2.1 Workspace offset and scaling

The workspace scaling is defined such that the slave manipulator can not be commanded to be fully outstretched, corresponding to the robot's external workspace boundary singularity, or to be bent into the unreachable inner area, denoted by the LWR elbow joint limit.

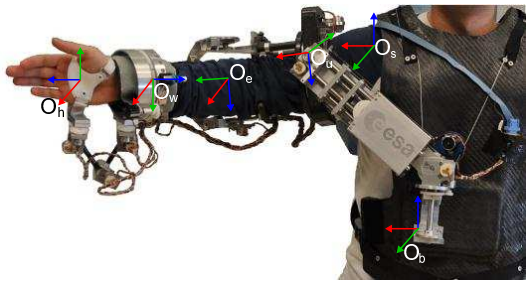


Figure 8.1: EXARM exoskeleton as worn by an operator ($O$) and frame assignment. The attachment points to the human operator in the upper arm ($O_u$), wrist ($O_w$) and palm ($O_h$) correspond to joints 4, 9 and 16 (end-effector) of the exoskeleton. The elbow frame ($O_e$) is attached to joint 7 and the shoulder frame ($O_s$) is static and defined on a user per user basis corresponding to a simple translation from the base to the estimated human operator shoulder. In this paper the XYZ axis are represented by the red, green and blue (RGB) colors, respectively.

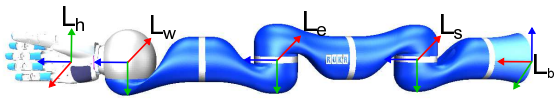


Figure 8.2: Lightweight Robot (LWR) with hand end-effector in standard mounting and base ($L_b$), shoulder ($L_s$), elbow ($L_e$), wrist ($L_w$) and hand ($L_h$) frame assignment.

Table 8.1: Kuka LWR D-H parameters and joint limits

| Joint | a | $\alpha$ | d | $\theta$ | $\theta_{min}$ | $\theta_{max}$ |
|---|---|---|---|---|---|---|
| 1 | 0 | $\pi/2$ | 310 | $\theta_1$ | $-170°$ | $170°$ |
| 2 | 0 | $-\pi/2$ | 0 | $\theta_2$ | $-120°$ | $120°$ |
| 3 | 0 | $-\pi/2$ | 400 | $\theta_3$ | $-170°$ | $170°$ |
| 4 | 0 | $\pi/2$ | 0 | $\theta_4$ | $-120°$ | $120°$ |
| 5 | 0 | $\pi/2$ | 390 | $\theta_5$ | $-170°$ | $170°$ |
| 6 | 0 | $-\pi/2$ | 0 | $\theta_6$ | $-120°$ | $120°$ |
| 7 | 0 | 0 | 78 | $\theta_7$ | $-170°$ | $170°$ |

The LWR commanded end-effector position $\mathbf{p}_{\mathrm{L}_h}$ can be determined from the EXARM end-effector position as

$$\mathbf{p}_{\mathrm{L}_h} = g \cdot (\mathbf{p}_{\mathrm{O}_h} - \mathbf{p}_{\mathrm{O}_s}) + \mathbf{p}_{\mathrm{L}_s} \tag{8.1}$$

where $\mathbf{p}_{\mathrm{O}_h}$ and $\mathbf{p}_{\mathrm{O}_s}$ are the current EXARM hand and shoulder position in base frame, $g$ is a scaling gain and $\mathbf{p}_{\mathrm{L}_s}$ is the LWR "shoulder" position in LWR base frame.

Considering the master-slave correspondence in the limit situations depicted in Figure 8.3, the gain boundaries can be computed as,

$$\frac{\sqrt{(L_{se}-L_{eh}sin(\theta_{max}))^2+(L_{eh}cos(\theta_{max}))^2}}{\sqrt{O_{se}^2+O_{eh}^2}} \leq g \leq \frac{L_{length}}{O_{length}} \tag{8.2}$$

where $L_{se}$ and $L_{eh}$ are the distances from shoulder to elbow and from elbow to hand of the slave manipulator, $\theta_{max}$ is the slave manipulator maximum elbow angle, $O_{se}$ and $O_{eh}$ are the distances from shoulder to elbow and elbow to hand of the human operator and $L_{length}$ and $O_{length}$ are the lengths of the slave manipulator and the human operator, respectively.

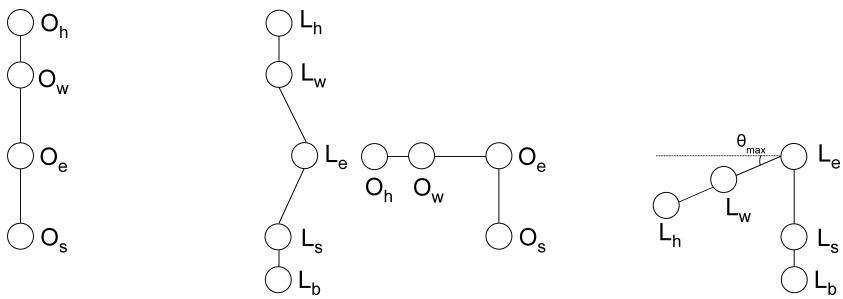


(a) Maximum gain (b) Minimum gain

Figure 8.3: Schematic illustration of geometrical correspondence between operator (on the left) and slave manipulator (on the right) in limit situations (top view).

The operator shoulder's center point and arm dimensions are estimated online from the EXARM sensor data using the method presented by Gamage and Lasenby in [114]. This closed-form algorithm estimates the center-of-rotation and radius of motion using the information of one frame and does not require any parameter adjustment. For this purpose the operator executes three motions before starting the slave controller, namely: shoulder rotation, elbow flexion-extension and wrist adduction-abduction. With the data captured during these motions, all the necessary human operator dimensions can be estimated online and the slave controller gains adjusted for each operator.

### 8.2.2 Slave end-effector mounting

The end-effector mounting is optimized to prevent the robot reaching into wrist singularities during operation. Recalling the frame assignment shown in Figure 8.1, the rotation limits for the human operator wearing the exoskeleton are ±20° around the X axis, ±80° around the Y axis and −90° to 40° around the Z axis in wrist reference frame.

Applying joint offsets of 90° and −90° to joints 5 and 6 of the LBR and mounting the hand as depicted in Figure 8.4 ensures that, for the hand orientation control, the joints are always kept within the limits and away from the wrist singularity.

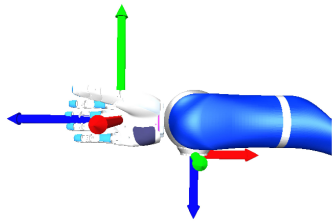

Figure 8.4: DLR-HIT hand front view of mounting on the LWR manipulator, with wrist (joint 7) and end-effector frames.

The LWR commanded hand-orientation in robot base frame is then taken directly from human operator hand orientation in exoskeleton base frame.

### 8.2.3 Redundancy mapping for configuration control

To control the robot redundant degree-of-freedom, the "arm angle" as defined by Kreutz-Delgado and Seraji [115] is used. This is a natural human redundancy resolution method and can be directly computed from the exoskeleton information.

Having a shoulder center point $\mathbf{p}_{O_s}$, an elbow point $\mathbf{p}_{O_e}$, a wrist point $\mathbf{p}_{O_w}$ and an arbitrary unit vector $\hat{\mathbf{V}}$ defined in a 3-dimensional Cartesian frame, the elbow and wrist vectors can be computed as $\mathbf{w} = \mathbf{p}_{O_w} - \mathbf{p}_{O_s}$, $\mathbf{e} = \mathbf{p}_{O_e} - \mathbf{p}_{O_s}$. The projection of the elbow vector onto the wrist vector is computed as $\mathbf{d} = (\hat{\mathbf{w}} \cdot \mathbf{e})\,\hat{\mathbf{w}}$, and the minimum distance from the vector $\mathbf{w}$ to the point $\mathbf{p}_{O_e}$ is represented by the vector $\mathbf{p} = \mathbf{e} - \mathbf{d}$. The unit vector of the reference plane is determined by $\mathbf{l} = \left(\mathbf{w} \times \hat{\mathbf{V}}\right) \times \mathbf{w}$. The arm angle can then be calculated as

$$\psi_O = atan2\left(\hat{\mathbf{w}} \cdot \left(\hat{\mathbf{V}} \times \mathbf{p}\right), \hat{\mathbf{V}} \cdot \mathbf{p}\right) \equiv \psi_L \tag{8.3}$$

The human operator and slave manipulator arm angle are computed using the shoulder, elbow and wrist points shown in Figures 8.1 and 8.2, respectively. The operator arm angle value ($\psi_O$) is used as the robot manipulator target arm angle ($\psi_L$) without any modification.

### 8.2.4 Slave base placement optimization

The mapping proposed in the previous sections avoids both joint limits and wrist singularities and guarantees geometric pose matching, but does not yet ensure teleoperation in the areas of highest manipulability. In this section, a slave robot base placement optimization is proposed to maximize manipulability and distance from joint limits during operation, minimizing the effects of the slave shoulder singularity.

The optimization input is a set of target points obtained by measuring the positions of an operator using the EXARM and the slave base orientation. Since the area in which useful operations can occur is located in front of the operator's chest [112], the optimization is limited to this area. Each of the generated target points from the exoskeleton is matched to the closest point in terms of position and arm angle of the precomputed LWR workspace. As the hand orientation was already ensured by mechanical mounting to be within joint

limits and without singularities (see previous section), only the workspace generated by the total motion range of joints 1 to 4 was considered. The manipulability measure and distance to joint limit are evaluated for each selected point. A genetic algorithm is then used to optimize the fitness function

$$\begin{aligned}\text{fitness}(\mathbf{R}^{base}_{\text{LWR,world}}, T_{pose}) = \\ -min(\sigma) + \textstyle\sum_{i=1}^{n} max(\mathbf{DJL}_i),\end{aligned} \tag{8.4}$$

where $\mathbf{R}^{base}_{\text{LWR,world}}$ is the manipulator base orientation, $T_{pose}$ is the set of all target poses, $min(\sigma)$ represents the lowest manipulability in the reachable area and $max(\mathbf{Q}_i)$ is the closest distance to the joint limit of joint $i$ in the reachable area. This worst-case scenario approach ensures that the manipulator will be within the controllable space throughout the entire range of possible commanded slave poses. Only the mounting orientation is optimized since the position could be adjusted, if needed, by adding an extra offset to (8.1).

The criteria used to determine the manipulability is the smallest singular value of the Jacobian matrix [116]. Using the Singular Value Decomposition (SVD), the Jacobian matrix can be defined as

$$\mathbf{J} = \mathbf{U}\Sigma\mathbf{V}^T \tag{8.5}$$

where $\mathbf{U} \in R^{m\times m}$ and $\mathbf{V} \in R^{n\times n}$ are orthogonal matrices and the singular values matrix $\Sigma$ is

$$\Sigma = \begin{bmatrix} \sigma_1 & & & \mathbf{0} \\ & \sigma_2 & & \\ & & \ddots & \\ \mathbf{0} & & & \sigma_m \end{bmatrix} \tag{8.6}$$

and $\sigma_1 \geq \sigma_2 \geq \ldots \geq \sigma_m \geq 0$. The smallest singular value $\sigma_m$ tends to 0 as the manipulator approaches a singular configuration. Figure 8.5 shows the manipulability map for the LWR manipulator in its original configuration. The map is obtained by discretizing the workspace of the manipulator in $75mm$ side cubes and determining the minimum position manipulability in each of the points.

The distance from the joint limits ($DJL$) criteria is adapted from [117] and is defined as

$$DJL(q_i) = \left| \frac{(q_{i,max}-q_{i,min})^2(2q_i-q_{i,max}-q_{i,min})}{(q_{i,max}-q_i)^2(q_i-q_{i,min})^2} \right| \tag{8.7}$$

where $q_i$ is the $i^{th}$ joint value, $q_{i,max}$ the joint upper limit, $q_{i,min}$ the joint lower limit. As shown in Figure 8.6 this function takes values close to 0 in most of the joint range and increases steeply when the minimum and maximum limits are approached. This function is used to guarantee minimum bias towards the joint center. Figure 8.7 shows the distance to joint limit map for joint 4 of the LWR manipulator.

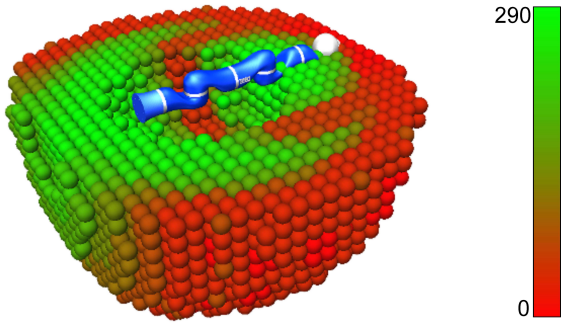


Figure 8.5: LWR position manipulability map. Larger values correspond to areas of higher manipulability. For better visualization only the bottom half of the workspace in the Z axis is shown, since the upper part is symmetrical

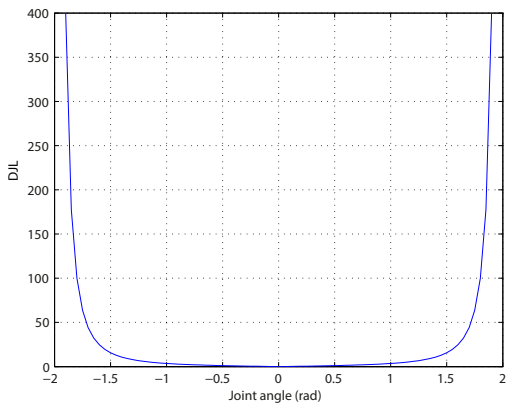


Figure 8.6: Distance to joint limit function response. The joint limit is equal to $\pm 2rad$.

## 8.3 Experimental setup

To validate the proposed mapping and slave manipulator mounting a test setup was prepared in which the EXARM exoskeleton can control a virtual kinematic model of the LWR.

The EXARM exoskeleton is connected to a control computer through a PCI analog input card. This machine computes the controller values, performs the mapping to desired slave manipulator end-effector positions and orientations, calculates the inverse kinematics and sends the manipulator joint values to the virtual reality computer. An overview of the experimental setup high-level architecture is shown in Figure 8.8.

The Jacobian transpose algorithm [102] augmented with the equations from [115] is used to compute the inverse kinematics.

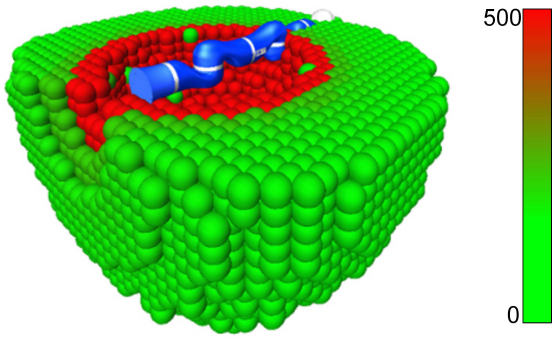


Figure 8.7: LWR distance to joint 4 limit map. Lower values correspond to larger distance from joint limit. For better visualization only the bottom half of the workspace in the Z axis is shown, since the upper part is symmetrical

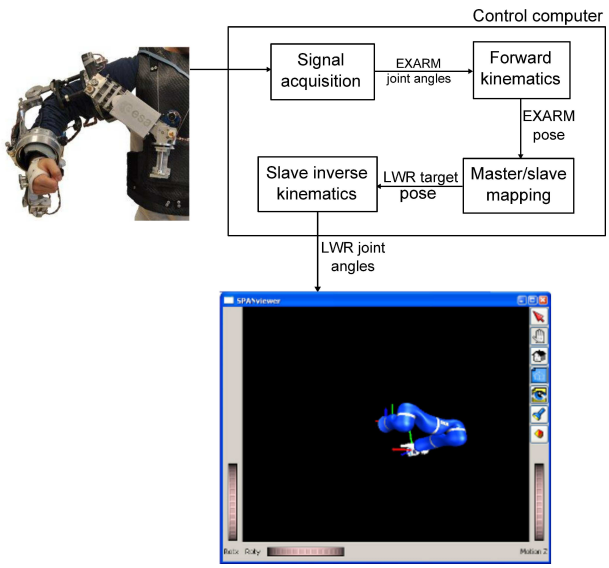


Figure 8.8: Experimental setup high-level architecture showing the EXARM and the LWR visualization

## 8.4 Results and discussion

In this section the optimization results and the performance of the optimized mounting in teleoperation are analysed.

Figure 8.9 shows a comparison between the reachable orientation manipulability for the default and optimized end-effector mounting. Analysing the two mounting performances it

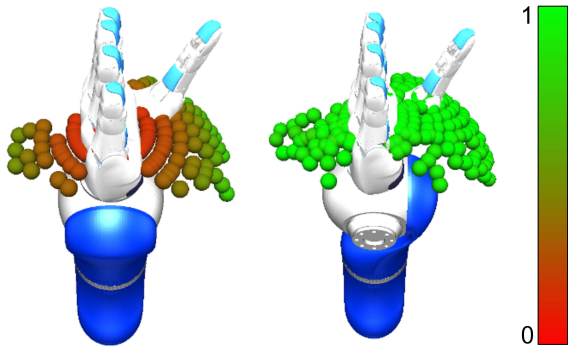


Figure 8.9: Manipulability comparison for reachable orientations between default (left) and optimized (right) end-effector mounting. Higher values correspond to areas of better manipulability.

is visible that the optimized mounting (right) places all the reachable target orientations in an area of maximum manipulability, distant from the wrist singularity.

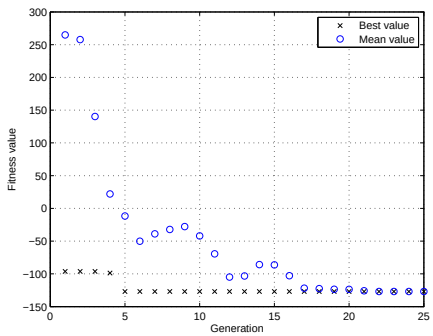


Figure 8.10: Best and average fitness evolution

A genetic algorithm with a population of 30 individuals, roulette selection, single-point crossover and a mutation probability of 5 percent is used to determine the optimal slave robot base placement. The best and average fitness evolution is shown in Figure 8.10. This optimization determines that the ideal mounting is $R_x = 40°$, $R_y = 52°$ and $R_z = 56°$ using XYZ Euler angle representation. As illustrated in Figure 8.11 the proposed slave manipulator mounting (right) clearly places the task-space area in the zone of highest manipulability of the manipulator. Thus, combining the proposed end-effector slave base mounting, any arbitrary motion by a human operator is within the controllable areas of the slave manipulator workspace.

The inverse kinematics tracking performance for the human reachable area is shown in Figure 8.12. The LWR is able to consistently follow the arbitrary motions without cartesian

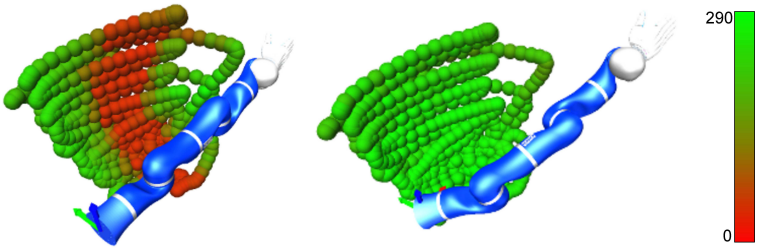


Figure 8.11: Comparison of manipulability performance between default and optimized slave manipulator placement

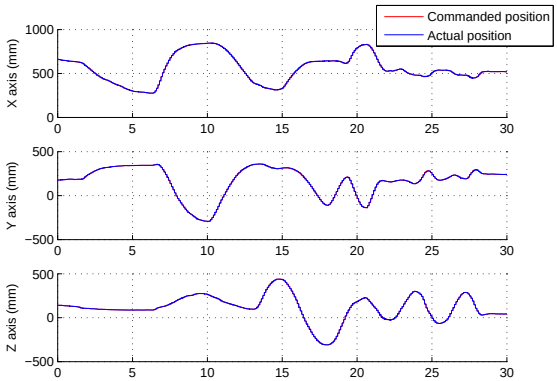


Figure 8.12: LWR inverse kinematics position tracking performance

deviations and, as seen in Figure 8.13, all the joints are away from its limits during operation. Using the proposed mapping the slave can track the operator robustly in a range of approximately 500$mm$ in each of its axis without reaching into singularities or joint limits. The good operator to LWR geometrical configuration correspondence is shown in Figure 8.14 for 3 different postures.

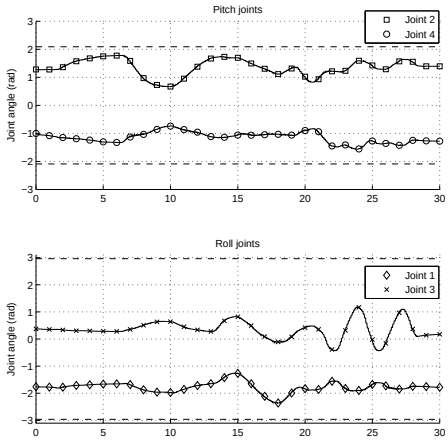


Figure 8.13: LWR distance to joint limits. The maximum and minimum joint angle is indicated by the dashed line.

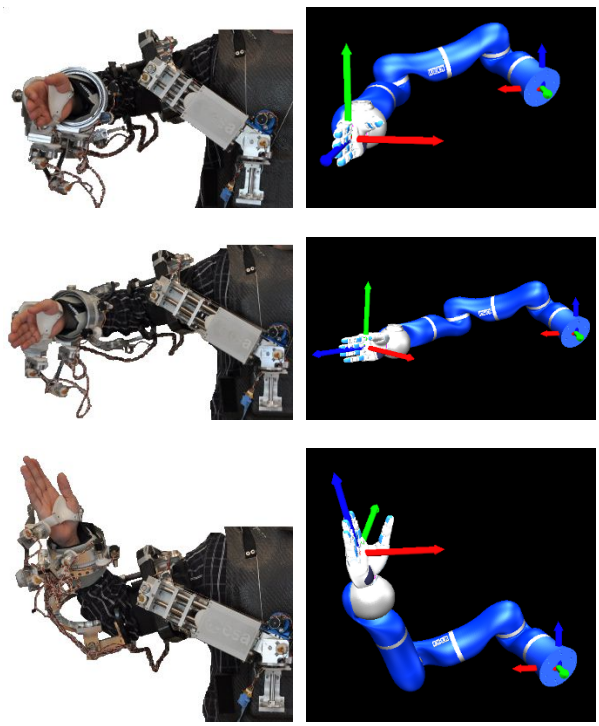

Figure 8.14: Operator to LWR posture mapping showing the geometrical configuration correspondence between the human operator and the slave robot arm.

## 8.5 Conclusion

The proposed mapping between the EXARM exoskeleton and the 7-DOF LWR together with the placement optimization ensures geometrical correspondence between the operator and the slave manipulator while simultaneously avoiding singularities and joint limits during real-time teleoperation.

Even though only a part of the slave workspace is available for teleoperated control this area is similar to the human operating area and corresponds to the zones of higher dexterity of the slave. Thus it is expected that several human-like handling tasks can be executed in a robust and intuitive manner in teleoperation with this configuration.

Additionally, since the human operator parameters are determined online the device is adaptable to a large range of users without any adjustment.

CHAPTER 9

# Conclusion

## 9.1 Recapitulation of the goal

It is the main goal of this research to achieve maximum transparency and time-delay robustness in bilateral teleoperation using dissimilar multi-dof master-slave devices, in particular when using impedance-type masters to command impedance-controlled slave manipulators.

This overall goal can be divided into the following sub-goals:

- Understand the influence of human operator, environment, control system parameters and time-delay on the stability and performance of a teleoperation system composed by an impedance-type master device and an impedance-controlled slave.
- Develop a control strategy that ensures system stability, independent of time-delay and other communication constraints, while still providing a maximum level of transparency to the operator.
- Propose a hardware and control architecture, as well as a master/slave position mapping, which allows transparent bilateral teleoperation using kinematically dissimilar multi-dof master-slave devices while being robust to time-delay and other communication channel constraints.

## 9.2 Discussion

The research work presented in this thesis enabled the implementation of a robust and transparent multi-dof bilateral teleoperation system under time-delay. The goal was achieved both by understanding the effects of the different system characteristics on the stability and performance of the system and having a control strategy that ensures stability independently of communication channel characteristics. The capabilities of the proposed control strategy were validated on a multi-dof bilateral teleoperation system using an impedance-type exoskeleton to command an impedance-control lightweight robot over a bandwidth limited mobile internet connection. In the remaining of this section, the obtained results and its implications and limitations are discussed in a global perspective.

### 9.2.1 System characteristics influence on stability and performance

The stability and performance analysis done in Part I has shown that, independently of the human operator and environment characteristics, with convenient parameter tuning, the

system can be made stable for constant time-delay in the communication channel. While these results could suggest that a system could be made stable by parameter tuning to arbitrary time-delay, these values are limited by the master and slave characteristics and can, therefore, be configured only to a limited range typically of up to a maximum of some tens of milliseconds. The analysis has also shown that, in free-air motion, the highest stability margin is obtained when having a master device with low controller stiffness settings commanding a slave with high stiffness. In rigid contact, the highest stability margin is achieved with the opposite settings, i.e. having a high master controller stiffness commanding a slave with low stiffness. In all cases, increasing the controller damping values of the system contributed to the system being stable up to higher time-delay values.

From the system performance analysis it can be observed that, in terms of steady-state transparency, as long as the transparency optimized tuning rules are kept, the stiffness rendered to the operator in steady-state is equal to that of the environment, independently of time-delay. To overcome the difficulties of quantifying transparency in free-air, the reflected damping criteria was introduced. This criterion shows that the damping felt by an operator interacting with the master device in bilateral teleoperation increases linearly with time-delay with a factor dependent on the master and slave controller stiffness settings. Relating the stability results with the performance analysis, it can be observed that parameters which contribute to a higher stability of the system results in the operator feeling a larger damping in free-air.

One situation which was not theoretically analysed, neither for performance nor stability, is the transition between free-air and contact. From the experimental results it can be observed that, as expected, with increasing time-delay, even when the system remains stable, the operator feels the transition between the free-air and contact as increasingly softer. This effect is also more visible with controller settings which ensure stability for longer time-delay.

When analysing the effects of human operator and environment characteristics on the stability of the system it was shown that a more rigid environment causes the system to become unstable for shorter values of time-delay. The presence of the human operator, despite being an active element in the system, always contributes to increasing the stability margin. These results confirm research done previously by Hogan [75] that reached identical conclusions.

Comparing the theoretical stability analysis with experimental results it was shown that, using the Lambert W method, an accurate stability border of the system can be computed. The stability analysis is based on a numerical method, which means that the actual results are only valid for the system for which the analysis was performed. Nonetheless, the guidelines obtained in the analysis have been empirically verified in other systems and the general results hold both in one-dof and multi-dof cases. While similar results could possibly be achieved using frequency-domain techniques, these require a complex loop reshaping [22] and do not give other information than the system stability boundary. It is expected that in the future, the poles of the system can be directly related to the performance and that controllers can be designed by pole-placement or other state-space control methods. The effects of transparency on human operator task performance are an open question in the field, which remains to be studied.

### 9.2.2 Time-delay robust stability

In Part II, an extension to the existing time-domain passivity control method was presented. The proposed method enables using time-domain passivity control for bilateral teleoperation with the 4-channel architecture. The method has been experimentally validated both for 1-dof and multi-dof bilateral teleoperation.

Even though stability is ensured, the overall behaviour of the system is highly dependent on how the human operator interacts with the master device, on the characteristics of the remote environment and on the controller parameter settings. Naturally, controller parameter settings which result in higher stability margins result in less energy dissipation by the passivity controller. Therefore, a trade-off between the performance and stability of the system is still required even when using the time-domain passivity control method.

Previous implementations of the time-domain passivity control were limited to position-force and position-position control architectures which have low transparency performance both with and without time-delay. Also, modelling the position controllers as current sources and applying parallel passivity controllers resulted in position drifts which are not desirable in the type of teleoperation scenario considered in this thesis.

The proposed extension to the time-domain passivity controller, models all the controllers as dependent voltage sources. Passivity of the system is ensured by using series passivity controllers which dissipate the excess energy introduced by the time-delay in the communication channel. The obtained results have shown that the system remains stable independently of communication constraints, such as variable time-delay and data loss, while still resulting in a high level of transparency to the operator. The drawback of this strategy is that the energy dissipation behaviour is noisy, resulting in vibrations in the system which can be clearly felt by the operator.

The method was extended to multi-dof bilateral teleoperation with similar results, as was described in Chapter 5. In multi-dof, different energy dissipation strategies can be selected. In this work, we have used a uniform distribution in every Cartesian direction. As in the one-dof situation, the energy dissipation behaviour is noisy and has clear influence on the motion of the operator. The effects of vibrations, as well as advantages and drawbacks of different energy dissipation strategies, possibly related with the task which is being executed, need to be further researched.

### 9.2.3 Multi-dof bilateral teleoperation

In Part III it was demonstrated that, using the system proposed in this thesis, it is possible to execute complex 6-DOF tasks over a packet switched communications link. Using the Sensoric Arm Master exoskeleton, an operator is able to command the LWR in a stable fashion, receiving accurate force-feedback from the remote environment while the system remains stable at all times.

To enable highly transparent multi-dof bilateral teleoperation, a fully integrated hardware solution using the SAM exoskeleton to command a Kuka Lightweight Robot in impedance-controlled mode was presented. The master architecture is based on the EtherCAT real-time communication bus whereas the communication between the master and the slave takes place over a classical UDP link. Using the EtherCAT protocol allowed reaching high performance control bandwidths while keeping a reduced hardware size and weight of the

master. The downside of the protocol is its complexity, especially the fact that each slave in the network needs to be configured individually at start-up and multiple algorithms are necessary on the master to handle the distributed clock of the system. Nonetheless, these are design and implementation difficulties which do not affect the usability and performance of the system.

Having the 4-channel architecture with the SAM exoskeleton controlling the LWR in impedance-control mode achieves a high level of transparency in both free-air and contact. The stiffness rendered to the operator for different surfaces allows a clear distinction to be felt between them. In free-air motion the dynamics of the master device are felt by the operator, in particular the effects of gravity and friction in the joints.

Given the mass of the device, the used DC motors are not able to fully compensate for gravity while still having enough power to generate force feedback to the operator. With 30% gravity compensation the user can operate the device more comfortably while the motors can still provide sufficient torque for accurate force-feedback rendering. The forces caused by friction are always below 10 N and are therefore causing little effect to the operator. Problems occur when not only translations but also rotation are commanded since the torques exerted by the user to keep the position of the master device are transmitted to the slave, thus causing a position offset. This problem highlights the need of having either a complete gravity compensation, which is not a problem in space environments, or an accurate model of the forces and torques caused by the weight of the device.

It is expected that using an absolute mapping, in which the operator arm configuration always corresponds to the same slave end-effector. The proposed mapping method, using the EXARM exoskeleton and the 7-DOF LWR together with the placement optimization ensures geometrical correspondence between the operator and the slave manipulator while simultaneously avoiding singularities and joint limits during real-time. Even though only a part of the slave workspace is available for teleoperated control this area is similar to the human operating area and corresponds to the zones of higher dexterity of the slave. Thus, several human-like handling tasks can be executed in a robust and intuitive manner in teleoperation with this configuration.

## 9.3 Future work

While the goal proposed for this work can be considered achieved, both new and known questions remain open for future research. In this section, possible points of future research, in particular human aspects, bilateral control with time-delay and shared control are further explored.

### 9.3.1 Human aspects

The focus on this thesis was on researching how to achieve a high transparency and time-delay robustness in bilateral teleoperation using dissimilar multi-dof master-slave devices. It was assumed that the higher the transparency, the easier it would be for an operator to execute a task in the remote environment. However, it has so far not been shown how transparency affects human operator performance when executing different tasks. The tele-

operation system presented in this thesis should enable such studies since a large range of transparencies can be achieved.

It was also discussed that the stabilizing action of the time-domain passivity controller introduces mechanical noise in the system which can be clearly felt by the operator. This noise is dependent on control system parameter settings and energy dissipation strategies. So far, it was shown that tasks such as peg-in-a-hole can be executed despite these effect. However, further studies are needed to understand how the combined effects influence the human operator task performance and what are the ideal.

As the main goal of a teleoperation system is to allow a human operator to execute tasks in a remote environment, these studies are needed to understand how to best align the system design and the operator task performance.

### 9.3.2 Bilateral control with time-delay

The stability analysis done in this work was based on the usage of the Lambert W function to determine the exact pole placement of a system described in state-space. While the used method allows computing accurate stability borders, several challenges remain open in this domain. On one side no closed form solution exists for the equation presented in Chapter 2. Finding a closed-form solution would enable, for example, state observers for the state-space delayed system to be implemented.

Since the system poles can be computed using this method, it should be investigated how the performance of the system and the pole placement are related. If these relations could be established, it would be possible to use pole placement design methods [72] to implement a system with a well defined performance under specific time-delay conditions.

### 9.3.3 Shared control

When time-delay between the master and the slave is short and enough bandwidth is available for transmitting good quality video data, bilateral teleoperation system which fully rely on the human operator are usable and can lead to good results. However, in many cases, either time-delay values are long or the communications bandwidth is too low. In these cases, the human operator performance will be reduced and it might be impossible to execute certain tasks.

To mitigate the effects of time-delay, shared control systems in which higher level control loops are implemented both on the master and the slave side could be used to provide additional cues to the operator or automatically move the slave robot. The additional information to the operator could be either in the visual form, using, for example augmented reality displays or haptic cues, in which the master device inputs additional guidance forces to the operator.

## 9.4 Main conclusions

The main conclusions of this thesis are:

(1) Having an impedance-type master device commanding an impedance-controlled slave manipulator using the 4-channel architecture combined with time-domain passivity control allows high transparent and time-delay robust bilateral teleoperation.

(2) Having a master device with soft controller stiffness setting commanding a rigid slave increases the stability margin in free-air motion whereas a master device with hard controller stiffness setting commanding a soft slave increases the stability margin in rigid contact.

(3) Increasing the damping of the system controllers results in system stability for larger time-delay values.

(4) The damping felt by an operator when moving in free-air increases linearly with time-delay with a factor dependent on the controller stiffness settings.

(5) Controller parameter settings which result in higher system stability will generally result in a higher damping being felt by the operator in free-air motion.

(6) Transparency in contact is independent of the stiffness and damping settings of an impedance controlled slave as long as the 4-channel architecture and the transparency optimized tuning rules are used and the system remains stable.

(7) The human operator always contributes to increase the stability of the bilateral teleoperation system.

(8) The larger the remote environment stiffness, the smaller the stability margin of the system.

(9) Using the proposed 4-channel time-domain passivity controller ensures that the system remains stable independently of the communication channel constraints and that the highest reflected contact stiffness can be achieved.

(10) Modelling the controllers as voltage dependent sources and implementing all the passivity controllers as series elements ensures that the position tracking of the system is never lost.

(11) Using only series passivity controllers results in a noisy energy dissipation behaviour.

(12) The optimized mapping allows the operator to command the slave device while avoiding singularities and joint limits during real-time teleoperation and ensuring geometrical correspondence between the operator and the slave manipulator.

(13) An optimal mapping is achieved by making use of only a part of the slave workspace for teleoperation which is similar to the human operating area and corresponds to the zones of higher dexterity of the slave.

# Appendices

APPENDIX A

# SPANviewer - A Visualization Tool for Advanced Robotics Applications

S. Kimmer, J. Rebelo and A. Schiele
*12th symposium on Advanced Space Technologies In Robotics and Automation (ASTRA)*, 2013

## A.1 Introduction

When developing control algorithms and systems for teleoperation, the need often arises for real-time debugging of new kinematic and dynamics algorithms, image recognition techniques and real/virtual image combination for teleoperation scenarios. Currently, no tool exists that allows a quick and adaptable definition of robotics structures that can be controlled in real-time and potentially serve as an overlay of real video images. The existing visualization tools for virtual reality focus on realistic image rendering but lack the specific robotics-oriented applications (e.g. structure kinematics representation), whereas robot simulators (e.g. Webots [118]) aim at emulating real-hardware and dynamics behavior which makes them very complex and reduces real-time capabilities.

The Space Portable Applications Network (SPAN) aims at being a set of highly reusable tools and libraries which can be used to allow quick implementation and debugging not only of new algorithms but also of more complete system implementations. The goal of this paper is to describe the visualization tool of this library, the SPANviewer, detailing its software structure and design while highlighting the use-cases and applications for which it was developed.

The SPANviewer allows the user to define any robot by a hierarchical XML (Extensible Markup Language) structure using parameters of standard representations common in robotics (e.g. Denavit-Hartenberg or frame coordinate system). The structures can be realistically represented using CAD (Computer Aided Design) models, but simple built-in models can be used instead if CAD models are not available. The XML input file also allows the definition of camera view-points in mono and stereoscopic view. Both the structure joint positions and the camera view-points can be adjusted in real-time through a UDP (User Datagram Protocol) or Shared Memory communications interface. In addition, the viewer is able to render a real-time video stream and overlay it with the virtual structures controlled in real-time. Given the need of using both Windows and real-time Linux-based operating systems, the viewer implementation is platform independent.

This paper is organized as follows: Section A.2 describes the software architecture and design, Section A.3 highlight the main applications of the viewer and the conclusions and

future developments are stated in Section A.4.

## A.2 Software overview

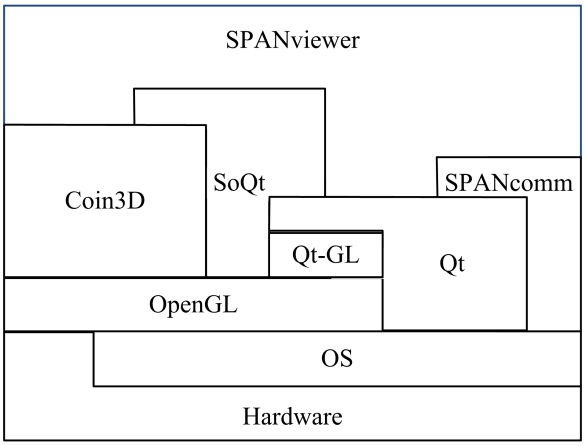


Figure A.1: Overview of the stack of used libraries. The OS can be any of the operating systems supported by Qt and OpenGL, e.g.: Microsoft Windows XP, 7, 8 or Linux

As explained in the introduction, the SPANviewer aims at being platform independent. For this reason it was implemented in C++ on top of Coin3D [119], a higher level library of the OpenGL [120] library. For windowing and other graphical user interface functionality the SoQt binding to the Qt library [121] is used. A diagram of the component stack is shown in Figure A.1.

Since all of the components are cross platform the SPANviewer is running on all major platforms. For newer Windows and Debian-based Linux distributions an installer and a package exist that enables fast deployment of the software. This section describes the main characteristics, such as the scene model, the camera model and the available communications mechanisms. Finally some of the additional capabilities of the SPANviewer, such as the stereoscopic view and the 3D model rendering are also presented.

### A.2.1 Scene definition

At the base of the viewer functionality stands the world model described in XML where the scene and cameras can be defined. This XML is described by the ESA-Telerobotics-Lab-SPAN schema. Under the <scene> tag all the objects and structures are defined. The viewer allows the simulation of both series and parallel structures defined by Denavit-Hartenberg parameters (using the convention in [102]) . An example of a parallel and a series joint structures model is shown in List. A.1 and the output in Figure A.2. The scenes resulting from these models are depicted in Figure A.2. Note that the only difference between implementing a series and a parallel structure is on the hierarchy of the XML model.

Listing A.1: SPANviewer example model file to generate a series structure. The structure is defined under the <scene> node using the DH convention. The visualization is visible in Figure A.2(a)

```
<?xml version="1.0"?>
<world xmlns="ESA-Telerobotics-Lab-SPAN">
  <scene units="0.2">
    <structure convention="dh">
      <joint a="0" alpha="-1.5708" d="0.5" offset="0" theta="0">
        <joint a="0.5" alpha="1.5708" d="0" offset="0" theta="0">
        </joint>
      </joint>
    </structure>
  </scene>
</world>
```

Listing A.2: SPANviewer example model file to generate Figure A.2(b). It is an XML-file which follows the XML schema under the namespace ESA-Telerobotics-Lab-SPAN. The parallel structure is defined under the <scene> node using the Denavit-Hartenberg convention.

```
<?xml version="1.0"?>
<world xmlns="ESA-Telerobotics-Lab-SPAN">
  <scene units="0.2">
    <structure convention="dh">
      <joint a="0" alpha="-1.5708" d="0.5" offset="0" theta="0">
      </joint>
      <joint a="0.5" alpha="1.5708" d="0" offset="0" theta="0">
      </joint>
    </structure>
  </scene>
</world>
```

Besides the robotic structures it is also possible to render pre-defined objects such as cubes, spheres, cylinders and arrows and to include custom position and rotation offsets. As already mentioned, the viewer is independent from any physics or kinematics engine, therefore it is the task of the user to implement the needed algorithms and send the actual joint values to be displayed through the viewer communications channel.

The viewer is able to import model parts written in the Virtual Reality Modelling Language (VRML). Most computer aided design program have the possibility to export their formats to VRML into a world file (*.WRL file). The WRL file can then be included at any point in the scene or at any joint of a structure.

Images which can be used to display a video stream can be added to a scene. This can be a shmimage object as in List. A.4.

### A.2.2 Camera definition

With the SPANviewer it is possible to visualize a scene with predefined point of views. Each point of view is thereby displayed in a separate window. The location of the appear-

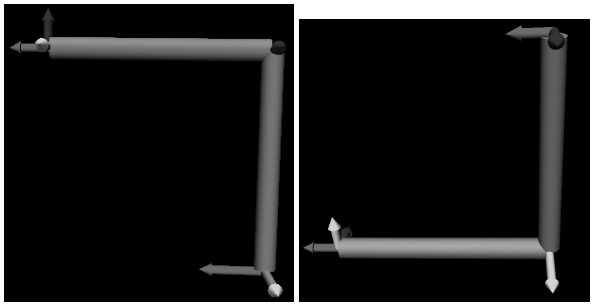

(a) Series joint (b) Parallel joint

Figure A.2: Example of simple series and parallel structures. Note that in both images the center point is represented by the axis on the lower right corner. In this scene, the default built-in models are used to represent the structure. The model files which can be used to generate this can be seen for (a) in List. A.1 and for (b) in List. A.2

Listing A.3: Example with three cameras viewing a cube. The three cameras will produce four windows, one for each mono-camera and two for the stereo-camera. The two windows of the stereo camera can be placed to two projectors of a passive stereoscopic viewing system. The resulting windows are shown in Figure A.3 and in Figure A.4

```
<?xml version="1.0"?>
<world xmlns="ESA-Telerobotics-Lab-SPAN">
  <camera>
    <monocamera window_title="monocamera␣X">
      <pose x="100" y="0" />
    </monocamera>
    <monocamera window_title="monocamera␣Y">
      <pose x="0" y="100" />
    </monocamera>
    <stereocamera>
      <pose x="700" z="200" z="0" />
      <screendef diameter="1016" />
    </stereocamera>
  </camera>
  <scene units="100">
    <cube sx="100" sy="10" sz="20" tx="200" axis_scale="5"/>
  </scene>
</world>
```

ance of each window can be configured for multi monitor systems. Hence it is possible to set up multiple view point human machine interfaces. In List. A.3 two viewpoints are configured with the <monocamera> tag. One camera enables the view of the back of a cube and the other a side-view of that cube. The resulting windows are shown in Figure A.3.

It is also possible to view a scene in a stereoscopic mode. Therefore two viewpoints will be created which represent the view of the left and right eye of the human. Each side can be displayed as a separate window which allows the usage of passive stereoscopic displays. A

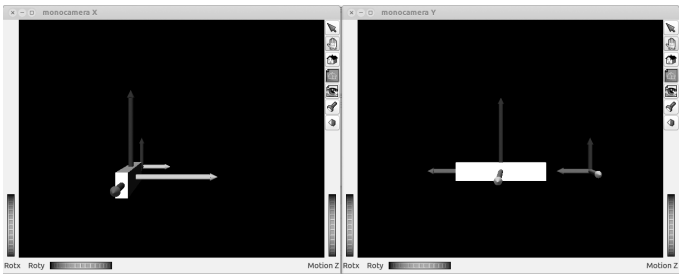


Figure A.3: Two windows of two mono-cameras as defined in List. A.3. The left window shows the cube from behind while the right window shows the same cube from the side.

passive system is often used with larger projections where each of the two projectors needs its own image source. A stereo-camera has been defined besides two other mono-cameras in List. A.3. This stereo-camera results in the two windows as shown in Figure A.4. Those two windows can be viewed by a passive stereoscopic display system. There a human observer will perceive the cube 200mm in front of the screen. The latter will be true if the observer is located 700mm in front and 200mm above the center of the screen because the pose of the stereocamera is configured as x="700" and z="200" (the global unit is assumed to be mm). The screen size can be configured as the diameter in a screendef tag. In this example it is set to a screen with a 40" (1016mm) diagonal. The cube will appear in the size it is specified in the XML model file, i.e 100mm long, 10mm wide and 20mm height.

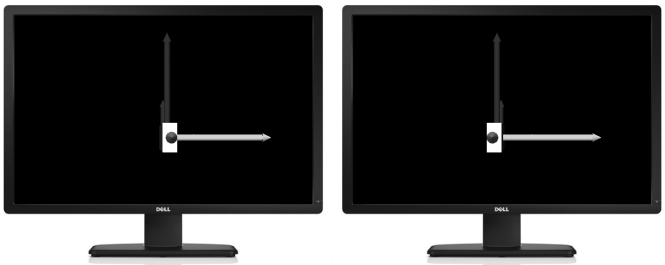

Figure A.4: Two windows of the stereo-cam output of List. A.3. The left window represents the view of the left eye and the right window for the right eye respectively.

### A.2.3 Communication Model

Another key functionality of the viewer is the ability to enable fast configurable communications with the model. To achieve this goal the user can, in the XML model file, reference to different communication channels that will receive new values for the objects characteristics. These characteristics can be e.g. position and orientation.

A general way of using different channels is shown in List. A.4. There the images could be used to display a video stream written in shared memory, the view-points of the virtual

Listing A.4: Example model file of the SPANviewer with the child nodes configured to listen on different communication channels. The letters k,m and n must be hereby be replaced by a valid identification number. A schematic plot of this configuration is shown in Figure A.5. The exact communication mechanism (the definition of the channels) is configured only at execution time. An example is shown in List. A.5.

```
<?xml version="1.0"?>
<world xmlns="ESA-Telerobotics-Lab-SPAN">
  <camera>
    <monocamera channel="1" />
    <stereocamera channel="k" />
  <camera>
  <scene>
    <structure channel="1" />
    <structure channel="m" />
    <shmimage channel="1" />
    <shmimage channel="n" />
  </scene>
</world>
```

Listing A.5: Example command line to load the xml.xml model file. For each communication category two channels are defined. Whereas the first channel get the identification number 1 and the second the identification number 2. The channel can be addressed by those identification numbers in the xml file.

```
spanviewer --input xml.xml --channel 25000 shm --cam-channel shmCam 18000
    --img-channel shmImg1 shmImg2
```

cameras could be controlled by a tracking mechanism and the structure could be controlled by an exoskeleton. The communication channels are grouped to enable different update speeds for each group. Those groups are: camera-channels to allow view-point updates, channels to allow scene object updates and image-channels to allow video streaming. An overview of the communication groups and how they are embedded in a SPANviewer model is given in Figure A.5. Inside a model file only the identification number of the channel can be configured, the channels itself can be configured at the command line options of the viewer. Each channel can be a UDP port to listen to or a shared memory key to read from. In the command line options a pure numerical argument represents a UDP port, others represent a key for a shared memory region. In List. A.5 an example is shown where various channels are defined. During execution each category is checked for changes at a periodic scheduled basis. For instance the image input data can be read with 25Hz while the camera input data can be read with 100Hz. This allows for a configurable and transparent way of prioritization to the different input device categories. If the viewer is unable to render in the desired speed a message will be displayed about the dropped input data frames. In the case input data is dropped the viewer renders as fast as possible. The communications are done by simple arrays of doubles and the order is identical to the one in which the objects are defined in the XML. This order can be printed to the command window when the SPANviewer is started for user reference. In List. A.6 a more concrete

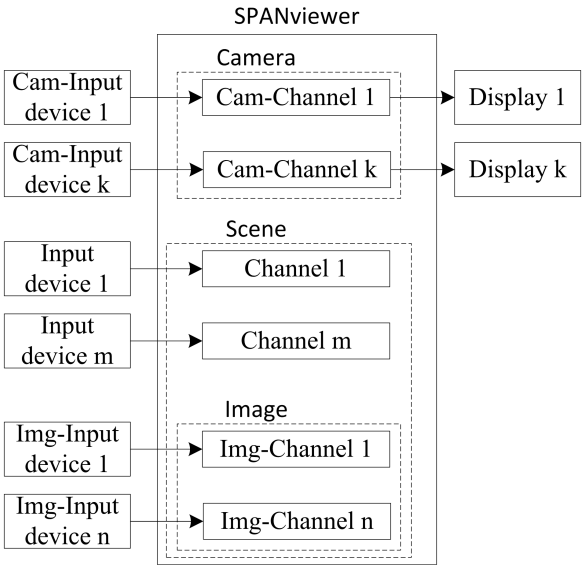


Figure A.5: The general communication model of the SPANviewer. A communication category for general, camera image input devices exists. Each camera will result in a new display (window).

Listing A.6: Example of objects of a SPANviewer model file. The structure contains two joints which can be controlled through communication channel 1. In addition a cube is located in the scene and can be controlled through communication channel 2.

```
<structure convention="dh" channel="1">
  <joint a="10" alpha="0">
    <joint a="20" alpha="1.5708" />
  </joint>
</structure>
<cube channel="2"/>
```

example is shown which contains a manipulator with two joints and a cube in the same scene. These two objects can be controlled through two different channels. The joints of the manipulator can be controlled by, e.g. a joystick through channel 1 and the cube can be controlled, e.g. by a computer simulation through channel 2. The model can be executed with:

```
spanviewer --input in.xml --channel 25000 shm
```

Then the joystick must send its data to UDP port 25000 (channel 1) and the computer simulation must write the data to the shared memory region with the key "shm" (channel 2). For test purposes values can be send with the enclosed sendvalues program. If for example the angle of joint 1 shall be 1.1 and the angle of joint 2 shall be 1.2 following python script can be used:

```
import socket, struct
sock = socket.socket(socket.AF_INET, socket.SOCK_DGRAM)
sock.sendto(struct.pack("dd", 1.1, 1.2), ("127.0.0.1", 25000))
```

## A.3 Applications

The SPANviewer is designed to be usable in various fields of robotics, nonetheless the main driver of these developments is the Multi-Purpose End-To-End Robotics Network (METERON) project [58]. In the next subsections three of the applications which are targeted specifically at METERON or related developments are outlined.

### A.3.1 Kinematic Studies

One of the main applications of the SPANviewer is to allow quick debugging and analysis of different types of control algorithms. For example, when controlling a 7 degree-of-freedom manipulator using an exoskeleton, the visualization is needed to ensure that the robot behavior is following exactly the commands given by the exoskeleton. Using the SPANviewer, a kinematic structure based on the same D-H parameters used for the kinematics computation can be defined. The kinematic algorithm (such as e.g. Jacobian transpose augmented with elbow control [122]) can be easily analyzed by sending the resulting joint values in real-time to the visualization tool. An example of simultaneous views of the exoskeleton and the simulation is shown in Figure A.6

It is also common in telerobotic applications that the user is provided with views from fixed cameras in different angles. To simulate these scenarios, the viewer allows the simultaneous implementation of different viewpoints. An example of a typical scenario with Top, Left and Front views of the LWR robot is shown in Figure A.7. This experimental setup was used to experiment on the effects of perception on the user performance on a positioning task.

### A.3.2 Overlay of Video Streams

In teleoperation scenarios, in particular in space teleoperation, it is common that the available bandwidths are very limited which allows only low-quality video to be transmitted. Naturally, this leads to extended difficulties in executing remote tasks. Nonetheless, since models of the manipulator and potentially of the environment can be available it is possible to enhance the video perception to the user by overlaying virtual scenes on top of the real video stream.

The SPANviewer allows simultaneous display and real-time update of both real and virtual scenes. The robot structure is identical to the one described in Figure A.8.This overlaid virtual robot gives the operator additional information about the structure position which allows a better evaluation of the current situation at the remote site. It is also possible to render additional items, e.g. color-coded arrows representing forces and velocities, which can transmit to the operator a complete and intuitive overview of the operations scenario within a single display.

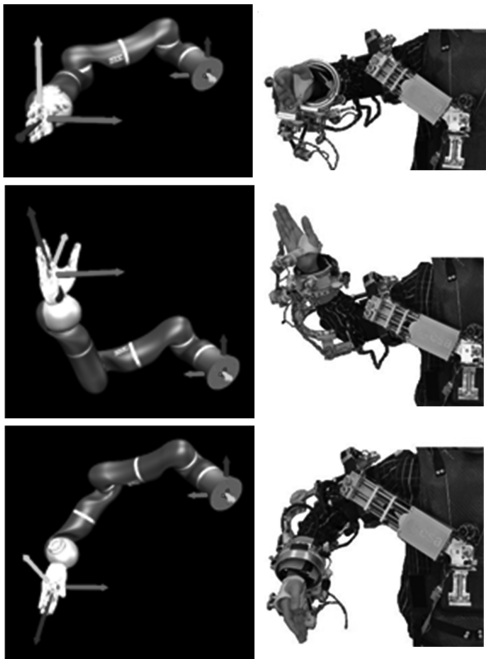

Figure A.6: Example of kinematic tracking debugging.


Figure A.7: SPANviewer showing three simultaneous views of the LWR

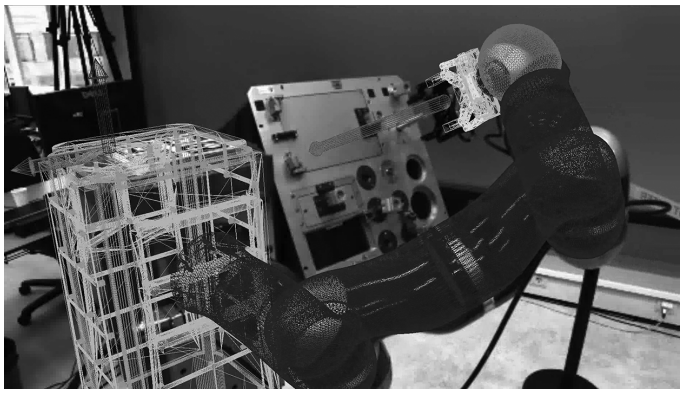

Figure A.8: Overlay of a real scene with a virtual scene. The real scene is a gray-scale video stream from a camera. The overlay is a model of the robot used in the real scene while seven joints are actuated. Additionally the force which is applied to the robot is displayed at the tool of the robot.

The virtual scene can be send to the viewer in predefined formats. The cross platform GStreamer [123] library can be used to stream various video sources to the desired image object inside the viewer. This achieved by the sending the video data to a identified shared memory. Any image object with that identifier of the running model of the SPANviewer will then be displayed with a configured frame-rate.

### A.3.3 Stereoscopic Visualization and Augmented Reality

It is often desirable to view an object from different viewpoints. If for instance an object has to be touched which lies in a three dimensional space, only one view point is not enough to determine its position in that space. For an intuitive solution the head of the user can be tracked and the point of view of the model will be adjusted accordingly. This results in static model in front of the displaying screen. The tracker values can be sent to the viewer in the same way as other values. A correct representation of such a model is dependent of the size of the displaying device. This can be configured within a SPANviewer model file.

The ability of visualizing objects in a real three dimensional space allows for a mixture of real objects (in front of the displaying device) with virtual objects. In Figure A.9 a copy of a real robot is displayed as a virtual object besides the real robot with determined and configurable geometric relationship in real space.

In addition the applied force to the robot is displayed as a red arrow which pops-up at the point of exertion in real space. If the operator is moving the appearance of the arrow will remain at the same point in space.

## A.4 Conclusion and Future Work

As described in this paper, the SPANviewer is currently in a state in which it can already be used to execute several tasks, ranging from control algorithm debugging to telerobotics

Figure A.9: Example of an augmented reality in front of a passive 3D-screen. The robotic arm is controlled by the operator which is wearing an exoskeleton. The head of the operator is tracked which enables the display of an arrow at the point in the three dimensional space where the corresponding force is exerted. In addition a copy of the robot is visualized behind and to the right of the real one.

operations with virtual overlaid information. The tool has been widely used in the activities of the ESTEC Telerobotics and Haptics Lab. Nonetheless, to further increase its usability and task range it is now planned to integrate the viewer with physics simulation software in which the same description language can still be used to create both the virtual scene and the virtual dynamics world. Also, the set of formats available for the video stream is currently very limited. To enable a more generic integration to other formats, the GStreamer library may be integrated into the SPANviewer. The entire range of SPAN tools aims at being self-contained and run on a distributed system. Currently the simple communication mechanisms available are adequate for direct interaction between two or three different systems. However, as more systems need to interact to create the simulation and visualization environments the simple communications techniques become unmanageable. The Data Distributed Service (DDS) communication middleware will be integrated into the viewer and future SPAN tools to allow a flexible and easy communication between each process. Once these tools and their documentation reach a high maturity level, they can be made available in open-source form to the community for further usage and enhancement.

# Bibliography


[1] T. B. Sheridan, *Telerobotics, automation and human supervisory control*. The MIT press, 1992.

[2] G. Guthart and J. K. Salisbury Jr, "The Intuitive$^{TM}$ Telesurgery System: Overview and Application," in *Proc. IEEE Int. Conf. on Robotics and Automation (ICRA)*, 2000, pp. 618–621.

[3] C. Preusche, D. Reintsema, K. Landzettel, and G. Hirzinger, "Rokviss–preliminary results for telepresence mode," in *Proc. IEEE/RSJ Int. Conf. Intelligent Robots and Systems (IROS)*, 2006, pp. 4595–4601.

[4] A. R. Lanfranco, A. E. Castellanos, J. P. Desai, and W. C. Meyers, "Robotic surgery: a current perspective," *Annals of surgery*, vol. 239, no. 1, p. 14, 2004.

[5] M. Kitagawa, A. M. Okamura, B. T. Bethea, V. L. Gott, and W. A. Baumgartner, "Analysis of suture manipulation forces for teleoperation with force feedback," in *Medical Image Computing and Computer-Assisted Intervention (MICCAI)*. Springer, 2002, pp. 155–162.

[6] Geomagic, "Touch," http://geomagic.com/en/products/phantom-omni/overview/, Accessed in January 2015.

[7] Force Dimension, "sigma.7," http://www.forcedimension.com/products/sigma-7/overview, Accessed in January 2015.

[8] W. S. Kim, B. Hannaford, and A. K. Bejczy, "Force-reflection and shared compliant control in operating telemanipulators with time delay," *IEEE Transactions on Robotics and Automation*, vol. 8, no. 2, pp. 176–185, 1992.

[9] R. Daniel and P. McAree, "Fundamental limits of performance for force reflecting teleoperation," *The International Journal of Robotics Research*, vol. 17, no. 8, pp. 811–830, 1998.

[10] A. Tobergte, P. Helmer, U. Hagn, P. Rouiller, S. Thielmann, S. Grange, A. Albu-Schaffer, F. Conti, and G. Hirzinger, "The sigma. 7 haptic interface for mirosurge: A new bi-manual surgical console," in *Proc. IEEE/RSJ Int. Conf. Intelligent Robots and Systems (IROS)*, 2011, pp. 3023–3030.

[11] T. F. Chan and R. V. Dubey, "Design and experimental studies of a generalized bilateral controller for a teleoperator system with a six dof master and a seven dof slave,"

in *Proc. IEEE/RSJ Int. Conf. Intelligent Robots and Systems (IROS)*, vol. 1, 1994, pp. 415–422.

[12] N. Hogan, "Impedance control: An approach to manipulation: Part II-Implementation," *Journal of Dynamic Systems, Measurement, and Control*, vol. 107, no. 1, pp. 8–16, 1985.

[13] G. A. V. Christiansson, "Hard master, soft slave haptic teleoperation," Ph.D. dissertation, TU Delft, 2007.

[14] G. Hirzinger, N. Sporer, A. Albu-Schaffer, M. Hahnle, R. Krenn, A. Pascucci, and M. Schedl, "DLR's torque-controlled light weight robot III-are we reaching the technological limits now?" in *Proc. IEEE Int. Conf. on Robotics and Automation (ICRA)*, vol. 2, 2002, pp. 1710–1716.

[15] R. O. Ambrose, H. Aldridge, R. S. Askew, R. R. Burridge, W. Bluethmann, M. Diftler, C. Lovchik, D. Magruder, and F. Rehnmark, "Robonaut: NASA's space humanoid," *IEEE Intelligent Systems and their Applications*, vol. 15, no. 4, pp. 57–63, 2000.

[16] R. Q. Van der Linde, P. Lammertse, E. Frederiksen, and B. Ruiter, "The hapticmaster, a new high-performance haptic interface," in *Proc. of the Eurohaptics conference*, 2002, pp. 1–5.

[17] A. Peer, "Design and control of admittance-type telemanipulation systems," Ph.D. dissertation, Technische Universitat Munchen, 2008.

[18] A. Schiele, "Fundamentals of ergonomic exoskeleton robots," Ph.D. dissertation, Delft Technical University, 2008.

[19] W. S. Kim, "Shared compliant control: A stability analysis and experiments," in *Proc. IEEE Int. Conf. Systems, Man and Cybernetics (SMC)*, 1990, pp. 620–623.

[20] S. Salcudean, K. Hashtrudi-Zaad, S. Tafazoli, S. P. DiMaio, and C. Reboulet, "Bilateral matched impedance teleoperation with application to excavator control," *IEEE Transactions on Control Systems*, vol. 19, no. 6, pp. 29–37, 1999.

[21] P. F. Hokayem and M. W. Spong, "Bilateral teleoperation: An historical survey," *Automatica*, vol. 42, no. 12, pp. 2035 – 2057, 2006.

[22] D. A. Lawrence, "Stability and transparency in bilateral teleoperation," *IEEE Transactions on Robotics and Automation*, vol. 9, no. 5, pp. 624–637, 1993.

[23] Y. Yokokohji and T. Yoshikawa, "Bilateral control of master-slave manipulators for ideal kinesthetic coupling-formulation and experiment," *IEEE Transactions on Robotics and Automation*, vol. 10, no. 5, pp. 605–620, 1994.

[24] J. E. Colgate and J. M. Brown, "Factors affecting the z-width of a haptic display," in *Proc. IEEE Int. Conf. on Robotics and Automation (ICRA)*, 1994, pp. 3205–3210.

[25] K. Hashtrudi-Zaad and S. E. Salcudean, "Transparency in time-delayed systems and the effect of local force feedback for transparent teleoperation," *IEEE Transactions on Robotics and Automation*, vol. 18, no. 1, pp. 108–114, 2002.

[26] ——, "Analysis of control architectures for teleoperation systems with impedance/-admittance master and slave manipulators," *The International Journal of Robotics Research*, vol. 20, no. 6, pp. 419–445, 2001.

[27] W. R. Ferrell, "Remote manipulation with transmission delay," *IEEE Transactions on Human Factors in Electronics*, no. 1, pp. 24–32, 1965.

[28] R. J. Anderson and M. W. Spong, "Bilateral control of teleoperators with time delay," *IEEE Transactions on Automatic Control*, vol. 34, no. 5, pp. 494–501, 1989.

[29] B. Hannaford, "A design framework for teleoperators with kinesthetic feedback," *IEEE Transactions on Robotics and Automation*, vol. 5, no. 4, pp. 426–434, 1989.

[30] G. Niemeyer and J.-J. E. Slotine, "Stable adaptive teleoperation," *IEEE Journal of Oceanic Engineering*, vol. 16, no. 1, pp. 152–162, 1991.

[31] ——, "Towards force-reflecting teleoperation over the internet," in *Proc. IEEE Int. Conf. on Robotics and Automation (ICRA)*, vol. 3, 1998, pp. 1909–1915.

[32] Y. Yokokohji, T. Imaida, and T. Yoshikawa, "Bilateral teleoperation under time-varying communication delay," in *Proc. IEEE/RSJ Int. Conf. Intelligent Robots and Systems (IROS)*, vol. 3, 1999, pp. 1854 – 1859.

[33] C. Benedetti, M. Franchini, and P. Fiorini, "Stable tracking in variable time-delay teleoperation," in *Proc. IEEE/RSJ Int. Conf. Intelligent Robots and Systems (IROS)*, vol. 4, 2001, pp. 2252–2257.

[34] B. Hannaford and J.-H. Ryu, "Time-domain passivity control of haptic interfaces," *IEEE Transactions on Robotics and Automation*, vol. 18, no. 1, pp. 1–10, 2002.

[35] J.-H. Ryu, J. Artigas, and C. Preusche, "A passive bilateral control scheme for a teleoperator with time-varying communication delay," *Mechatronics*, vol. 20, no. 7, pp. 812–823, 2010, Special Issue on Design and Control Methodologies in Telerobotics.

[36] J. Artigas, J. H. Ryu, and C. Preusche, "Time domain passivity control for position-position teleoperation architectures," *Presence: Teleoperators and Virtual Environments*, vol. 19, no. 5, pp. 482–497, 2010.

[37] C. Preusche, G. Hirzinger, J.-H. Ryu, and B. Hannaford, "Time domain passivity control for 6 degrees of freedom haptic displays," in *Proc. IEEE/RSJ Int. Conf. Intelligent Robots and Systems (IROS)*, vol. 3, 2003, pp. 2944–2949.

[38] K. Hertkorn, T. Hulin, P. Kremer, C. Preusche, and G. Hirzinger, "Time domain passivity control for multi-degree of freedom haptic devices with time delay," in *Proc. IEEE Int. Conf. on Robotics and Automation (ICRA)*, 2010, pp. 1313–1319.

[39] J.-P. Kim, C. Seo, and J. Ryu, "Multirate energy-bounding algorithm for high-fidelity stable haptic interaction control," *IEEE Transactions on Control Systems Technology*, vol. 19, no. 5, pp. 1195–1203, 2011.

[40] C. Seo, J.-P. Kim, J. Kim, H.-S. Ahn, and J. Ryu, "Robustly stable bilateral teleoperation under time-varying delays and data losses: an energy-bounding approach," *Journal of Mechanical Science and Technology*, vol. 25, pp. 2089–2100, 2011.

[41] M. Franken, S. Stramigioli, S. Misra, C. Secchi, and A. Macchelli, "Bilateral telemanipulation with time delays: A two-layer approach combining passivity and transparency," *IEEE Transactions on Robotics*, vol. 27, no. 4, pp. 741–756, 2011.

[42] R. J. Adams and B. Hannaford, "A two-port framework for the design of unconditionally stable haptic interfaces," in *Proc. IEEE/RSJ Int. Conf. Intelligent Robots and Systems (IROS)*, vol. 2, 1998, pp. 1254–1259.

[43] A. Jazayeri and M. Tavakoli, "Revisiting Llewellyn's absolute stability criterion for bilateral teleoperation systems under non-passive operator or environment," in *Proc. IEEE/RSJ Int. Conf. Intelligent Robots and Systems (IROS)*, 2012, pp. 70–75.

[44] J. E. Colgate and G. G. Schenkel, "Passivity of a class of sampled-data systems: Application to haptic interfaces," *Journal of robotic systems*, vol. 14, no. 1, pp. 37–47, 1997.

[45] L. Eusebi and C. Melchiorri, "Force reflecting telemanipulators with time-delay: stability analysis and control design," *IEEE Transactions on Robotics and Automation*, vol. 14, no. 4, pp. 635–640, 1998.

[46] S.-I. Niculescu, D. Taoutaou, and R. Lozano, "Bilateral teleoperation with communication delays," *International Journal of Robust and Nonlinear Control*, vol. 13, no. 9, pp. 873–883, 2003.

[47] H. Kazerooni, T.-I. Tsay, and K. Hollerbach, "A controller design framework for telerobotic systems," *IEEE Transactions on Control Systems Technology*, vol. 1, no. 1, pp. 50–62, 1993.

[48] G. M. H. Leung, B. A. Francis, and J. Apkarian, "Bilateral controller for teleoperators with time delay via $\mu$-synthesis," *IEEE Transactions on Robotics and Automation*, vol. 11, no. 1, pp. 105–116, 1995.

[49] I. Polushin, P. X. Liu, C.-H. Lung, and G. D. On, "Position-error based schemes for bilateral teleoperation with time delay: Theory and experiments," in *Proc. IEEE Int. Conf. on Mechatronics and Automation*, 2006, pp. 312–317.

[50] A. Sano, H. Fujimoto, and M. Tanaka, "Gain-scheduled compensation for time delay of bilateral teleoperation systems," in *Proc. IEEE Int. Conf. on Robotics and Automation (ICRA)*, vol. 3, 1998, pp. 1916–1923.

[51] I. Polat and C. W. Scherer, "Stability analysis for bilateral teleoperation: An IQC formulation," *IEEE Transactions on Robotics*, vol. 28, no. 6, pp. 1294–1308, 2012.

[52] W.-H. Zhu and S. E. Salcudean, "Stability guaranteed teleoperation: an adaptive motion/force control approach," *IEEE Transactions on Automatic Control*, vol. 45, no. 11, pp. 1951–1969, 2000.

[53] J.-H. Ryu and D.-S. Kwon, "A novel adaptive bilateral control scheme using similar closed-loop dynamic characteristics of master/slave manipulators," *Journal of Robotic Systems*, vol. 18, no. 9, pp. 533–543, 2001.

[54] H.-K. Lee, K. Tanie, and M. J. Chung, "Design of a robust bilateral controller for teleoperators with modeling uncertainties," in *Proc. IEEE/RSJ Int. Conf. Intelligent Robots and Systems (IROS)*, vol. 3, 1999, pp. 1860–1865.

[55] J. H. Park and H. C. Cho, "Sliding mode control of bilateral teleoperation systems with force-reflection on the internet," in *Proc. IEEE/RSJ Int. Conf. Intelligent Robots and Systems (IROS)*, vol. 2, 2000, pp. 1187–1192.

[56] H. C. Cho, J. H. Park, K. Kim, and J.-O. Park, "Sliding-mode-based impedance controller for bilateral teleoperation under varying time-delay," in *Proc. IEEE Int. Conf. on Robotics and Automation (ICRA)*, vol. 1, 2001, pp. 1025–1030.

[57] D. Lee and K. Huang, "Passive-set-position-modulation framework for interactive robotic systems," *IEEE Transactions on Robotics*, vol. 26, no. 2, pp. 354–369, 2010.

[58] A. Schiele and G. Hirzinger, "A new generation of ergonomic exoskeletons - The high-performance X-Arm-2 for space robotics telepresence," in *Proc. IEEE/RSJ Int. Conf. Intelligent Robots and Systems (IROS)*, 2011, pp. 2158–2165.

[59] A. Schiele, "METERON - validating orbit-to-ground telerobotics operations technologies," in *11th Symposium on Advanced Space Technologies for Robotics and Automation (ASTRA)*, 2011.

[60] G. Hirzinger, J. Heindl, K. Landzettel, and B. Brunner, "Multisensory shared autonomy-a key issue in the space robot technology experiment rotex," in *Proc. IEEE/RSJ Int. Conf. Intelligent Robots and Systems (IROS)*, vol. 1, 1992, pp. 221–230.

[61] S. W. Squyres, R. E. Arvidson, E. T. Baumgartner, J. F. Bell, P. R. Christensen, S. Gorevan, K. E. Herkenhoff, G. Klingelhöfer, M. B. Madsen, R. V. Morris *et al.*, "Athena mars rover science investigation," *Journal of Geophysical Research: Planets (1991–2012)*, vol. 108, no. E12, 2003.

[62] A. Haddadi and K. Hashtrudi-Zaad, "Stability analysis of haptic interfaces for different types of sampled signals and virtual environment implementations," in *Proc. IEEE Haptics Symp.*, 2010, pp. 293–299.

[63] F. M. Asl and A. G. Ulsoy, "Analysis of a system of linear delay differential equations," *Transactions-American Society of Mechanical Engineers Journal of Dynamic Systems Measurement and Control*, vol. 125, no. 2, pp. 215–223, 2003.

[64] S. Yi and A. G. Ulsoy, "Solution of a system of linear delay differential equations using the matrix Lambert function," in *Proc. American Control Conference (ACC)*, 2006, pp. 6–14.

[65] S. Yi, W. Choi, and T. Abu-Lebdeh, "Time-Delay Estimation using the Characteristic Roots of Delay Differential Equations," *American Journal of Applied Sciences*, vol. 9, no. 6, p. 955, 2012.

[66] S. Yi, P. W. Nelson, and A. G. Ulsoy, *Time-delay systems: Analysis and control using the Lambert W function*. World Scientific Publishing Company, 2010.

[67] ——, "Proportional-Integral Control of First-Order Time-Delay Systems via Eigenvalue Assignment," *IEEE Transactions on Control Systems Technology*, 2012.

[68] K. B. Fite, L. S., and M. Goldfarb, "Loop shaping for transparency and stability robustness in bilateral telemanipulation," *IEEE Transactions on Robotics and Automation*, vol. 20, no. 3, pp. 620–624, 2004.

[69] A. Peer and M. Buss, "Robust stability analysis of a bilateral teleoperation system using the parameter space approach," in *Proc. IEEE/RSJ Int. Conf. Intelligent Robots and Systems (IROS)*, 2008, pp. 2350–2356.

[70] R. M. Corless, G. H. Gonnet, D. E. Hare, D. J. Jeffrey, and D. E. Knuth, "On the LambertW function," *Advances in Computational mathematics*, vol. 5, no. 1, pp. 329–359, 1996.

[71] K. Ogata, *Modern Control Engineering*. Prentice-Hall International, 1990.

[72] S. Yi, P. W. Nelson, and A. G. Ulsoy, "Eigenvalue assignment via the Lambert W function for control of time-delay systems," *Journal of Vibration and Control*, vol. 16, no. 7-8, pp. 961–982, 2010.

[73] H. Shinozaki and T. Mori, "Robust stability analysis of linear time-delay systems by Lambert W function: some extreme point results," *Automatica*, vol. 42, no. 10, pp. 1791–1799, 2006.

[74] L. Ljung, *System Identification: Theory for the User*. Prentice Hall, New Jersey, 1999.

[75] N. Hogan, "Controlling impedance at the man/machine interface," in *Proc. IEEE Int. Conf. on Robotics and Automation (ICRA)*, 1989, pp. 1626–1631.

[76] K. Kosuge, H. Murayama, and K. Takeo, "Bilateral feedback control of telemanipulators via computer network," in *Proc. IEEE Int. Conf. on Intelligent Robots and Systems (IROS)*, vol. 3, 1996, pp. 1380–1385.

[77] S. Hirche, A. Bauer, and M. Buss, "Transparency of haptic telepresence systems with constant time delay," in *Proc. of IEEE Conf. on Control Applications (CCA)*, 2005, pp. 328–333.

[78] J. Kim and P. H. Chang, "Extended transparency as a quantitative performance measure in bilateral teleoperation," in *Proc. IEEE/RSJ Int. Conf. Intelligent Robots and Systems (IROS)*, 2007, pp. 3119–3124.

[79] J. Rebelo and A. Schiele, "State-space stability analysis of 4-channel bilateral teleoperation under constant time-delay," *IEEE Transactions on Control Systems Technology (submitted)*, 2015.

[80] J. Artigas, J. Vilanova, C. Preusche, and G. Hirzinger, "Time domain passivity control-based telepresence with time delay," in *Proc. IEEE/RSJ Int. Conf. Intelligent Robots and Systems (IROS)*, 2006, pp. 4205–4210.

[81] J. Artigas, C. Preusche, G. Hirzinger, G. Borghesan, and C. Melchiorri, "Bilateral energy transfer in delayed teleoperation on the time domain," in *Proc. IEEE Int. Conf. on Robotics and Automation (ICRA)*, 2008, pp. 671–676.

[82] J. Artigas, J.-H. Ryu, C. Preusche, and G. Hirzinger, "Network representation and passivity of delayed teleoperation systems," in *Proc. IEEE/RSJ Int. Conf. Intelligent Robots and Systems (IROS)*, 2011, pp. 177–183.

[83] J. Artigas, C. Preusche, and G. Hirzinger, "Time domain passivity for delayed haptic telepresence with energy reference," in *Proc. IEEE/RSJ Int. Conf. Intelligent Robots and Systems (IROS)*, 2007, pp. 1612–1617.

[84] J. Rebelo and A. Schiele, "Time domain passivity controller for 4-channel time-delay bilateral teleoperation," *IEEE Transactions on Haptics*, 2014.

[85] C. Ott, J. Artigas, and C. Preusche, "Subspace-oriented energy distribution for the time domain passivity approach," in *Proc. IEEE/RSJ Int. Conf. Intelligent Robots and Systems (IROS)*, 2011, pp. 665–671.

[86] P. Letier, M. Avraam, S. Veillerette, M. Horodinca, M. De Bartolomei, A. Schiele, and A. Preumont, "SAM: A 7-DOF portable arm exoskeleton with local joint control," in *Proc. IEEE/RSJ Int. Conf. Intelligent Robots and Systems (IROS)*, 2008, pp. 3501–3506.

[87] G. Schreiber, A. Stemmer, and R. Bischoff, "The fast research interface for the kuka lightweight robot," in *IEEE Workshop on Innovative Robot Control Architectures for Demanding (Research) Applications How to Modify and Enhance Commercial Controllers (ICRA 2010)*, 2010.

[88] J. Rebelo, T. Sednaoui, E. Den Exter, T. Krueger, and A. Schiele, "An intuitive and portable haptic arm exoskeleton workstation for bilateral robot teleoperation," *Robotics and Automation Magazine*, 2014.

[89] G. Clement, J. Vertut, R. Fournier, B. Espiau, and G. Andre, "An overview of CAT control in nuclear services," in *Proc. IEEE Int. Conf. on Robotics and Automation (ICRA)*, vol. 2, 1985, pp. 713–718.

[90] D. Yoerger and J.-J. Slotine, "Supervisory control architecture for underwater teleoperation," in *Proc. IEEE Int. Conf. on Robotics and Automation (ICRA)*, vol. 4, 1987, pp. 2068–2073.

[91] V. Abbasi, B. Azria, E. Tabarah, V. Menon, and M. Bedirian, "Improved 7-DOF control of ISS robotic manipulators," in *Proceeding of the Eigth International Conference on Space Operations*, 2004.

[92] A. Peer, B. Stanczyk, and M. Buss, "Haptic telemanipulation with dissimilar kinematics," in *Proc. IEEE/RSJ Int. Conf. Intelligent Robots and Systems (IROS)*, 2005, pp. 3493–3498.

[93] T. Hulin, K. Hertkorn, P. Kremer, S. Schatzle, J. Artigas, M. Sagardia, F. Zacharias, and C. Preusche, "The DLR bimanual haptic device with optimized workspace," in *Proc. IEEE Int. Conf. on Robotics and Automation (ICRA)*, 2011, pp. 3441–3442.

[94] L. I. Lugo-Villeda, A. Frisoli, S. Pabon, M. A. Padilla, E. Sotgiu, and M. Bergamasco, "Light-exoskeleton and data-glove integration for enhancing virtual reality applications," in *Proc. Int. Conf. on Advanced Robotics (ICAR)*, 2009, pp. 1–6.

[95] H. Kazerooni, "Exoskeletons for human power augmentation," in *Proc. IEEE/RSJ Int. Conf. Intelligent Robots and Systems (IROS)*, 2005, pp. 3459–3464.

[96] H. S. Lo and S. Q. Xie, "Exoskeleton robots for upper-limb rehabilitation: State of the art and future prospects," *Medical engineering & physics*, vol. 34, no. 3, pp. 261–268, 2012.

[97] R. Gopura, K. Kiguchi, and D. Bandara, "A brief review on upper extremity robotic exoskeleton systems," in *Proc. 6th IEEE Int. Conf. on Industrial and Information Systems (ICIIS)*, 2011, pp. 346–351.

[98] C. Carignan, M. Liszka, and S. Roderick, "Design of an arm exoskeleton with scapula motion for shoulder rehabilitation," in *Proc. 12th Int. Conf. on Advanced Robotics (ICAR)*, 2005, pp. 524–531.

[99] D. Jansen and H. Buttner, "Real-time ethernet: the ethercat solution," *Computing and Control Engineering*, vol. 15, no. 1, pp. 16–21, 2004.

[100] "Simple open ethercat master (online)," http://soem.berlios.de/, Accessed on February 2014.

[101] G. Pardo-Castellote, "OMG data-distribution service: Architectural overview," in *Proc. 23rd Int. Conf. on Distributed Computing Systems Workshops*, 2003, pp. 200–206.

[102] L. Sciavicco and B. Siciliano, *Modelling and Control of Robot Manipulators*, 2nd ed. Springer-Verlag, 2000, ch. 3, pp. 113–117.

[103] S. Kimmer and A. Schiele, "Investigations towards low-bandwidth real-time video for teleoperation," in *Proceedings of the 12th Symposium on Advanced Space Technologies in Robotics and Automation (ASTRA)*, 2013.

[104] G. Hirzinger, B. Brunner, J. Dietrich, and J. Heindl, "Rotex – the first remotely controlled robot in space," in *Proc. IEEE Int. Conf. on Robotics and Automation (ICRA)*, 1994, pp. 2604–2611.

[105] J. Rebelo and A. Schiele, "Time-domain passivity control in 4-channel multi-dof bilateral teleoperation," in *Proc. IEEE/RSJ Int. Conf. Intelligent Robots and Systems (IROS) (submitted)*, 2015.

[106] T. Hulin, M. Sagardia, J. Artigas, S. Schaetzle, P. Kremer, and C. Preusche, "Human-scale bimanual haptic interface," in *Proc. of the 5th International Conference on Enactive Interface*, 2008.

[107] C. W. Wampler, "Manipulator inverse kinematic solutions based on vector formulations and damped least-squares methods," *IEEE Transactions on Systems, Man, and Cybernetics*, vol. 16, no. 1, pp. 93–101, 1986.

[108] A. Liegeois, "Automatic supervisory control of the configuration and behavior of multibody mechanisms," *IEEE Transactions on Systems, Man and Cybernetics*, vol. Vol. SMC-7, pp. 868–871, 1977.

[109] Y. Tsumaki, P. Fiorini, G. Chalfant, and H. Seraji, "A numerical SC approach for a teleoperated 7-DOF manipulator," in *Proc. IEEE Int. Conf. on Robotics and Automation (ICRA)*, vol. 1, 2001, pp. 1039–1044.

[110] G. J. A. Pamanes and S. Zeghloul, "Optimal placement of robotic manipulators using multiple kinematic criteria," in *Proc. IEEE Int. Conf. on Robotics and Automation (ICRA)*, 1991, pp. 933–938.

[111] L. Tian and C. Collins, "Optimal placement of a two-link planar manipulator using a genetic algorithm," *Robotica*, vol. 23, no. 02, pp. 169–176, 2005.

[112] F. Zacharias, I. S. Howard, T. Hulin, and G. Hirzinger, "Workspace comparisons of setup configurations for human-robot interaction," in *Proc. IEEE/RSJ Int. Conf. Intelligent Robots and Systems (IROS)*, 2010, pp. 3117–3122.

[113] A. Schiele, *Wearable Robots: Biomechatronic Exoskeletons*. John Wiley & Sons Ltd., 2008, ch. 8.3, pp. 248–255.

[114] S. S. U. Gamage and J. Lasenby, "New least squares solutions for estimating the average centre of rotation and the axis of rotation," *Journal of Biomechanics*, vol. 35, no. 1, pp. 87 – 93, 2002.

[115] K. Kreutz-Delgado, M. Long, and H. Seraji, "Kinematic analysis of 7 DOF anthropomorphic arms," in *Proc. IEEE Int. Conf. on Robotics and Automation (ICRA)*, 1990, pp. 824–830.

[116] C. A. Klein and B. E. Blaho, "Dexterity measures for the design and control of kinematically redundant manipulators," *The International Journal of Robotics Research*, vol. 6, no. 2, pp. 72–83, 1987.

[117] T. F. Chan and R. V. Dubey, "A weighted least-norm solution based scheme for avoiding joint limits for redundant joint manipulators," *IEEE Transactions on Robotics and Automation*, vol. 11, no. 2, pp. 286–292, 1995.

[118] Cyberbotics, "Webots," http://www.cyberbotics.com/overview, Apr. 2013.

[119] Kongsberg Oil & Gas Technologies, "Coin3d," http://www.coin3d.org, Apr. 2013.

[120] The Khronos Group, "Opengl," http://www.opengl.org/, Apr. 2013.

[121] Digia Plc, "Qt," http://qt.digia.com, Apr. 2013.

[122] J. Rebelo and A. Schiele, "Master-slave mapping and slave base placement optimization for intuitive and kinematically robust direct teleoperation," in *International Conference on Control, Automation and Systems (ICCAS)*, 2012.

[123] GStreamer, "Gstreamer," http://www.gstreamer.com/, Apr. 2013.

# Acknowledgements

First and foremost I would like to thank Dr. Schiele for giving me the opportunity to pursue this research in his lab and for his consistent support and incentive. It's still hard for me to believe that just 5 years ago the lab was only a construction site and we are now close to demonstrating bilateral teleoperation from the International Space Station. It has been a great journey and I am very glad to have been part of it.

I would also like to thank my promotor, Prof. van der Helm for supporting my work and for the good discussions and advices especially during the critical phases of the thesis.

The support of all the people in the ESA Telerobotics Lab has also been essential for this work. I would therefore like to thank Frank van der Hulst, Manuel Aiple, Thomas Krüeger, Thomas Sednaoui, Emiel den Exter, and Eloise Matheson for their professional support and friendship throughout my research. A particular thank you goes to my two fellow Ph.D. colleagues in the lab, Stefan Kimmer and Jan Smíšek, with whom I have had many fruitful research discussions and a great time over many lab demos, dinners and Friday afternoon beers.

I would also like to acknowledge all the people in ESA who have directly or indirectly supported my research, in particular Robert Blommestijn and Quirien Wijnands as well as all my colleagues at TEC-SW for showing me my way around when I first came to ESA and for their patience answering my many questions about spacecraft simulators and software. I would also like to thank Wilhelm van Hoogstraten, Kees van der Luijt and the people at the ESA workshop for all their help preparing test setups.

As writing a Ph.D. thesis is as much a professional as a personal endeavour, I would like to thank the many people around me who helped make this time memorable. I have to thank everyone in the Võ-Đạo-Việt-Nam group for all the great fun during training which helped me keep both physically and mentally fit, especially Stan for always insisting that limits can be pushed a bit further and Torsten for all the great advices and shared wisdom not only about martial arts but life in general. To my brother Pedro and my friend Hugo, who have been around for most of the time in the Netherlands, I have to thank them for always showing up in a good mood and making life here feel a lot more like home. To all the other people I had the luck of meeting here, especially Manuel, Sara, César, David, Catarina, Inês, Tatiana, Lucie, Duarte, Francis, Laura, Jesús, Marco Panunzio, Marco de Rosa and Corianne, thanks for making my stay in The Netherlands such a great time. To my friends Nuno, Rodrigo and Tó Mané in Portugal; Luzia, André, Héctor and Ania in Denmark; and Wiebke in Aachen, thanks for always keeping in touch even through the most busy times.

Last but not least I would like to thank my family, especially my parents for being always encouraging and supportive of my goals even when that meant long times without news and being away from home. The last and biggest thanks of all goes to my wife Adéla, without whose love, extraordinary logistic support and care none of this would have been possible.

# Curriculum Vitæ

João Luis Pinto Rebelo
Born on July 29th, 1984
in Lamego, Portugal

## Education/Professional Experience

| | |
|---|---|
| 2015– now | **Telerobotics Engineer**<br>European Space Agency, Noordwijk, The Netherlands |
| 2011– 2015 | **PhD. Candidate**<br>European Space Agency, Noordwijk, The Netherlands<br>Delft University of Technology, The Netherlands |
| 2009– 2011 | **Satellite Simulation Engineer**<br>European Space Agency, Noordwijk, The Netherlands |
| 2007– 2009 | **Software Engineer**<br>Danfoss Drives, Gråsten, Denmark |
| 2002– 2007 | **Graduate in Electrical and Computers Engineering**<br>Faculty of Engineering of University of Porto, Portugal |
| 1999– 2002 | **High school**<br>Escola Secundária Latino Coelho, Lamego, Portugal |